ROYAUME DU MAROC
Université Mohammed V - RABAT -
جامعة محمد الخامس – الرباط –
Faculté des sciences
كلية العلوم
CENTRE D'ETUDES DOCTORALES - SCIENCES ET TECHNOLOGIES

=

N° d'ordre 3075

THESE

En vue de l'obtention du : ***DOCTORAT***

Structure de Recherche : Laboratoire de Matière Condensée et Sciences Interdisciplinaires (LaMCScI)
Discipline : Physique Informatique
Spécialité : Matière condensée et modélisation des systèmes

Présentée et soutenue le : 03/03/2018 par :

Abderrahim AIT RAISS

Le titre de la thèse :
Ab initio study of magnetic properties and Faraday rotation of diluted magnetic semiconductors (CdTe, ZnSe)

JURY

Mr. Najem HASSANAIN PES, Université Mohammed V, Faculté des Sciences, Rabat
Président
M r. Larbi LAANAB PES, Université Mohammed V, Faculté des Sciences, Rabat
Examinateur
Mr. Abdelilah BENYOUSSEF PES, Membre résident à l'académie Hassan II des Sciences et techniques, Rabat *Examinateur*
Mr. Lahoucine BAHMAD PES, Université Mohammed V, Faculté des Sciences, Rabat
Directeur de Thèse
Mr. Hamid EZ-ZAHRAOUY PES, Université Mohammed V, Faculté des Sciences, Rabat
Examinateur & Rapporteur
Mr. Mohammed Aggour PES, Université Ibn Toufail, Faculté des Sciences, Kenitra
Examinateur & Rapporteur
Mr. Mohamed Kerouad PES, Université Moulay-Ismaïl, Faculté des Sciences, Meknès
Examinateur & Rapporteur

Dedication

I would like to dedicate my thesis dissertation to my mother and father, to whom I'm grateful and thankful for all what they have done and sacrifice, to help me and push me to reach this high honorable degree.

Thank you for all your moral and financial support.

A special feeling of love and gratitude goes to my brothers Boubker, Abdelaziz, Mohammed, and my sister Fatima for their support and encouragement.

A dedication to all my friends who shared with me this wonderful period of thesis preparation.

Acknowledgments

This work was carried out in the laboratory of condensed matter and interdisciplinary Sciences (LaMCScI), Mohammed V University, Faculty of Sciences, Rabat, under the supervision of the Professor Lahoucine Bahmad.

First and foremost, I would like to expres my deepest thanks and gratitude to allah the almighty for his help and support throughout whole my life, especially in my study and research project.

With gratitude, I would like to express my sincere thanks to Prof. Lahoucine Bahmad for supervising this thesis and for his availability, his advices, support and encouragement throughout the preparation period of this thesis.

It is a pleasure for me to express my gratitude and appreciation to the professor Mr. Najem HASSANAIN to be the president of this thesis as well as his relevant comments and advices.

A special thanks and gratefulness, go to the professor Mr. Hamid EZ-ZAHRAOUY for accepting to report and to examine this thesis as well as his advices and moral support during the preparation of this thesis.

A special thanks and gratitude go to the Professor Mr. Abdelilah Benyoussef, for teaching me in bachelor, and for his support and encouragement for me and all the Ph.D students in (LaMcSI) laboratory.

Special thanks and gratefulness, go to the professor Mr. Larbi LAANAB for his relevent comments and advices during the deffense of this thesis.

It is a great pleasure for me to express my gratitude and thanks to the professor Mr. Mohammed AGGOUR from Faculty of Sciences-Kénitra, for his great efforts and disponibility to report and to examine this work, as well as his relevant comments and advice. Thank you, Mr for teaching me in Master and for your unforgettable positive attitudes.

I would like to extend my gratefulness and thanks to the professor Mr. Mohamed KEROUAD from Faculty of Sciences-Meknès, for accepting to report and to examine this work as well as his pertinent comments and personal advice in the forthcoming projects.

I would like to extend my sincere gratitude to my friends and colleagues in the laboratory (LaMcSI), Sbai Younes, Zarhri Zakaryaa, Arejdal Mustapha, Houmad Mohamed, and all members who showed a spirit of collaboration and respect.

I also want to thank all the professors who taught me during my university courses, either at the faculty of Rabat or Kenitra. The same thanks go to all my primary, middle school and high school teachers.

Special thanks to my family member El houzali Mohammed, for his moral support, and continuous encouragement during my study period, and for his pieces of advice in my personal life.

I would like to thank my best friends, Abdelmjid Timzitine, Yassine Libtinioui, Younes El yousfi, for their support, and encouragment during my research project.

At last, my Sincere gratitude and appreciation go to my parents, for their great support and sacrifices. Without their pure efforts, I would not reach this honorable position.

I expand my gratitude and thanks to my dear sister Fatima, to my dear brothers Boubker, Abdelaziz and Mohamed. I really appreciate all your moral, and physical support during my period of study.

Abstract

The spintronic is a new kind of electronic which will replace the classical microelectronic when using the spin of the electron besides to its charge. This kind of electronics is based on diluted magnetic semiconductors (DMS). The main objective of this thesis is to study the magnetic properties and Faraday rotation of DMSs, such as CdTe and ZnSe, doped with different transition metals (TM). This study is carried out by Ab initio calculations, based on Density Functional Theory (DFT), which we will describe in detail, later in the manuscript. Firstly, we have investigated that doping CdTe with Mn impurity, induces a magnetism in the host compound. But the doping with Fe atoms does not contribute to magnetism. While the codoping with both Mn and Fe improves well the Faraday rotation according to an experimental work, cited in the first chapter of part two. Secondly, we have investigated that Cd or Te vacancy defects in $CdMn_{0.38}Te$, affects the magnetic state, as the codoping with N atoms in Te sites does. Thereafter, we have investigated that doping CdTe with the Vanadium impurity (V) for the concentrations (0.05; 0.07; 0.09; 0.11), shows a half-metallic behavior, and stabilizes the ferromagnetic state for all those concentrations. We have found out that the critical temperatures approximate 621(K) in this case. In addition, we have investigated that adding 0.03 of vacancy defects, improves well the ferromagnetic state, while the critical temperature has increased. Concerning the Faraday rotation, we have found out that Vanadium doping improves this property, affecting the exchange interactions $N0\alpha$. While in the case of adding vacancies, this property is improved, thanks to the contribution of the exchange interactions $N0\beta$. For ZnSe doped with Chromium impurity, we have found that this type of doping induces a half-metallic behavior, for all the studied concentrations (0.01; 0.05; 0.1; 0.15; 0.2; 0.25). This behavior is affected when introducing vacancy defects besides to the Cr doping. The critical temperature is found to increase with the increase of doping concentrations and vacancies. The Faraday effect is not affected in this case. In addition, we have investigated that doping ZnSe with Mn impurity, induces a magnetism behavior, which is stable in anti-ferromagnetic state for all the studied concentrations (0.05; 0.1; 0.15; 0.2). While introducing 0.05 of vacancy defects in Zn sites, affect the magnetic state, by changing it to a stable ferromagnetic state. this also gives birth to the half metallic behavior and improves the critical temperatures. Also, the Faraday effect seems to be as not affected either by Mn doping or vacancy defects.

Keywords: CdTe; ZnSe; Ab initio calculations; Spintronic; DMS; Magnetism; Half metal; Curie temperature; Faraday rotation.

Resumé

La spintronique est un nouveau type d'électronique qui va remplacer la microélectronique classique en utilisant le spin de l'électron en plus de sa charge. Ce type d'électronique est basé sur des semi-conducteurs magnétiques dilués (DMS). L'objectif principal de cette thèse est d'étudier les propriétés magnétiques et la rotation de Faraday des DMS, tels que CdTe et ZnSe, dopés avec différents métaux de transition (TM). Cette étude est réalisée par des calculs Ab initio, basés sur la théorie fonctionnelle de la densité (DFT), que nous décrirons en détail plus loin dans le manuscrit. Premièrement, nous avons étudié que le dopage CdTe avec l'impureté Mn, induit du magnétisme dans le composé hôte (CdTe). Mais le dopage avec des atomes de Fe ne contribué pas au magnétisme. Alors que le co-dopage à la fois avec Mn et Fe améliore bien la rotation de Faraday selon un travail expérimental cité dans le premier chapitre de la deuxième partie. Deuxièmement, nous avons étudié que les défauts d'inoccupation Cd ou Te dans CdMn0.38Te, agit sur l'état magnétique, comme le fait le co-dopage avec des atomes d'azote (N) dans les sites Te. Par la suite, nous avons découvert que le dopage CdTe avec l'impureté de vanadium (V) pour les concentrations (0.05; 0.07; 0.09; 0.11) montre un comportement semi-métallique et stabilise l'état ferromagnétique pour toutes ces concentrations. Nous avons également trouvé que les températures critique sont supérieur à l'ambiante, et elles s'approchent de 621 (K). En outre, nous avons découvert que l'ajout de 0.03 de défauts de lacunes, améliore bien l'état ferromagnétique, tandis que la température critique devient plus élevée. Concernant la rotation de Faraday, nous avons découvert que le dopage au Vanadium améliore cette propriété, affectant les interactions d'échange N0α. Cependant, dans le cas de l'ajout des sites vacants, cette propriété est améliorée, grâce à la contribution des interactions d'échange N0β. Pour le ZnSe dopé avec l'impureté de chrome, nous avons trouvé que ce type de dopage induit un comportement semi-métallique, pour toutes les concentrations étudiées (0.01; 0.05; 0.1; 0.15; 0.2; 0.25) . Ce comportement, est influencé par l'apparition des défauts de lacunes dans le composé ZnSe dopé avec du chrome (Cr). La température critique augmente avec l'augmentation des concentrations de dopage et celle des lacunes. L'effet Faraday n'est pas affecté dans ce cas. En outre, nous avons vérifié que le dopage du composé ZnSe avec l'impureté Mn, induit un comportement magnétique. Nous avons trouvé que le magnétisme induit est stable dans l'état anti-ferromagnétique pour toutes les concentrations étudiées (0.05; 0.1; 0.15; 0.2). Dans le cas d'introduire un taux de 0.05 de défauts de lacunes dans les sites Zn, nous avons découvert que cela agit sur l'état magnétique, en le changeant en un état ferromagnétique stable. Cela donne aussi naissance au comportement semi-métallique et améliore les températures critiques. De plus, l'effet de Faraday ne semble pas être influencé, ni par le dopage Mn, ni par les défauts d'inoccupation.

Mots-clés: CdTe; ZnSe; Calculs ab initio; Spintronique; DMS; Magnétisme; semi-métal; Température de Curie; La rotation de Faraday.

Contents

Dedication.....1
Acknowledgment.....2
Abstract.....4
Contents.....6
Abreviations list.....10

Dedication.....1
Acknowledgment.....2
Abstract.....4
Contents.....6
Abreviations list.....10

***I. GENERAL INTRODUCTION*.....11**
I.1 Thesis overview and motivation.....12

I.2 Objective and Structure of the thesis.....12

PART ONE: Background information……..……...14

CHAPTER I: Spintronic & DMSs ……..……15

***I. Introduction*..... 16**

***II.** Spin electronics*.....…..…..16**

1.The Giant Magneto-Resistance (GMR)..... ……..16

2.The Tunnel Magnetic Resistance (TMR)..... …… ……..18

3. Magnetic Random Access Memory (MRAM)……21

4. Spin Field Effect Transistor(SPINFET)……22

***III. The difficulty of spin injection* .....……24**

IV. Diluted magnetic semiconductors (DMS).....…….....**24**

1. Definition and types..... 24

2. DMS crystal growth techniques.....26

3. Different types of DMSs……28

3.a. DMS based on IV semiconductors……28

3.b. DMS based on II-VI semiconductors.....28

3.c. DMS based on III-V semiconductors.....28

4. Advantages of DMSs based on III-V and II-VI semiconductors.....28

5. CdTe semiconductor.....29

6. ZnSe semiconductor.....30

V. Faraday rotation (magneto-optical effect) 31

VI. Different exchange interactions in DMSs……32

1. Direct exchange ……33

2. Indirect exchange……33

a. Double exchange ……33

b. Super-exchange……34

c. RKKY interactions (Ruderman-Kittel-Kasuya-Yoshida)……34

CHAPTER II: Ab-initio calculation method…….....36

I. Density Functional Theory…….....37

I.1 Introduction..... .37

I .2 Schrödinger equation for many-body problem……37

I.2.1 Born-Oppenheimer approximation……39

I.3 Hartree approximation……39

I.4 Density Functional Theory ……40

I.4.1 The Hohenberg and Kohn Theorems……40

I.4.2 The Kohn and Sham equations……41

I.4.3 The exchange-correlation functional……42

I.4.4 The Local Density Approximation (LDA)……43

I.4.5 The local spin density approximation (LSDA)……43

I.4.6 The Generalized Gradient Approximation (GGA)……44

I.4.7 Resolving the Kohn Sham equations……44

II. Korringa Kohn Rostoker method……..…..46

II.1. Introduction……46

II.2 Definition and general properties of the Green function……47

II.2.1 Green's function time depending……47

II.2.2 Green's function energy depending……49

II.2.3 Relation between disturbed and non-disturbed system of the transition matrix or T-matrix……50

II.2.4 Scattering of a single site……53

2.4 Multiple diffusion theory……56

II.2.5 Representation of KKR method……59

II.2.6 Coherent potential approximation (CPA)……61

III. FPLAPW method implemented in Wien2k……62

III.1 The basic of Augmented Plane Wave (APW) ……62

III.2 The basic of linear augmented plane wave (LAPW)……63

III.3 GW approximation……65

III.4 Modified Becke and Johnson potential (mBJ)……65

PART TWO: Results and discussion on magnetic and magneto-optical properties of DMSs (CdTe, ZnSe)……66

Chapter I: Magnetic and Magneto-optical properties of doped and co-doped CdTe with (Mn, Fe): Ab-initio study……67

I. Magnetic and Magneto-optical properties of doped and co-doped CdTe with (Mn, Fe): Ab-initio study……69

1. Introduction……69

2. Computational method……70

3. Results and discussion……71

3.a . CdTe doped with Mn impurity……72

3.b. CdTe doped with Fe impurity……74

3.c. CdTe codoped with Mn and Fe impurity……75

II. Study of the magnetic properties of CdMnTe1-yNy and CdMnTe with defects by Ab initio calculations……83

II.1. Introduction……83

II.2. Results and discussion ……83

2.a.case of $Cd_{0.62}Mn_{0.38}Te$……83

2.b. case of $Cd_{0.62}Mn_{0.38}Te$ co-doped with Nitrogen (N)……84

2.c- case of vacancy defects in Te sites of $Cd_{0.62}Mn_{0.38}Te$……86

2.d- case of vacancy defects in Cd sites of $Cd_{0.62}Mn_{0.38}Te$ ……88

III. Study of electronic structure and magnetic properties of Vanadium doped CdTe with vacancy defects: Ab initio approach……93

1. Introduction……93

2. Results and discussion……..93

2.a. case of Vanadium doped CdTe……..93

2.b. the case of vacancy defects in Cd sites of Vanadium doped CdTe……96

2.c. discussion of Faraday rotation……100

IV. Conclusion……...101

Chapter II: Magnetic properties and Faraday rotation of doped ZnSe (Cr, Mn)……..103

I. Magnetic properties and Faraday rotation of Cr doped ZnSe with defects: First principles calculations ……105

1. Introduction……..105

2. Computational method……106

3. Results and discussion……..107

3.a. case of undoped ZnSe…….107

3.b. case of Chromium doped ZnSe……108

3.c. introducing vacancy defects in Cd sites of Chromium doped ZnSe……111

II. The vacancy defects in ZnMnSe induces a half-metallic behavior and stabilizes the ferromagnetic state: Ab initio study……119

1. Results and discussion……..119

2.a. magnetic properties and Faraday rotation of Mn-doped ZnSe……119

2.b. case of Mn-doped ZnSe with 0.03 of vacancy defects in Zn sites……121

*2.*c. *the case of Mn-doped ZnSe with 0.05 of vacancy defects in Zn sites……123*

III. Conclusion…… …125

General Conclusion*……..128*

List of publications……..131

References……133

Abbreviations list

DLM	Disordered local moment
DMS	Dilute magnetic semiconductor
MTJ	Magnetic tunnel junction
HM	Half metal
FM	Ferromagnetic
Tc	Curie Temperature
TDOS	Total Density of States
GMR	Giant Magnetic resistance
TMR	Tunnel magnetic resistance
RKKY	Ruderman-Kittel-Kasuya-Yoshida
PDOS	Partial Density of States
DFT	Density Functional Theory
FP-LAPW	Full Potential- Local Approximation Plane Wave
KKR	Korringa Kohn Rostoker
CPA	Coherent Potential Approximation
PBE	Perdew-Burke-Ernzerhof
GGA	Generalized Gradient Approximation
LSDA	Local Spin Density Approximation
MBJ	Modified Becke and Johnson
MRAM	Magnetic Random Access Memory
TM	Transition Metal
AFM	Antiferromagnetic
BZ	Brillouin Zone
Tc	Curie Temperature
EF	Fermi Energy
VBM	Valence Band Maximum
CBM	Conduction Band Maximum
MS	Magnetic Semiconductor
NMS	Non Magnetic semiconductor
MBE	Molecular Beam Epitaxy
MO	Magneto-Optical
FE	Faraday Effect

General Introduction :

Seventy years ago, The Microelectronics was born with the physicist Shockley and his colleagues. That was after the discovery of the transistor in 1947. This magical component gives birth to many electronic devices, which is widely used in our daily life. However, this kind of electronic has a limit. According to Moore'slaw, the number of transistors implanted in surface doubles every eighteen months, so it means that we will reach the limit in one day. A lot of research works are focused on finding other solution to reduce the energy consumption of electronic devices and develop a new technology as well as transport information, storage capacity and so on. Spintronic is a new technique that exploits the spin of the electron besides to its charge. This, to study the properties of new materials such as DMSs (diluted magnetic semiconductors), in order to develop new efficient electronic devices, so as to improve the existing ones. Some components of spintronics are already widely used by industry, such as the hard disk drive heads based on the GMR (Giant Magneto Resistance). Other applications are on the way to be born, as MRAM (Magnetic Random Acces Memory), which may replace the current memory (RAM) of computers. Research in the field focuses mainly on creating and controlling the spin current to transmit the information. Responding to the need for fast access to digital data is in the origin of a lot of works in the field of spintronics. Among them, many are focused on finding new spintronic systems and devices, with interesting magnetic properties, such as the ferromagnetism (FM) and the half-metallic(HM). So far two main effects of spintronic, have been observed, which are the Giant Magnetoresistance(GMR), and the Tunnel-effect magnetoresistance(TMR). These discoveries, which may be seen as the starting point, will lead to the development of Random access memory (MRAM), which allows replacing the current RAM memories, as said before. Therefore, the integration of this new science in multidisciplinary research will lead to the development of many applications. As an example of application, we name the hard disks of modern computers, which are based on TMR. The planned development of spin electronics is aimed to improve the semiconductor heterostructures, making it possible to increase the density of the components, as well as to improve the performance, in addition to lower the cost. The aim of Spintronic is to associate magnetic and semiconductor materials, allowing to integrate into the same device, memory functions, detection and signal processing.

1.1 Thesis overview and motivation :

The research on diluted magnetic semiconductors (DMSs) and their properties have attracted much interest from physics scientists from all over the world. This research was carried out, either in developed laboratories, or using computational methods, such as Ab initio, Monte Carlo, or other computational methods. This field of research still has many questions and concerns, for example, seeking a ferromagnetism and half-metallic behavior at room temperature. As well as dealing with structural defects, such as the vacancy sites in the host material, in addition to impurities, which can affect the properties of the compound.

1.2 Objective and Structure of the thesis :

The main objective of this work is to study the magnetic properties of CdTe and ZnSe, doped with different TM impurities. As well as to check the evolution of the Faraday rotation as a magneto-optical property. This study was performed by ab initio calculations, using the KKR and Wien2k codes, based on Density Functional Theory (DFT). This study, aims to contribute to the developing of spintronic devices and photovoltaic applications. The progress of presenting the work in the manuscript is divided on two parts :

1 . **Part one**: is about the background information. It is devided into two chapters. In the first chapter, we give an overview and introduction about the Spintronic, in addition to a brief description on DMSs.

The second chapter is dedicated to the calculation method, Ab initio, besides to DFT approach and exchange mechanism. Also, we give a description of the used codes during the preparation of this thesis.

2. **Part two**: This part, is divided into two chapters. In the first chapter, we present the results and the discussion of the published papers about cadmium telluride (CdTe), in addition to the calculation method. The first section is dedicated to CdTe doped with Mn, Fe and codoped with both. This in order to study the effect of Mn or Fe doping on magnetic properties and Faraday effect. The second section is about studying the effect of vacancy defects in Cadmium (Cd), or Tellurium (Te) sites. In addition to the effect of replacing (Te) by Nitrogen(N) impurity. This defects may affect, either the magnetic and/or the magneto-optical properties. In the third section, we present our results about the compound CdTe, doped with Vanadium(V) impurity, and discuss its effect on the magnetic properties and Faraday rotation. The second chapter is divided into two sections, in the first one we will present and discuss the results about the compound Zinc Selenide (ZnSe), doped with Chromium (Cr), then with

vacancy defects in Zn sites. After that, in the second section, we will present a similar work to the previous one. Instead of chromium atoms, this time we will substitute the Zn atoms of the studied compound by Mn impurity for different concentrations. This to investigate its effect on the magnetic properties as well as the Faraday rotation. Later, we will conclude with a general conclusion on the work carried out.

Part one :
Background Information

Chapter I :
Spintronic and DMSs

I . Introduction :

The microelectronic technology encompasses all the standard electronic devices, based on classical semiconductors such as silicon, which is the most used in modern microchips. In these semiconductors, the signal processing is based on the charge of the electrons and controlled by the electric field. The observation of a ferromagnetism behavior in compounds of II-VI and III-V diluted magnetic semiconductors (DMSs), has opened the door to a new field of research. Therefore, a lot of works, are focused on using the spin of the electron, besides to its charge. Relying on the spin, as well as on the charge, gives birth to a new kind of electronic, which is called spintronic or spin electronic. Many of spintronic applications are based on DMSs, in which we substitute a part of nonmagnetic atoms by magnetic impurities, which are in general transition metals (TM). This will make it possible to realize new applications, which are not available with classical semiconductor devices. The diluted magnetic semiconductors may hold a ferromagnetism behavior above room temperature. They also could present a 100% of spin polarization. This could lead to spin current polarization, as well as the control of the spin current injection. Future spintronic applications are already expected, such as spin valve transistor, spin FET, and magnetic random access memory (MRAM). Spintronics devices could be smaller, more flexible and more efficient than those currently based on Silicon wafers. The spin transistor, which uses two ferromagnetic layers as an injector and spin analyzer, illustrates the potential semiconductor capability to increase the performance of integrated circuits, for spintronic applications. For example, a single spin transistor may be used as non-volatile memory cells, where the binary data are stored by magnetizing one of the ferromagnetic electrodes. This can lead to improving the storage capacity of the memories. However, controlling the spin injection in semiconductors at room temperature has been a major obstacle for the spintronic devices. One of the advantages of the II-VI or III-V semiconductors is the possibility of incorporating magnetic atoms (Mn, spin 5/2), and using the very strong interaction between these localized spins and charge carriers (electrons in the conduction band, holes in the valence band), to give the semiconductor new and exceptional magnetic, optical and magneto-optical properties.

II.Spin electronics

1.The Giant Magneto-Resistance (GMR)

Giant Magneto Resistance (GMR) is a quantum effect which is the main characteristic of the first manifestation of spintronic applications. It was discovered in 1988 in Orsay by the team of Albert Fert [1] and Peter Grünberg [2]. This effect was observed in thin film nanostructures composed of alternating ferromagnetic and nonmagnetic conductive layers. GMR effect is widely used in many spintronic applications such as a spin valve that is in the origin of the development and efficiency improvement of the hard disk read heads. A significant variation of the resistance occurs when an external magnetic field is applied. The macroscopic magnetizations of the magnetic layers, Successively, switches from an antiparallel configuration to an aligned parallel configuration, see (Figure I.1).

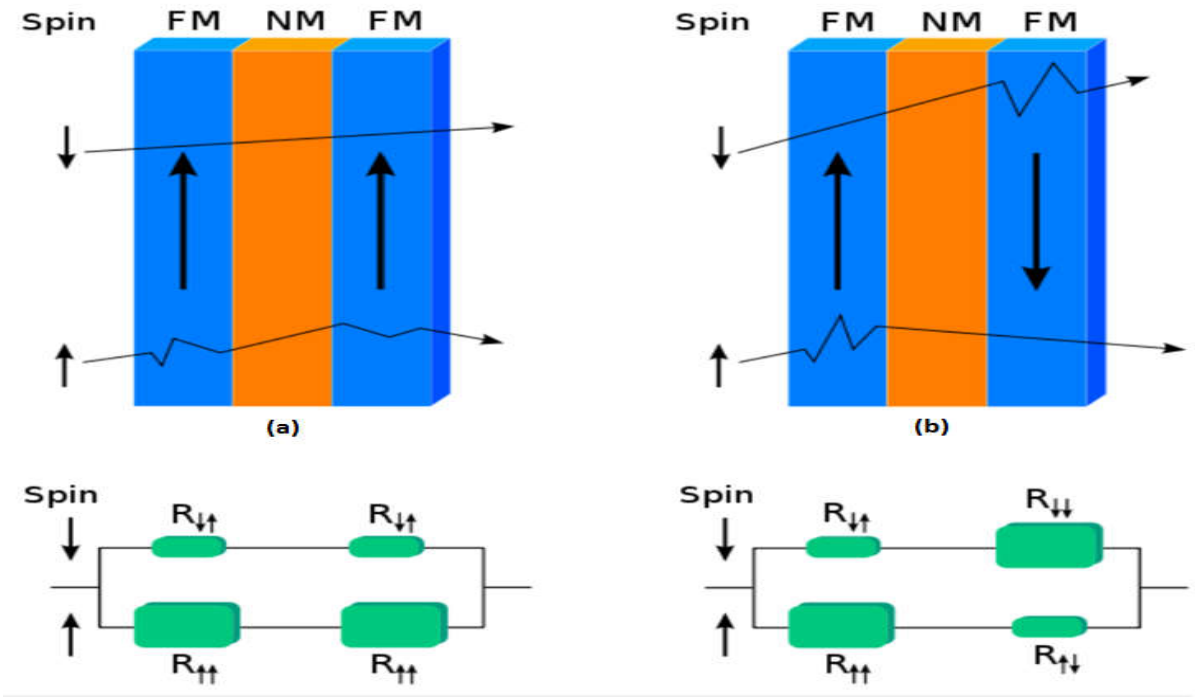

Figure I.1: Operating principle of Giant Magneto-Resistance. (a) parallel Magnetization and (b) antiparallel magnetization [3].

In this figure, we consider that a current is carried by two different channels, one is called up channel, and the other is called down channel. In a conventional semiconductor, the two channels are equivalent. But in a ferromagnetic semiconductor, there may be a difference between them, depending on the density of states in the Fermi level. Therefore, when the two layers have the same polarization, the conduction could be ensured by one of the channels. This behavior is called half-metallic, and it makes the material work as a spin valve, it allows to pass the spins of a privileged orientation and avoid the other spin orientation to pass.

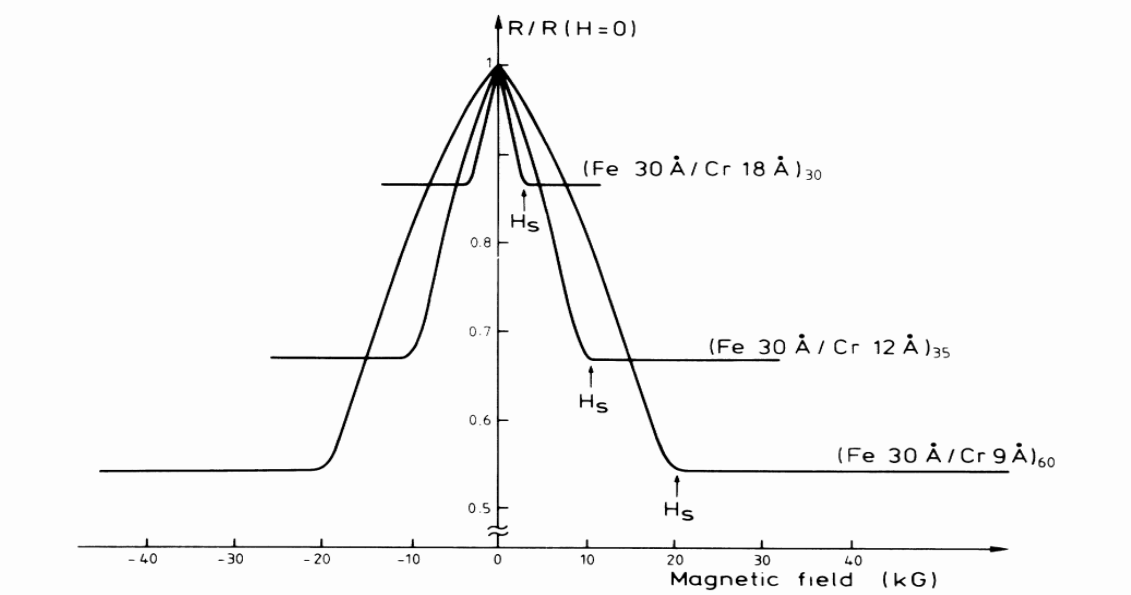

Figure I.2 The evolution of GMR resistance as a function of nonmagnetic chromium layer thickness.

At zero field, the opposite ferromagnetic layers have an anti-parallel magnetization. This stops any type of electrons from passing through, thus a high electrical resistance occurs.

When an external magnetic field is applied, respective magnetizations of the layers become aligned with the magnetic field orientation, this leads to a suddenly decreasing the resistance [1].

2.The Tunnel Magnetic Resistance (TMR)

A tunnel magnetic effect is similar to that of the giant magnetoresistance. This effect was examined in metal/insulator/metal tunnel junctions. Where each of the metallic electrodes is magnetic. Thus, a new significant variation of the junction resistance is observed when the relative directions of the magnetization of the ferromagnetic layers change. The relative estimation of tunnel magneto-resistance at room temperature is three times higher than the giant magnetoresistance. This makes it possible to predict the application of these structures as storage cells in non-volatile magnetic random access memories(MRAM). Storing the information in MRAM will no longer be based on the form of a charge in a capacitor, as the case of current DRAM or flash memories. However, the information will be stored as a magnetization in the magnetic tunnel junction. This principle makes it possible to maintain the type of magnetism more stable. Also, it preserves the three following aspects that are,

the speed of SRAM, the density of DRAM and the non-volatile character of Flash memories. In 1975, the first experiments on spin-dependent tunnel transport were realized by Tedrow et al, and Jullière [4;5] showed the magnetoresistance tunnel effect in a Fe / GeOx / Co trilayer, at low temperature. However, the rise in temperature or the application of a low voltage, lead to the attenuation of this magnetoresistive effect. Inspired by the work of its predecessors, Jullière developed a model based on two hypotheses to explain this TMR:

- The first hypothesis is that the spin of the electron is preserved during the tunnel transportation.
- The second is that the probability of the transmission of electrons through the barrier is proportional to the density of states at the Fermi level in the receiving electrode.

The number of electrons candidates to pass, in the emitting electrode, is proportional to the density of states at Fermi level. The current for each spin channel, is therefore proportional to the product of the density of states at Fermi level, for both electrodes.

The Figure I.3 is a schematic representation of the previous model. The density of states of the majority and minority spins(D↑, D↓) are represented by parabolas shifted into energy. This energy shift induces what Jullière defines as the polarization P of ferromagnetic materials:

$$P = \frac{D\uparrow - D\downarrow}{D\uparrow + D\downarrow} \quad \text{(I.1)}$$

In a parallel configuration of the magnetization of the two ferromagnetic materials, the density of states of majority spins is important at Fermi level, for both the emitter and receiver electrodes, respectively F1 and F2. Thus, the corresponding resistance r↑, is weak for this spin channel, whereas the density of states at Fermi level, is lower for the minority spins, in both electrodes. In this case, the tunnel resistance R↓ is important. Therefore, the current is mainly due to the majority spins channel. The total resistance of the magnetic tunnel junction in the parallel state is given by:

$$R\uparrow\uparrow = \frac{r\downarrow R\uparrow}{r\downarrow + R\uparrow} \quad \text{(I.2)}$$

In the configuration of antiparallel magnetization, the density of states at Fermi level is weak, either for the minority or the majority spins, in both emitter(F1) and receiver(F2) electrodes. Therefore, the conduction of the two channels is similar and lower than the case of the parallel configuration. Accordingly, the tunnel resistance of the electrons of majority spins R↑, as well as that of the minority spins R ↓ are averages. The total resistance of the magnetic tunnel junction, in this case, is given as:

$$R\uparrow\downarrow = \frac{R\downarrow R\uparrow}{R\downarrow + R\uparrow} \quad \text{(I.3)}$$

The weak value of the resistance r↑ makes the total resistance R↑↑ lower than R↑↓. Therefore, changing the magnetic configuration, from an antiparallel to a parallel state, leads to a variation in the electrical current flow through the tunnel barrier.

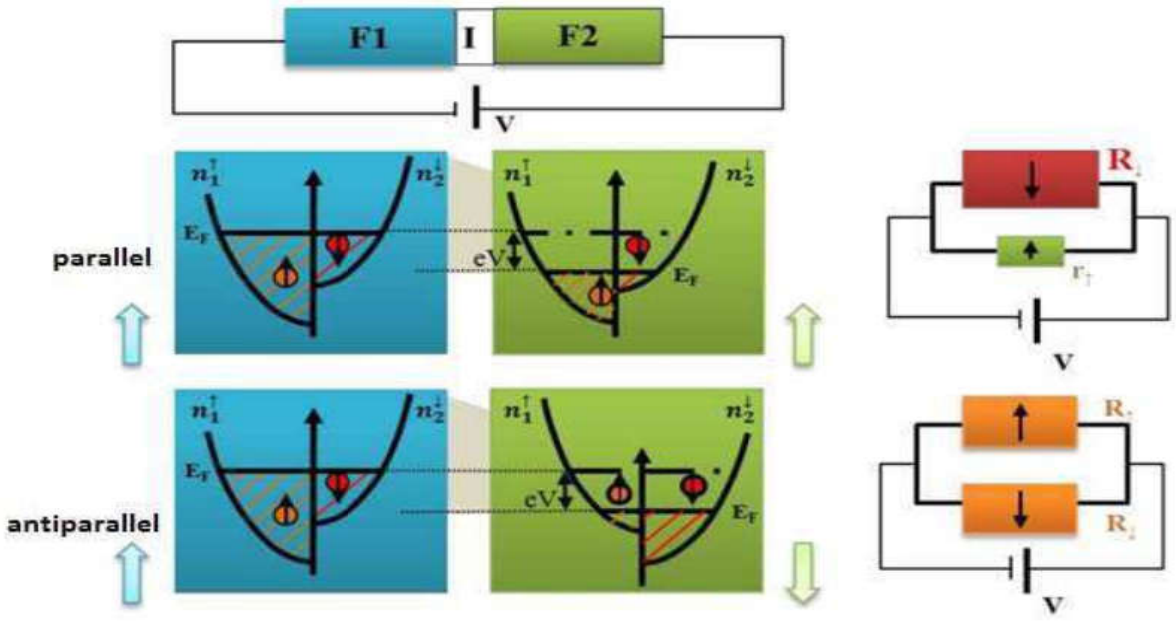

Figure I.3: Tunnel effect between two ferromagnetic layers F1 and F2 separated by an insulating barrier I [6].

Tunnel magnetoresistance (TMR), is defined as the relative variation of the system resistance, between its two extreme values:

$$TMR = \frac{R\uparrow\downarrow - R\uparrow\uparrow}{R\uparrow\uparrow} = \frac{2P1P2}{1-P1P2} \quad \text{(I.4)}$$

Where R↑↓ and R↑↑ have been already defined above as the MTJ total resistance, respectively in both antiparallel and parallel configuration. As After several attempts and experiments, in 1995, Moodera et al have observed a consistent TMR effect at room temperature.This effect was observed and measured at a junction of CoFe / Al2O3 / Co, or NiFe / Al2O3 / Co. The TMR value has reached about 11.8% at 295 K. As a future application of the TMR, is the MTJ junction, which is very small, and can be the basis of a new type of memories,where each junction can store a bit of data, "0" for the parallel configuration of the magnetization of the electrodes and "1" for the antiparallel configuration, see figure I.4 [7;8].

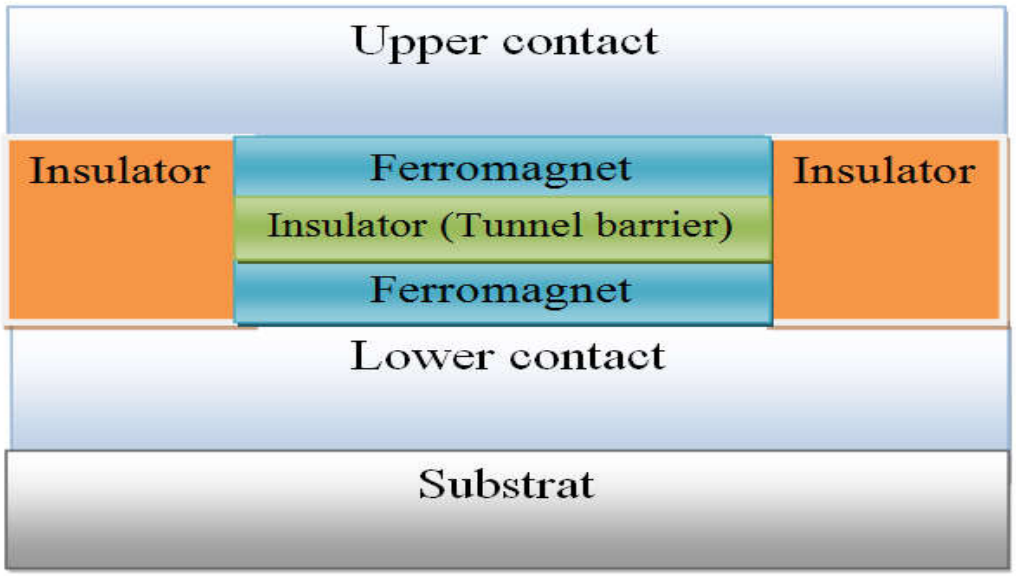

Figure I. 4: Schematic of a tunnel junction (MTJ)

3. Magnetic Random Access Memory (MRAM)

thanks to the MTJ junctions, the classical RAMs can be replaced by new memories based on TMR junction matrices.Therefore, data will no longer be stored as an electrical charge on a capacitor, but as a magnetization state (spin up or spin down) on MTJ junctions. The state "0" corresponds to the parallel configuration (low resistance) and the state "1" corresponds to the antiparallel configuration (high resistance). This storage method has the following advantages:

• the non-volatility of information, when there is no external power supply.

• the power consumption is theoretically lower since there is no heat dissipation caused by the mobility of charge carriers, and the resistance of the material to this movements.The

permanent intrinsic magnetism makes it a promising candidate for the next generation of memories, which can combine the speed of SRAM, the density of DRAM, as well as the non-volatility of Flash memories.

Figure I.5 illustrates the MRAM architecture, where magnetic tunnel junctions are connected in series with a selector transistor, a bit line, and a word line. A bit Writing is performed by closing the transistor and passing a current through the transistor bit line and a word line.The cross between those currents at the same location, which is the addressed location, create thus two orthogonal magnetic fields at the junction. These two fields are sufficient to change the orientation of the free layer. Each magnetic field taken independently does not allow the magnetization of the free layer to be reversed because the induced magnetic field at the intersection of the two currents must be greater than the coercive field of the free layer *[9]*.

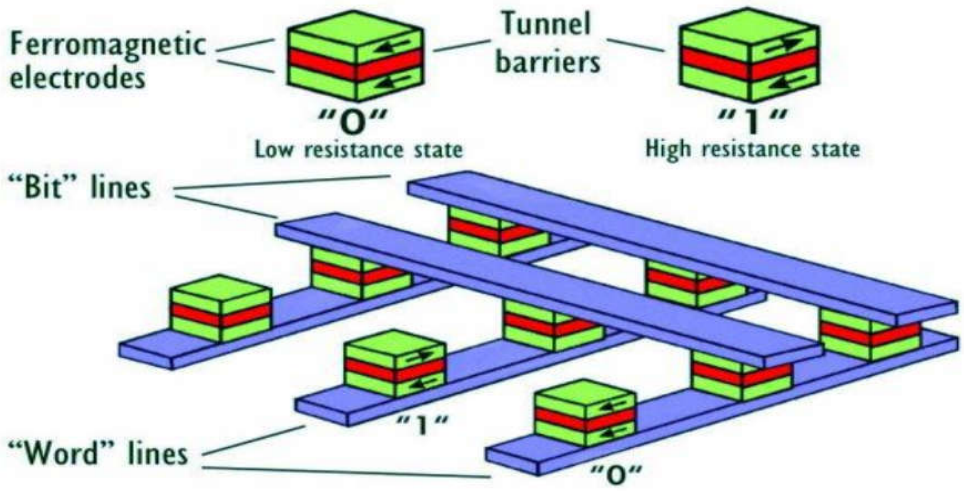

Figure I.5: Architecture of an MRAM memory consisting of a matrix of Magnetic tunnel junctions.

The principle of reading a bit digit is to pass a current through a word line and a bit line. Thus, the resistance value measured, corresponds to the state of a weak or high resistance, in other words, it corresponds to '0' or '1'. However, applying a voltage between two lines, a set of possible paths for current flowing through one or more magnetic tunnel junctions are superposed. To avoid this reading problem, a series of transistors had been added to each cell, in order to address each one individually during the reading.

4. Spin Field Effect Transistor(SPINFET)

The first device of a SpinFET has been proposed by Datta and Das [10]. In this device, the carriers are injected into the channel of a spin-polarized electrode (called a polarizer or source), which may be a ferromagnetic metal or a diluted magnetic semiconductor, connected via a channel with another spin-polarized electrode (called an analyzer or drain), see figure I.6. The current depends on the relative orientation of the spins of the electrons, as well as the moments of the magnetic source and drain. The current will be maximum when all the spins are aligned in the same direction. Various mechanisms have been proposed for manipulating the spin of the carriers in the semiconductor channel by a gate potential in a spin-FET, the application of a relatively low voltage causes an interaction between the electric field and the spins of carriers. Via the Rashba's spin-orbit interaction [11], and with this tension we can act on the polarization of the channel, which can allow us to control the flow of the current, this requires less energy compared to the case of controlling the electronic charge. The realization of such devices has encountered several difficulties, which is being understood. Thus, with a source and a ferromagnetic metal drain, it is now accepted that the current injected into the semiconductor is spin-polarized only if the source and the drain are interposed and the semiconductor of the spin-dependent interface resistors is sufficiently high. This holds even for a strongly spin-polarized conduction in the metal electrodes. Tunnel junctions seem to be the best suited to fulfill this role. But it is not enough to inject a spin-polarized current into the semiconductor channel, it is also necessary to retain the polarization in this channel in order to obtain a strong current difference between the two magnetic configurations. In the antiparallel configuration of the magnetizations, the carriers of a certain direction of spin are preferentially injected but difficult to be ejected, thus they are accumulated in the semiconductor. This blocking decreases the current compared to the parallel configuration, where the selected injected spins are also the same to be ejected. From a practical application point of view, an important parameter should have the electronic device, is to find a ferromagnetic semiconductor operating at room temperature. Great efforts have been made to observe the effect of the spin valve, with semiconductors as an intermediate layer [12;13]. A good candidate semiconductor, could be ferromagnetic at room temperature and present a half-metallic behavior, which means that it has a 100% of spin polarization.

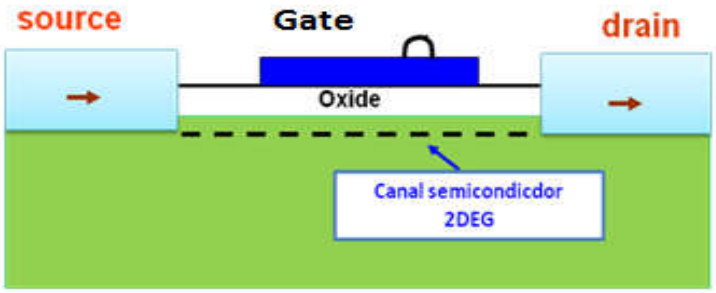

Figure I.6: schematic illustrating the SpinFET consisting of a semiconductor channel between the ferromagnetic source and drain

III. The difficulty of spin injection

For decades ago, optical pumping was the well-known method to generate an imbalance between the population of minority and majority spin carriers in a semiconductor, G. Lampel has obtained very convincing results in the case of silicon [14]. However, optical injection has met with a fundamental obstacle to create effective industrial devices. To avoid this problem, it is, therefore, necessary to use an electric injection, that is to say, to use a material in which the current is highly polarized (half metal type), and to inject this current into a semiconductor. Indeed, the known materials having this type of property which are in general the transition metal alloys, are all conductors. The major limitation, in this case, is the quality of the interfaces and the disagreement of the electronic structures between the ferromagnetic electrode and the insulating barrier.

The use of ferromagnetic semiconductors enables an epitaxy of the electrode on the semiconductor, therefore a dual competence, both a polarization and a solution for spin injection by allowing the use of the semiconductor as electrode and barrier. The problem that remains is to find a magnetic semiconductor whose Curie temperature is sufficiently high to make it useful and practical under normal temperature conditions. This problem has been particularly intense research in the last decade. in this work, our main research objective is oriented in this direction.

IV. Diluted magnetic semiconductors (DMS)

1. Definition and types

To create new, and more efficient spintronic components, we need to find a type of semiconductors which will replace the silicon. This new material should combine both the semiconducting and the magnetic properties. This, in order to serve as a base of the spintronic applications. Therefore, the research has led to the discovery of the new diluted magnetic semiconductors (DMS). Those compounds, are based on classical semiconductors, with a low doping with magnetic atoms. After substituting a part of the host material's cations with magnetic impurities, which are in general transition metals(TM). The resulted alloy is called then, a diluted magnetic semiconductor(DMS). To give some examples, we name following compounds:

CdTe, doped with Mn, Fe, Cr...

ZnSe doped with Mn, V, Co...

GaAs doped with Cr, Mn, Ti...

The following figure illustrates the difference between a magnetic semiconductor(MS), a nonmagnetic semiconductor (NMS), and a diluted magnetic semiconductor (DMS) [15]:

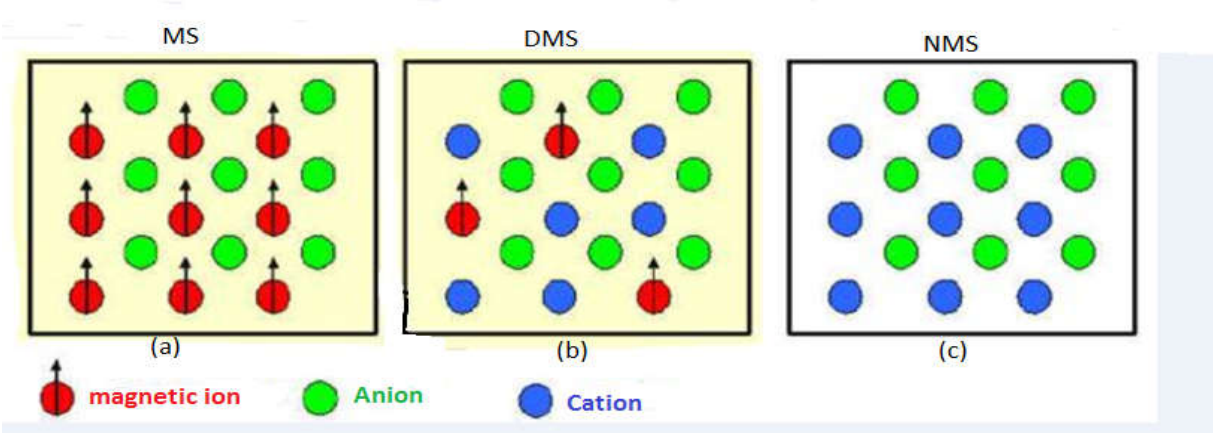

Figure I.7: Different types of semiconductors

The figure above illustrates the difference between the three types of semiconductor alloys, which we define as follows:

- (a): a magnetic semiconductor, which is composed of magnetic atoms(red balls), and nonmagnetic elements(green balls). In this type of material, a lot of magnetic impurities are introduced into the host compound. Therefore, the magnetic atoms are

arranged in a periodic lattice, forming a defined crystalline structure with the other type of atoms(figure I.7.a). The most known of this type is the chalcogenides, such as (CdCr2Se4, FeCr2S4, EuO)[16-19].The integration of these materials on microelectronics is very limited, due to their crystalline structure, which is too different from the classical semiconductors(Si, GaAs).

- (b): in this case, the semiconductor is completely composed of nonmagnetic atoms, such as the classical semiconductors(GaAs, ZnO, Si).

- (c): DMS, is a diluted magnetic semiconductor, in which a part of nonmagnetic atoms of a nonmagnetic semiconductor, are substituted by magnetic atoms. We distinguish several types of DMSs(figure I.7.c), the main of them are named as follows:

- -Type III-V, such as GaTMAs, GaTMN, InMnAs (where TM: Transition Metals).
- -Type IV, based on Si or Ge, doped with TM such as Mn, Fe, Cr.
- -Type IV-IV, as Pb1-x-ySnxMnyTe.
- -Type II-VI, such as CdTMTe,ZnTMSe,ZnTMO.

2. DMS crystal growth techniques

For the crystal growth and doping of a semiconductor, there are several interesting methods which can be useful in this process. Among the DMSs elaboration methods, we can name the following examples:

-The implant method, which consists of bombarding the substrate of the host semiconductor with ionized magnetic atoms, with controlled kinetic energy. This method allows controlling the phase obtained after the implant of impurities, which is similar to the phase before implanting the selected concentration of magnetic elements.However, the way of bombarding to insert the magnetic atoms may generate an amount of structural defects, which could affect the quality of the compound and as well as the properties.

-The chemical vapor deposition (CVD), this method uses the chemical processing to bring the targeted elements to the surface of the substrate, in order to produce high quality and efficient thin films. in typical CVD, the wafer (substrate) is exposed to one or more volatile precursors,

which react on the substrate surface, to produce the desired deposit. During this process, some volatile by-products could be produced, but they are removed by gas flow through the reaction chamber. This method is widely used in the microfabrication processes to deposit materials in various forms, such as monocrystalline, polycrystalline, amorphous, and epitaxial. These materials include as examples the silicon SiO2, germanium, carbide, nitride, oxynitride, carbon nanotubes, diamond, and graphene.

-The molecular beam epitaxy(MBE), which takes place in a high vacuum or high ultra vacuum. the most important aspect of this method is the slow rare of disposition, in order to produce high-quality thin films. MBE method allows to control the processes of the compound growth, by controlling and acting on the following parameters:

- The flow of each chemical element, which control the relative concentration of doping an impurity in the host material.
- The flow rate of atoms, which controls and determines the speed of the growth. Therefore, the quality of the obtained material.
- The substrate heating, which is controlled by the processes of impurities diffusion, nucleation, until the thin layer formation.
- The properties of the host substrate, which include (the cell lattice, lattice parameter, the surface shape...)[20].

The following figure illustrates the processes of crystal growth by MBE method :

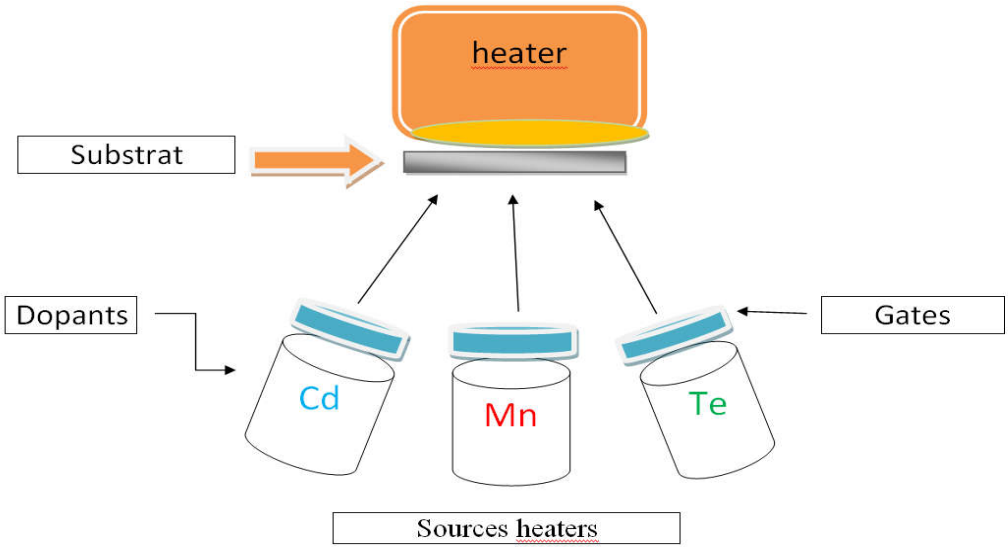

Figure I .8: Operating process of MBE method

3. Different types of DMSs

a. DMS based on IV semiconductors :

This type includes the classical semiconductors, such as Si and Germanium, which are the most used in classical microelectronic, as electronic circuits. Silicon doped with different transition metals such as Fe, Ni or Mn, has shown a ferromagnetic behavior induced by the magnetic atoms [21]hshown a magnetic. The same for Germanium when doping with Mn or Cr atoms [22;23].

b. DMS based on II-VI semiconductors :

This type of DMS has a high density of carriers, which strengthen the ferromagnetic interactions than the antiferromagnetic ones. This type of materials has a high solubility, which goes towards 77% for Mn impurities[24;25]. The control of the ferromagnetic phase in this materials was revealed in Pb1-x-ySnxMnyTe since 1986 [26]

c. DMS based on III-V semiconductors :

A lot of works were focused on III-V semiconductors, such as (Ga, Mn)As [27]. In addition, the first tested DMS was the thin film of InAs(Indium Arsenide) doped with Mn atoms, for which was declared that there is a homogeneous ferromagnetic phase for In1-xMnxAs [28].

4. Advantages of DMSs based on III-V and II-VI semiconductors

DMSs based on group III-V and II-VI semiconductors have many advantages to be used in spintronic applications, for example, we name the following:

- compatibility with the existing devices.

- long life carriers(up to 100 ns)
- high efficiency in polarization and spin injection.
- adjustment of the gap, the lattice parameter. In addition to the presence of the ferromagnetic behaviour at room temperature.
- at the same time, the II-VI has an advantage of high solubility to host doping impurities, comparing to III-V semiconductor.

5. CdTe semiconductor

The CdTe compound is found to be stable in the Zinc-Blende structure, with the following parameters:

Cd(48) (0;0;0), Te(52) (1/4;1/4;1/4). The lattice parameters are a=6.48A° and α=β=γ= 90o [29]. This material is an n-type semiconductor, with a band gap Eg=1.45 eV[30]. In addition, The European Photovoltaic Industry Association has reported that photovoltaic energy has the potential to contribute up to 13% to the global electricity supply by 2040. A part of that energy supply will come from thin film technology, such as CdTe solar cells, which are the low-cost available in the market of photovoltaic cells. Furthermore, CdTe-PV can be considered as the market leader with about 5% of the annual production. However, there are two major concerns about CdTe Cells, which are the potential negative environmental impacts of cadmium contamination from CdTe-PV; and the possible shortage of the metal tellurium in the future. Because of these concerns, the recycling of production scrap and end-of-life PV modules is essential. Fortunately, the possibility of recycling the scrap and the end-of-life modules could solve this problem, Also the cadmium in CdTe is not toxic as the case of cadmium batteries or other components[31;32].

The following figure illustrates the Zinc blende structure of CdTe, with an example of substituting a part of Cd atoms by Mn atoms :

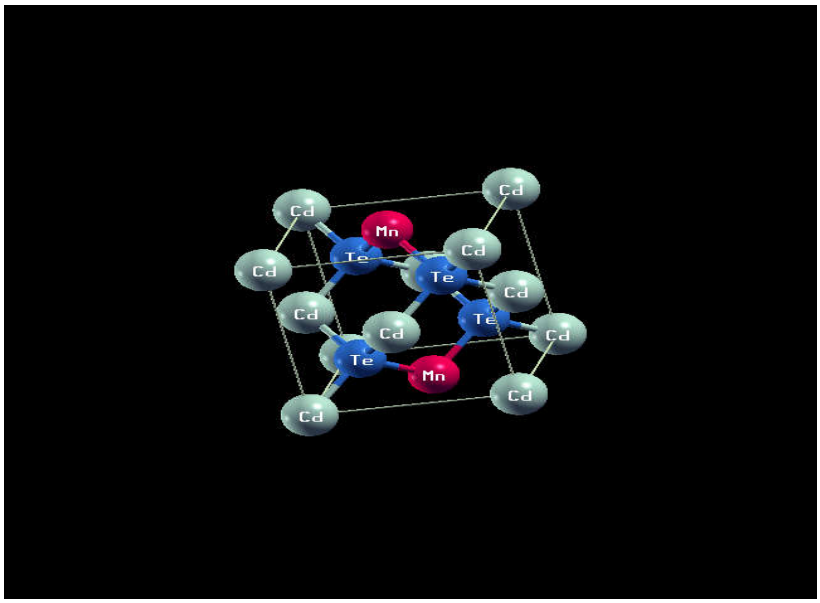

Figure I.9: The unit cell of CdTe, Cd atoms (green-grey); magnetic impurity Mn (magenta) ; Te atoms (blue).

6. ZnSe semiconductor

ZnSe is a wide-bandgap classical semiconductor of the II-VI group. This alloy, doped with chromium atoms (ZnSe: Cr) has been used as an infrared laser gain medium emitting at about 2.4 µm[33]. Furthermore, It is used as an infrared optical material with a remarkably wide transmission wavelength range (0.45 µm to 21.5µm). Thus, ZnSe is considered as a semiconductor that is optically active in the visible region, with a potential use in thin film devices, especially in optoelectronic devices such as light emitters (blue laser diodes), photodetectors and photovoltaic devices. This, due to its direct and wide-bandgap Eg=2.7 eV [34]. In our work, we studied the zinc blende structure of this material, in order to study its magnetic properties.

The unit cell of ZnSe is similar to that of CdTe described above. The only difference is the parameter lattice and the type of atoms. The following figure shows the unit cell structure of ZnSe :

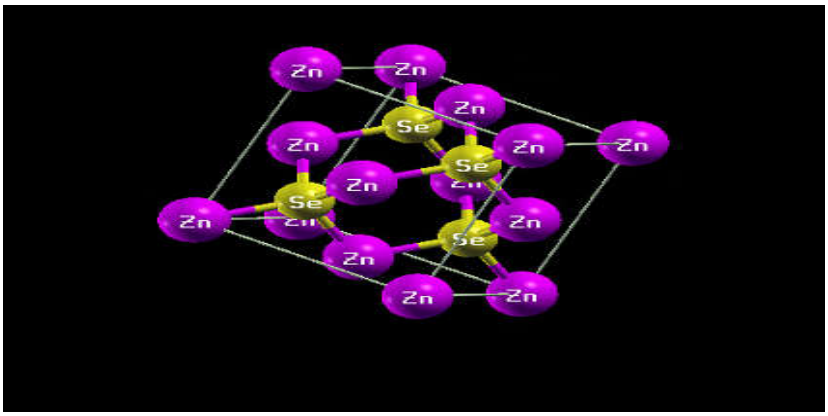

Figure I.10: The unit cell of ZnSe, Zn atoms (magenta); Se atoms (yellow).

V. Faraday rotation (Magneto-Optical effect)

The interaction of light with the matter affects the electronic structure of the matter. This means when a polarized incident light passes through a medium which presents a magnetic state, this magnetism affects the polarization of the emerged light. This gives rise to the magneto-optical effects, such as the Faraday rotation or Kerr effect.The first magneto-optic (MO) effect was observed in 1845 by Michael Faraday. He found that a linearly polarized light is rotated after passing parallel to a magnetic medium induced in a glass rod with polished faces. The following figure illustrates that experiment[35]:

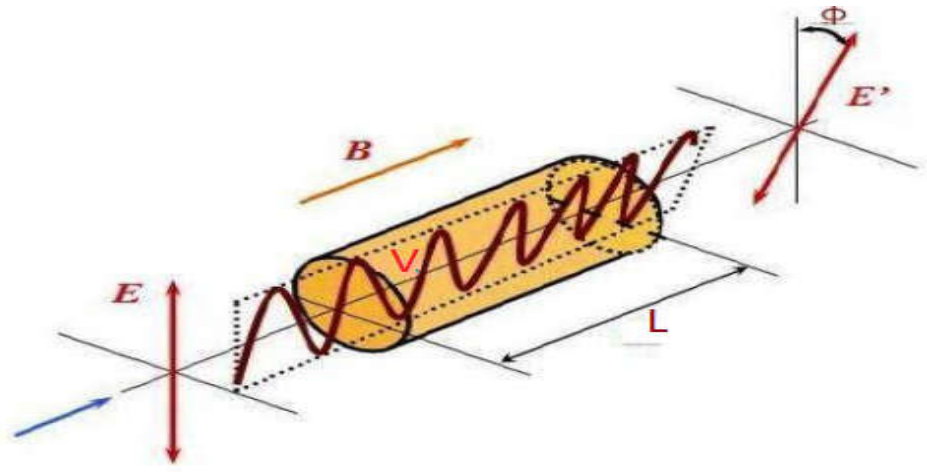

Figure I.11: Faraday effect illustration, where B is the magnetic field direction and Φ is the Faraday angle.

The azimuth rotation is found to be linearly proportional to the applied magnetic field B, as well as the length of the glass rod L, in addition to the Verdet constant V. The following equation expresses this relationship:

$$\boldsymbol{\Phi} = \mathrm{B.L.V} \qquad \text{(I.5)}$$

Where V is called verdet's constant and it's wavelength dependent [36].

This previous rotation, which expresses the Faraday effect, is called Faraday rotation. And this notation which we will use to name this effect so far in this manuscript. Magneto-optical effects have a lot of applications, we name some as follows[36]:

-determination of the average free carrier effective mass.

- detection of magnetic impurities.

-dynamic studies of film growth.

- MO filters as atomic line filters.

- MO devices: MO memories, MO magnetic field

sensors, MO modulators, and integrated optoelectronic

devices, like optical circulators, isolators, and switches.

-Magneto-optical drives using thermomagnetic

recording and MO sensing of recording information, with a minimum of 50 years of shelf life;

- MO microscopy.

- Spintronics.

VI. Different exchange interactions in DMSs

The magnetism appearing in DMSs results from the coexistence of magnetic ions, and charge carriers in the same material. The localized magnetic ions can interact each other, or with the

delocalized charge carriers. These magnetic interactions are called exchange interactions, and they can manifest in different types, which we will describe in the following:

1. **Direct exchange**

the direct exchange interactions occur between the localized magnetic impurities, without any intermediate element. This type of interaction is called d-d interaction or coupling, because it occurs between d-bands of the magnetic atoms. The direct exchange Hamiltonian of the interacting spins S_i, S_j is described by the following equation:

$$H(d-d) = \sum_{i \neq j} j(Ri - Rj).Si.Sj \qquad (I.6)$$

Where, $j(Ri - Rj)$ represents the coupling between the spin moment $Si\ and\ Sj$, located in Ri, Rj sites.

2. **Indirect Exchange**

This type of exchange occurs between the magnetic ions, but in an indirect way, which means that magnetic elements interact via nonmagnetic element. The three types of indirect exchange interactions are as follows:

a. Double exchange

In this case, the interactions occur by exchanging an electron of the 3d band between magnetic ions(cations) via nonmagnetic anion. for example, in ZnO doped Mn, the double exchange is done by exchanging electrons between Mn ions, via oxygen ions, this to transport electrons between magnetic ions which are far from each other. The following figure illustrates this example:

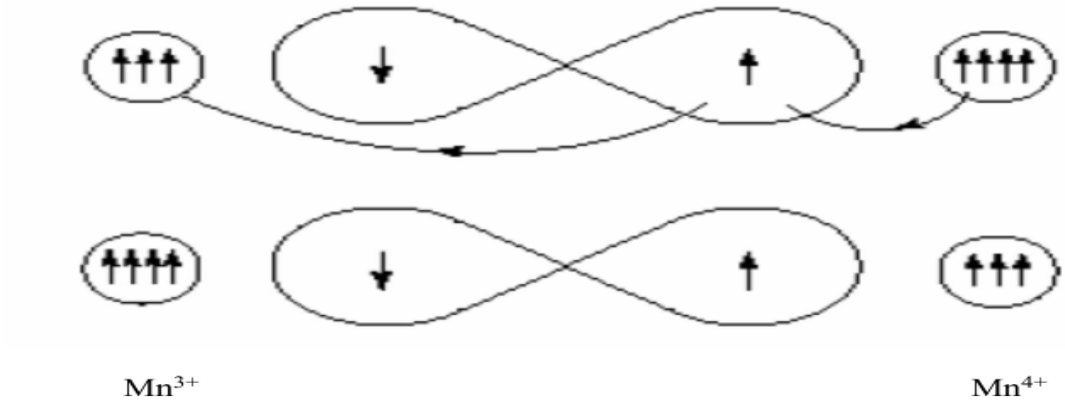

Figure I.12: a double exchange between Mn4+ and Mn 3+ via an oxygen ion.

In this case, when the electron of the nearest Mn ion jumps to the oxygen, simultaneously, an electron jumps from the oxygen to the other Mn ion. This exchange is not possible unless the two electrons have the same orientation of the spin. This phenomenon is known to occur in DMSs[37;38].

b. Super-exchange

The super-exchange is an indirect mechanism, where the interaction between the magnetic impurities is mediated by non-magnetic atoms. The antiferromagnetism by super-exchange interaction has been shown for crystals of LaMnO3 [39]. Goodenough et al. [40] formalized the super-exchange interaction, which resulted in the Goodenough-Kanamori rules. The Goodenough-Kanamori rule states that superexchange interactions are antiferromagnetic where the virtual electron transfer is between overlapping orbitals that are each half-filled, but these interactions are ferromagnetic where the virtual electron transfer is from a half-filled to an empty orbital, or from a filled to a half-filled orbital[41]. The figure above illustrates the phenomenon of super-exchange [42]:

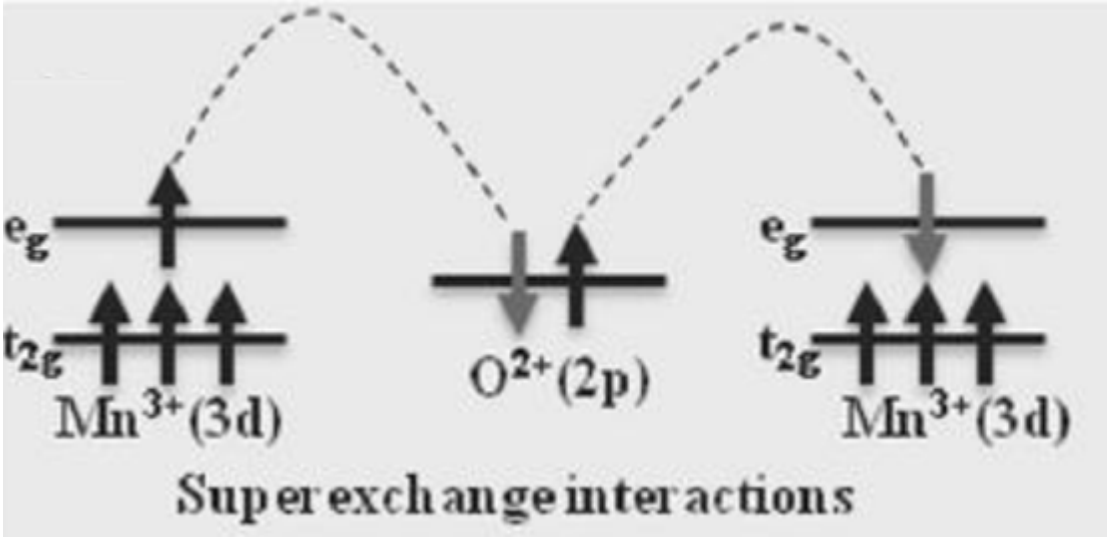

Figure I.13: super-exchange interaction between magnetic cations, via nonmagnetic anions.

c. RKKY interactions (Ruderman-Kittel-Kasuya-Yoshida)

The mechanism RKKY manifest as an indirect exchange interaction between magnetic ions, through intermediate charge carriers. The localized moments can lead to a ferromagnetic

direct exchange with electrons on the same site or can manifest as antiferromagnetic interaction, due to the hybridization between the local moments and electrons on neighboring sites. In the case of a weak coupling, this exchange is called RKKY coupling. Each two interacting magnetic ions a and b, are a function of coupling constant J, which depends on the distance between these ions, as well as the magnetic state, which may be ferromagnetic or antiferromagnetic. The J coupling is damped as a function of the distance between the interacting ions, See Figure I.14.

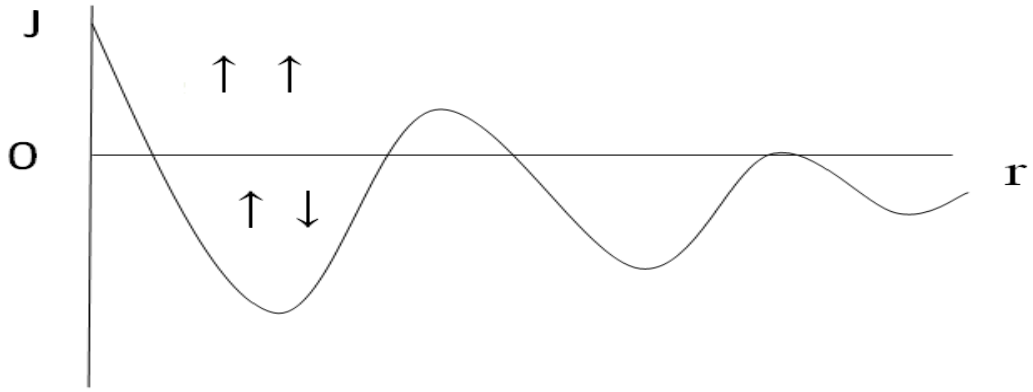

Figure I.14: RKKY exchange interactions, where J is the coupling coefficient

This kind of interaction is described by the following equation:

$$H_{ex} \sum_{ij} J \frac{2kf.\delta.\cos(2Kf.\delta) - \sin(2Kf.\delta)}{(2Kf.\delta)^4} \overrightarrow{Si} . \overrightarrow{Sj} \qquad (I.7)$$

Where Kf is the Fermi radius of an electron gas, this effect is dominant for metals where there is non-overlap between the neighboring orbitals of the magnetic ions. Thus, the localized ions polarize the electrons spins around. This serves as a field which influences the polarization of neighboring localized ions, in an oscillating manner. the exchange becomes important when the number of electrons becomes larger. This model applied then, to explain the ferromagnetic/antiferromagnetic coupling between two thin layers of a ferromagnetic material separated by a thin layer of a non-magnetic one, giving rise to a ferromagnetic or antiferromagnetic coupling between two layers according to the thickness of the non-magnetic layer [42;46].

Chapter II :
Ab-initio calculation method

Chapter II :
Ab-initio calculation method

I. Density Functional Theory

I.1 Introduction

Computational physics is getting widely used to study the properties of the materials, besides to the experimental works. These theoretical calculations have many methods of modeling, such as ab initio, Monte Carlo, Mean Field Theory, and so on. The aim of these methods is to resolve the Schrödinger equation for N electrons, in order to investigate their behavior, which allows characterizing the material. This complex equation couldn't be resolved with N electrons, that's why many searchers proposed some approximations such as density functional theory (DFT) to simplify the calculations. In this work, we have focused on bulk materials, with the finite crystal structure. Therefore, studying the properties of atoms, molecules, or solids, has become reachable for theoretical physicists, based on the basic tool which is the simplified Schrödinger equation. The time-independent Schrödinger equation has the following formula:

$$\hat{H}\psi = E\psi \qquad \text{(II.1)}$$

All the electrons of each studied system are interacting with each other, under Colombian forces. Thus, only in a few cases, which has been proven to quite exactly solve the problem with one nucleus and one electron, such as the hydrogen atom. however, a solid system is described by a many-electron wave function ψ (x_1,x_2,x_3, ...,x_N) which becomes very complicated, where x_i gives the position and the spin of the i-th particle. This would require a solution of a Schrödinger equation with too many simultaneous differential equations. because of the complexities of the use of these techniques, such as ab initio, then comes the use of different approximations to facilitate the process. In the following, we will describe and give a detailed information about the density functional theory as well as the approximations. In addition, we will provide a definition about the exchange-correlation approximations. Furthermore, a description of the used codes will be given later in this chapter.

I .2 Schrödinger equation for many-body problem

The matter in the solid state is formed on the basis of a successive and compact patterns consist of a primitive unit cell containing atoms and repeated periodically all over the space. The theory we are going to present is applied to any kind of solid, such as semiconductors or metals. To explain more, we take a quantum system which contains N_0 nuclei, and N electron. These particles are interacting one with each other. R_k and r_i refer to the position of the nuclei and the electrons, respectively. This system can be characterized by a wave function, which results from solving the Schrödinger equation (II.1).

Where ψ is the eigenfunction and $\widehat{H}$ is the Hamiltonian of the system. The distance between the i-th electron and k-th nucleus is $r_{ik} = | r_i - R_k |$. The distance between i-th and j-th electron is $r_{ij} = | r_i - r_j |$, where $R_{kk'} = | R_k - R_{k'} |$ is the distance between the k-th nucleus and k'-th nucleus. Thus, the Hamiltonian of the system can be written as follows:

$$\widehat{H} = T_{core} + V_{core\text{-}core} + T_e + V_{e\text{-}e} + V_{core\text{-}e} \qquad (II.2)$$

Where :

$T_{core} = -\sum_{k=1}^{N0} \frac{1}{2M_k} \Delta R_k$, is the operator related to the kinetic energy of the nuclei .

$V_{core\text{-}core} = \sum_{k<k'} \frac{Z_k Z_{k'}}{R_{kk'}}$, is the operator related to the interaction energy between the nuclei.

$T_e = -\sum_{i=1}^{N} \frac{\mathbf{1}}{\mathbf{2}} \Delta_{\boldsymbol{ri}}$, is the operator related to the kinetic energy of the electrons.

$V_{e\text{-}e} = \sum_{i<j} \frac{1}{r_{ij}}$, the operator related to the interaction energy between electrons.

$V_{core\text{-}e} = -\sum_{i,k} \frac{Z_k}{r_{ik}}$, is the operator related to the interaction energy between the nuclei and the electrons.

This leads to write the theprevious equation as follows:

$$\widehat{H} = -\sum_{k=1}^{N0} \frac{1}{2M_k} \Delta R_k + \sum_{k<k'} \frac{Z_k Z_{k'}}{R_{kk'}} - \sum_{i=1}^{N} \frac{\mathbf{1}}{\mathbf{2}} \Delta_{\boldsymbol{ri}} + \sum_{i<j} \frac{1}{r_{ij}} - \sum_{i,k} \frac{Z_k}{r_{ik}} \qquad (II.3)$$

With N_0 is the total number of nuclei in the system, and N is the total number of electrons.

The parameters k and k', refers as indexes of the nuclei. Where i and j, refers the electrons.

r_i is the position of the electron i, and R_k is the position of the nucleus k, where Z_k is the charge of the nucleus k.

I.2.1 Born-Oppenheimer approximation

The Born-Oppenheimer approximation [48] plays an important role in the electronic structure calculations. The main of this approximation is that the mass of the nuclei are much heavier then those of electrons, as an overview, if we consider just one proton of the nuclei, we found that its mass is about 3000 times higher that of the electron. Therefore, the mobility of the nuclei is too slowly than that of the electrons. As an approximation, we can consider the electrons moving in a field produced by a fixed nuclei, which allow separating between the motion of electrons and nuclei. with the Born-Oppenheimer approximation, the first and the second terms in the equation (II.3) are neglected, where the last term of the repulsion between nuclei, can be treated as a constant for a fixed configuration of the nuclei. Then, the simplified Hamiltonian is called electronic Hamiltonian $\widehat{H}_{elec}$:

$$\widehat{H}_{elec} = T_e + V_{e\text{-}e} + V_{core\text{-}e} \qquad (II.4)$$

With this approximation, the Schrodinger equation (II.1) with the electronic Hamiltonian becomes :

$$\widehat{H}_{elec}\psi_{elec} = E_{elec}\psi_{elec} \qquad (II.5)$$

Where $\psi_{elec} = \psi_{elec}(r_i, R_k)$ (II.6)

I.3 Hartree approximation

the other approximation to solve the equation (II.6) is the Hartree method, which was introduced to solve the complexity caused by the electron-electron interactions. It aims to consider electrons as being independent. Thus, each one of them is considered to be evolving

in a field created by the surrounding electrons. Then, the total wave function of this system can be written as a product of N wave functions of N electrons in the following form:

$$\psi_{elec}(r_i, R_k) = \prod_{i=1}^{N} \psi_{elec}(r_i) \qquad (II.7)$$

Considering the previous equation, it was found the Pauli principle was not respected. Thus, the other approximation which is the Hartree-Fock was introduced, based on the Slater determinant. This determinant, include the aspect of indiscernibility of electrons. Therefore, the proposed solution is to write the wave function of N electrons taking into account the indiscernibility aspect of the electrons [49;50]. As a result, each electron is now undergoing an external field created by the nuclei, in addition to the field created by the other electrons of the system. The later is called Hartree potential.

The HF approximation is then a basis of several methods studying the properties of the crystal structure. It is found that this method is widely used in quantum chemistry dealing with molecules, but less accurate for studying solids with a high number of electrons. Thus, more sophisticated methods are required. To this purpose, the density functional theory was introduced.

I.4 Density Functional Theory

Nowadays, the calculations of materials properties, based on DFT have become a very active field of research. The basic idea of DFT is to use the charge density of the electron ρ(r) instead of the many-electron wave function, used in Hartree–Fock theory. Recently, DFT has become the most widely used method to deal with electronic structure approach. In condensed matter physics, this approximation has provided the framework for fast and efficient calculations of a crystal structure properties. The first form of DFT was proposed by Thomas [51] and Fermi [52] in 1927, but this formula was largely overlooked due to serious deficiencies in their approximations. In 1964 Hohenberg and Kohn [53] introduced the proofs for their two theorems which demonstrate the fundamental importance of the electronic density, and in 1965 Kohn and Sham [54] improved this theory to push it to give more realistic calculations.

I.4.1 The Hohenberg and Kohn Theorems

The density functional theory(DFT) described above, was firstly established by Hohenberg and Kohn. As said before, these authors have proved that the density of electrons ρ(r) is used to determine all the aspects of the electronic structure, instead of the electron wave function. Therefore, their theorems have become the basis of the density functional theory. This finding led them to win the Chemistry Noble prize in 1998, thanks to its strong contribution in computing the electronic structure of solids. First, they proved that the total energy of a gas of electrons, in the presence of an external potential is reduced to a unique function of electronic density:

$$E = E(\rho) \qquad \text{(II.8)}$$

After that, they proved that the energy of the ground state is exactly the minimum value of this function. Moreover, the other properties of the ground state are functional of this density:

$$E(\rho) = E(\rho_0) \qquad \text{(II.9)}$$

with ρ_0 is the electronic density of the ground state

The functional of the total energy of the ground state is then :

$$E[\rho(r)] = F[\rho(r)] + \int \hat{V}_{ext}(r)\, \rho(r) d^3r \qquad \text{(II.10)}$$

Where $F[\rho(r)] = \langle \psi | T+V | \psi \rangle$ (II.11)

The functional F[ρ] is common for any system with N electrons. Thus, when this function is known, one can easily determine the total energy as well as the electronic density of the ground state, for a given external potential. However, this theorem doesn't provide any information about the form of the density F[ρ] [55;56].

I.4.2 The Kohn and Sham equations

For further simplification of DFT theory, Kohn and Sham have proposed to write the electron density as the sum of the densities of free electrons, and they used the variational principle to obtain the energy of the ground state, as well as the density that gives the functional $E_{xc}[\rho]$. Therefore, the energy functional $E_{ext}[\rho]$ is given in the following formula [57]:

$$E_{ext}[\rho] = T_0[\rho] + V_H[\rho] + V_{xc}[\rho] + V_{ext}[\rho] \qquad \text{(II.12)}$$

Where:

$T_0[\rho]$: represents the kinetic energy of the system.

$V_H[\rho]$: Hartree term (classical Coulomb interaction between electrons)

$V_{xc}[\rho]$: represents the exchange-correlation energy.

$V_{ext}[\rho]$: includes the Colombian interactions of the electrons with the nuclei and those of the nuclei between each other.

Where $V_H[\rho]=\frac{e^2}{2}\int d^3r\, d^3r' \frac{\rho(\vec{r})\rho(\vec{r'})}{|\vec{r}-\vec{r'}|}$ (II.13)

These terms are the most important in the treatment of the electrons interactions. The difference between the real interaction energy and that of Hartree, have been taken into consideration in the exchange-correlation energy $V_{xc}[\rho]$

The Kohn Sham (KS) equations are:

$$\left[\frac{-\hbar^2}{2m_e}\overrightarrow{\nabla_i^2} + \frac{e^2}{4\pi\varepsilon_0}\int\frac{\rho(\vec{r})}{|\vec{r}-\vec{r'}|}\,dr + \hat{V}_{xc} + \hat{V}_{ext}\right]|\Phi_i> = \varepsilon_i|\Phi_i> \;;\; i=1,\ldots, N \qquad (II.14)$$

While the exchange-correlation potential is given by the derivative function as follows :

$$\hat{V}_{xc} = \frac{\partial V_{xc}[\rho(r)]}{\partial\rho(r)} \qquad (II.15)$$

and the density of the ground state is given by the sum of the occupied orbitals, then:

$$\rho(\vec{r}) = \sum_{i=1}^{N}\Phi_i(\vec{r})^*\,\Phi_i(\vec{r}) \qquad (II.16)$$

To determine the functional state of the system requires to solve the set of equations(II.14), called Kohn and Sham equations, in a self-consistent way. The sum of three terms (V_H+V_{xc}+V_{ext}) forms an effective potential V_{eff} that may be qualified as a local potential, because it depends only on r. This method is formally accurate but for the practical calculation, the exchange and correlation which is a density functional needs to introduce some approximations.

I.4.3 The exchange-correlation functional

In the Kohn-Sham Hamiltonian expression, we need to know the form of the exchange-correlation energy functional, in order to make DFT and the Kohn-sham equations useful in the practice. That's why, it is necessary to suggest a formulation of the exchange-correlation

energy, which represents the smallest contribution of energy. To do so, one has to go through different approximations for this purpose. It is essential to have an accurate exchange energy functional or potential, in order to give a satisfactory description of a realistic condensed-matter system. for this reason, It is necessary to approximate it, and there are many different options available to use, such as the forthcoming examples.

The simplest approximation is the local density approximation (LDA) which is the most widely used in applied density functional theory. It is based on the homogeneous electron gas model (HEG), which has the same electron density at the point. Afterwards, comes the local spin density approximation approach (LSDA) which is an LDA model taking into account the spin aspect, then generalized gradient approximation (GGA) where the exchange-correlation energy depends on the density besides to its derivatives. Also, there are many others such as the hybrid functional, and mBJ which we will introduce later.

I.4.4 The Local Density Approximation

The local density approximation (LDA) is based on the homogeneous electron gas model (HEG). This approach is considered to be the simplest one to express the exchange-correlation energy.

This method consists of treating the inhomogeneous system as being locally homogeneous, so the terms of the exchange-correlation depend only on the local value of ρ(r).

$$E_{xc}^{LDA}[\rho] = \int \rho(\mathrm{r})\, \varepsilon_{xc}(\rho)\mathrm{dr} \qquad \text{(II.17)}$$

With $\varepsilon_{xc}(\rho)$ represents the exchange-correlation energy per particle of a homogeneous electron gas (HEG) of charge density ρ. The exchange-correlation energy is decomposed into exchange and correlation terms linearly :

$$E_{xc}=E_x+E_c \qquad \text{(II.18)}$$

I.4.5 The local spin density approximation (LSDA)

LSDA approximation comes to improve the LDA in order to treat the magnetic systems that need to include the spin aspect as an improvement of the LDA. LSDA introduces the spin effect in the calculation of the term of exchange-correlation, where the exchange and

correlation energy is a function of two densities which are the spin-up and spin-down densities:

$$E_{xc}^{LSDA}[\rho_\uparrow, \rho_\downarrow] = \int \rho(\mathrm{r})\, \varepsilon_{xc}(\rho_\uparrow, \rho_\downarrow)\mathrm{dr} \qquad \text{(II.19)}$$

The analytical expression of the exchange energy of $(\rho_\uparrow, \rho_\downarrow)$ can be obtained from the Hartree-Fock approximation. The calculation of the correlation energy of $(\rho_\uparrow, \rho_\downarrow)$ is based on the results of Monte Carlo for the homogeneous electrons gas (HEG) [58;59].

I.4.6 The Generalized Gradient Approximation (GGA)

The GGA approximation is usually used when LDA doesn't give reliable results, or when these results are far from the experimental finding. Most of the corrections that have been introduced to the LDA take into account the local variations in the density.

In the approximation GGA, the exchange-correlation energy is given as a function of the electronic density besides to its gradient:

$$E_{xc}^{GGA}[\rho_\uparrow, \rho_\downarrow] = \int \rho(\mathrm{r})\, \varepsilon_{xc}\left(\rho_\uparrow, \rho_\downarrow, \vec{\nabla}_{\rho_\uparrow}, \vec{\nabla}_{\rho_\downarrow}\right)\mathrm{dr} \qquad \text{(II.20)}$$

$\varepsilon_{xc}\left(\rho_\uparrow, \rho_\downarrow, \vec{\nabla}_{\rho_\uparrow}, \vec{\nabla}_{\rho_\downarrow}\right)$ is the exchange-correlation function, which depends on the electronic density in addition to its gradient. The additional information in the local gradient has participated in improving the description of the studied systems. Several different parameters of GGA have been proposed and used in studying a wide range of materials. GGA was supposed to add a significant improvement to the properties of the ground state of atoms, molecules, and simple solids [60-62].

I.4.7 Resolving the Kohn Sham equations

The idea of Kohn and Sham has led to suggest a simplified kind of Schrödinger equation known as Kohm-Sham equations:

$$H\Phi_i = \left[-\frac{\nabla^2}{2m} + V_{ext} + V_H + V_{xc}\right]\Phi_i = \varepsilon_i \Phi_i \qquad \text{(II.21)}$$

Resolving these equations must be numerically computed pursuing an iterative process:

Firstly, we must choose a basis for the wave functions that should be taken as a linear combination of the orbitals. This later is called Kohn-Sham orbitals (KS):

$$\psi_j(\mathrm{k,r}) = \sum C_{ji}\Phi_i(k,r) \qquad \text{(II.22)}$$

$\Phi_i(k,r)$ are the basic functions, and C_{ji} the development coefficients. In order to solve the Kohn-Sham equations, we need to determine the coefficients C_{ji} for the occupied orbitals that minimize the total energy. As a simplification of the calculation process, we take in account the symmetry points in the first Brillouin zone for Solving KS equations. There are many other possibilities and approximations that are used to solve the Schrödinger equation as it is shown in the following figure:

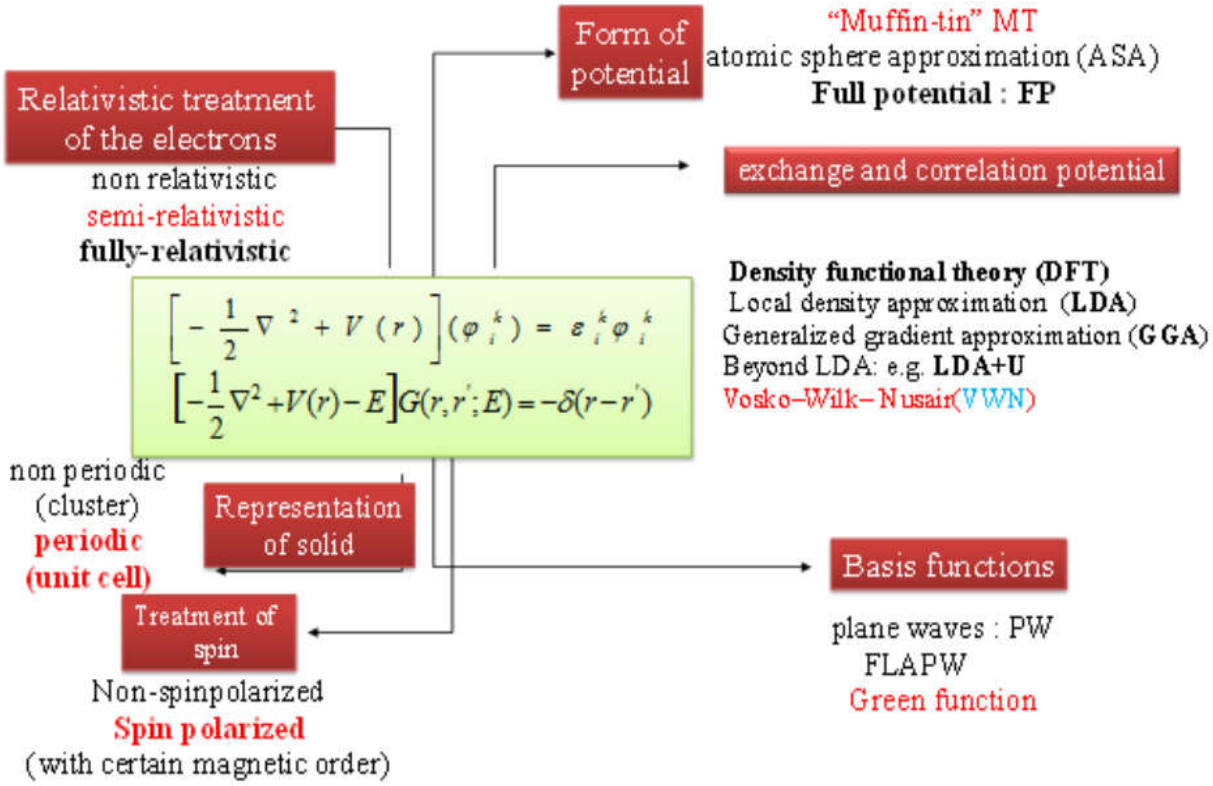

Figure II.1 : Schematic representation of different methods of DFT calculation

The resolution of the Kohn-Sham equation can be performed by several methods, such as linearized Muffin-Tin Orbitals, linearized Augmented Plane Wave LAPW, KKR theory (Kohn Korringa Rostoker), pseudo-potential approximation, and so on. To perform the calculation with any of these methods, the potential is calculated in a self-consistent way, because the density that is the solution of these equations, should theoretically be equal to that introduced initially to solve these self-coherent equations. Thus, Kohn and Sham equations

must be solved by an iterative technique that aims to diagonalize the Hamiltonian matrix that can be summarized as follows:

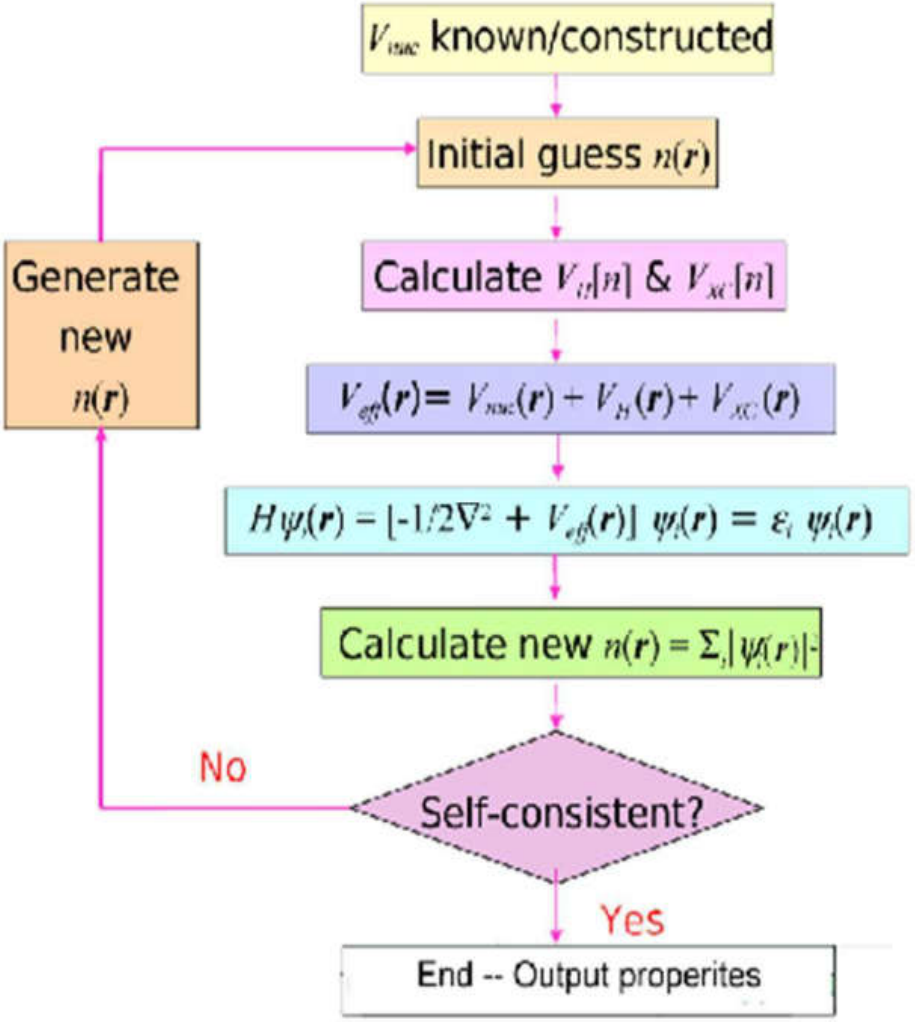

Figure II.2: Self-consistent flowchart for solving the Kohn-Sham equations

II. Korringa, Kohn and Rostoker method

II.1 Introduction

The Korringa-Kohn-Rostocker (KKR) method is a very efficient technique for calculating the Green's function based on the multiple-scattering formalism. In this approach, each site is treated as a scattering center, and the solution of the original equation is obtained by demanding the self-consistency of scattering at all sites. One of the advantages of this method is that the charge density and the local density of states can be directly calculated from the

Green's function. This method was introduced in 1947 by Korringa [63] and in 1954 by Kohn and Rostoker [64]. The Characteristic of this method is the use of multiple-scattering theory

for the solution of the Schrödinger equation and the determination of the electron band structure. A further significant development of the KKR scheme results when it was reformulated as a Green function method [65;66]. Once more separating the single-site scattering problem from the multiple-scattering effects, the method is able to produce the crystal Green function efficiently by relating it to the Green function of free space via the Dyson equation. In a second step, the crystal Green function can be used as a reference in order to calculate the Green function using Dyson equation, for an impurity in the crystal [67]. This way of solving the impurity problem is extremely efficient, avoiding the construction of huge supercells which are needed in wavefunction methods. In addition, this method can treat disordered alloys within the coherent potential approximation (CPA)[68].

II.2 Definition and general properties of the Green function

The physical meaning of the Green function G(r, r', E) is a function that describes the movement of the spread of free particle from r to r' with the energy E. The power of Green's function consists in its largest amount for the calculation of physical quantities. where this function is determined, all quantities such as the density of states, charge density, besides to the total energy or the magnetic moments can then be extracted. On the other hand, the Green function of the pure and perfect crystal (without defects) can be used to calculate the Green's function of an impurity in a system with defects from the Dyson equation as well. Chemically disordered systems can also be treated by the KKR method in the context of the coherent potential approximation CPA.

II.2.1 Green's function time depending

henceforth, we will use the atomic units $\left[\hbar = 1,\ m_e = \frac{1}{2},\ \mathrm{e} = -\sqrt{2}\right]$ (II.23)

Considering an electron under the influence of a potential $V(\vec{r})$, the Hamiltonian is :

$$H = -\nabla^2 + V(\vec{r}) = H_{free} + V(\vec{r}) \qquad \text{(II.24)}$$

The Schrödinger equation is time depending.

The time evolution of the electron's wave function $\psi(t)$ is determined by the following equation:

$$i\frac{\partial}{\partial t}\psi(t) = H\psi(t) \qquad \text{(II.25)}$$

The solution of the previous equation is:

$$\psi(t) = e^{-iHt}\psi(0) \qquad \text{(II.26)}$$

$\psi(0)$ is the representation of the preparation of the wave packet as an initial condition. The quantity U(t)= e^{-iHt} is the operator of time evolution in quantum mechanics.

Then, we define two propagators, related to Green's function $G^R(t)$ and the advanced Green's function $G^A(t)$, such as:

$$(i\frac{\partial}{\partial t} - H)\, G^{R,A}(t) = \delta(t) \qquad \text{(II .27)}$$

With the following boundary conditions

$G^R(t) = 0 \qquad t<0 \qquad (1)$ (II.28)

$G^A(t) = 0 \qquad t>0 \qquad (2)$

The formal solution of these equations is :

$$G^R(t) = \begin{cases} -ie^{-iHt} & t > 0 \\ 0 & t < 0 \end{cases} \quad (1) \qquad \text{(II.29)}$$

$$G^A(t) = \begin{cases} 0 & t > 0 \\ ie^{-iHt} & t < 0 \end{cases} \quad (2)$$

Green's functions coincide up to a factor with the operator of evolution time. $G^R(t)$ is used to propagate the wave function before the time t and propagate the wave function after the time t.

$$\begin{cases} \psi(t) = iG^R(t - t')\,\psi(t') & t < t' \quad (1) \\ \psi(t) = iG^A(t - t')\psi(t') & t' > t \quad (2) \end{cases} \qquad \text{(II.30)}$$

In the following, we will limit the discussion to the retarded Green's function G^R.

The equation (II.28.1), where the Green function corresponding to Hamiltonian $H_1 = H_0 + \Delta V$ is linked to the Green's function G0 corresponding to H0 through the integral equation of Dyson:

$$G_1(t) = G_0(t) + \int_0^1 G_0(t - t')\,\Delta V G_1(t')\,dt' \qquad \text{(II.31)}$$

In addition, $\psi(0)$ corresponds to the wave function without interaction with ΔV which evolves as $\psi(0)$, its transformation of the wave function $\psi(t)$ as:

$$\psi(t) = \psi_0(t) + \int_{-\infty}^{t} G_0(t - t')\,\Delta V \psi(t')dt' \qquad \text{(II.32)}$$

this equation (II.32) is called the equation of Lippmann-Schwinger.

II.2.2 Green's function energy depending

The Fourier transformation of the Green's function is :

$$G(E) = \int_{-\infty}^{+\infty} G(t) e^{i(E+i\varepsilon)t}\,dt \qquad \text{(II.33)}$$

The regular solution of the transformation is the next one :

$$G(E) = (E + i\varepsilon - H)^{-1} \qquad \text{(II.34)}$$

ε is a positive real number, which has been introduced to ensure the convergence of the integral in equation (II.32) for $t \longrightarrow \infty$.

In general, we can define the Green's function (time-independent) as a solution of the Schrödinger equation time independent through the operator equation

$$G(E) = (E - H)^{-1} \qquad \text{(II.35)}$$

When $Im(E) > 0$, then G(E) is an analytic function of E. In terms of a full set of the proper functions of H, $|\psi_i>$ correspond the eigenvalues ε_i, and the following spectral representation may be obtained by:

$$G(E) = \sum_i \frac{|\psi_i><\psi_i|}{E - \varepsilon_i} \qquad \text{(II.36)}$$

After representing in a real space, the above equation becomes:

$$G(\vec{r}, \vec{r'}, E) = \sum_i \frac{\psi_i(\vec{r})\ \psi_i^*(\vec{r'})}{E - \varepsilon_i} \qquad \text{(II.37)}$$

If there is a limit of $Im(E) = \varepsilon \longrightarrow 0$, an outgoing wave at $\vec{r}$ with term $\vec{r'}$ can be seen from the previous equation. The imaginary part of G is directly linked to the resolution of the spectral and spatial density of states $n(\vec{r'}; E)$ (for real E):

$$n(\vec{r'}; E) = -\frac{1}{\pi} \text{Im } G(\vec{r}, \vec{r'}, E) \quad \text{(II.38)}$$

This follows the Dirac identity :

$$\int_{-\infty}^{+\infty} \frac{f(x)}{x-x_0 \pm i\varepsilon} dx = P\left(\int_{-\infty}^{+\infty} \frac{f(x)}{x-x_0} dx\right) \pm i\pi f(x_0) \quad \text{(II.39)}$$

Such as P represents the main part of Cauchy's integral. We can deduce the relationship of the equation (39):

$$n(E) = -\frac{1}{\pi} \text{Im} \int \text{Im } G(\vec{r}, \vec{r'}, E)\, d^3r = -\frac{1}{\pi} \text{ImTr}G(E) \quad \text{(II.40)}$$

The operator trace G(E) can be taken in any base, not just in real space. The charge density is found as an integral part $n(\vec{r'}; E)$ of the energy above until the Fermi level:

$$\rho(\vec{r}) = -\frac{1}{\pi} \text{Im} \int_{-\infty}^{E_F} G\left(\vec{r}, \vec{r'}, E\right) dE = -\frac{1}{\pi} \text{Im} \int_{-\infty}^{E_F} \text{Tr}(\hat{r} G(E)) dE \quad \text{(II.41)}$$

As $\hat{r} = |\vec{r}\rangle \delta\left(\vec{r} - \vec{r'}\right) < \vec{r'}|$ is the operator position.

In general, the average value of the physical quantity represented by an operator can be defined by this relation:

$$\langle A \rangle = -\frac{1}{\pi} \text{Im} \int_{-\infty}^{E_F} \text{Tr}(\hat{A} G(E)) dE \quad \text{(II.42)}$$

Hence the Green function contains all the information which is provided by the proper functions. When the Green's function is calculated, then all the physical properties of the system can be found.

II.2.3 Relation between disturbed and non-disturbed system of the transition matrix or T-matrix

The Dyson equation(II.31) depends on the time and its counterpart depends on energy. Taking account of equation (II.33) for the reference systems $G_0^{-1}(E)=(E-H)$, whereas for the perturbed system $G_1^{-1}(E)=E-(H_0 + \Delta V)$, we conclude that both Green functions are linked through:

$$G_1^{-1}(E) = G_0^{-1}(E) - \Delta V \quad \text{(II.43)}$$

The Dyson equation can be rewritten in the following forms :

$$G_1(E) = [1 - G_0(E)\, \Delta V]^{-1} G_0(E) \quad (1) \quad \text{(II.44)}$$

$=G_0(E)[1-\Delta V G_0(E)]^{-1}$ (2)

$=G_0(E) + G_0(E)\Delta V G_1(E)$ (3)

The last Expression (II.44.3), provides an interpretation of the Dyson equation via multiple scattering events by the potential ΔV. If we develop G_1 on the right side we have:

$G_1(E) = G_0(E) + G_0(E)\Delta V G_0(E) + G_0(E)\Delta V G_0(E)\Delta V G_0(E) + \ldots\ldots$ (II.45)

This is similar to a series development of Born for the Green function.

Also, Lippmann-Schwinger equation (II.32) has an independent counterpart depends on time. Observing the Schrödinger equation for the perturbed system which is written as :

$(E - H)|\psi_1\rangle = \Delta V|\psi_1\rangle$ (II.46)

By substitution; we can verify that the $\psi_1\rangle$ solution can be written in terms of proper undisturbed $|\psi_0\rangle$ a statement such as :

$$|\psi_1\rangle = |\psi_0\rangle + G_0(E)\Delta V\psi_1\rangle \quad \text{(II.47)}$$

We developed $\psi_1\rangle$ the right side of the Lippmann-Schwinger equation which leads to the series of Born

$$|\psi_1\rangle = |\psi_0\rangle\, G_0(E)\Delta V|\psi_0\rangle + G_0(E)\Delta V G_0(E)\Delta V|\psi_0\rangle + \ldots\ldots \quad \text{(II.48)}$$

In this case, E does not belong to the spectrum of the unperturbed Hamiltonian $|\psi_0\rangle = 0$, Then we get:

$$|\psi_1\rangle = G_0(E)\Delta V|\psi_1\rangle \quad \text{(II.49)}$$

This expression can be used to obtain the discrete spectrum of H_1.

Now we will introduce the transition matrix or T-matrix of a scattering system.

The state of the perturbed Hamiltonian $|\psi_1\rangle$ is connected to the undisturbed system state $|\psi_0\rangle$ through the following equation :

$$\Delta V\,|\psi_1\rangle = T(E)|\psi_0\rangle \quad \text{(II.50)}$$

The Lippmann-Schwinger equation (II.47) is written in terms of transition matrices:

$|\psi_1\rangle = |\psi_0\rangle + G_0(E)T(E)|\psi_0\rangle$ (II.51)

The Dyson equation is :

$G_1(E) = G_0(E) + G_0(E)T(E)G_0(E)$ (II.52)

While the following relations can be easily verified:

$T(E) = \Delta V\,[1 - G_0(E)\,\Delta V]^{-1}$ (1) (II.53)

$= [1 - \Delta V G_0(E)]^{-1}\,\Delta V$ (2)

$= \Delta V + \Delta V G_0(E)T(E)$ (3)

If we develop the right side of the last equation, this will lead again to a series of Born:

$T(E) = \Delta V + \Delta V G_0(E)\Delta V + \Delta V G_0(E)\Delta V G_0(E)\Delta V + \ldots\ldots$ (II.54)

While for the small perturbations, it will lead to Born approximation of the first order $T \approx \Delta V$.

The change in integrated density of states $\Delta N(E)$ between the disturbed and undisturbed system can be expressed using the transition matrix (T-matrix).

The change of the density of states is picked from the equation (II.41).

$$\Delta n(E) = n_1(E) - n_0(E) = -\frac{1}{\pi}\,\mathrm{Im}\mathrm{Tr}[G_1(E) - G_0(E)] \quad \text{(II.55)}$$

Equation (II.33) provides us the identity: $G = \frac{\partial(ln\ G^{-1})}{\partial E}$

Combining this with the equation (II.55):

$$\Delta n(E) = -\frac{1}{\pi}\,\mathrm{Im}\mathrm{Tr}\,\frac{\partial}{\partial E}[\ln G_1^{-1} - \ln G_0^{-1}] = -\frac{1}{\pi}\,\mathrm{Im}\mathrm{Tr}\,\frac{\partial}{\partial E}\,\ln[G_0\,G_0^{-1}]$$

$$= -\frac{1}{\pi}\,\mathrm{Im}\,\frac{\partial}{\partial E}\,\mathrm{Tr}\,\ln[1 - G_0\Delta V] \quad \text{(II.56)}$$

$$= -\frac{1}{\pi}\,\mathrm{Im}\,\frac{\partial}{\partial E}\,\mathrm{Tr}\,\ln[T^{-1}\Delta V]$$

In the last two steps, we used the Dyson equation(II.53) and the property of the T-matrix.

The integrated change in the density of states is:

$$\Delta N(E) = \int_{-\infty}^{E} \Delta n(E')dE' = -\frac{1}{\pi}\,\mathrm{Im}\mathrm{Tr}\,\ln[T^{-1}(E)\Delta V]\ {}^{E}_{-\infty} \quad \text{(II.57)}$$

By definition, we can say that $[T^{-1}(E)\Delta V]$= ln T^{-1}(E)+lnΔV.

Note that the ΔV contribution is neglected because it does not depend on energy.

$$\Delta N(E)=\frac{1}{\pi}\,\mathrm{ImTrlnT(E)} \qquad \text{(II.58)}$$

In the following section, we will associate the perturbation ΔV with a spherically symmetric potential of the set over in the free space. So we have a diffusion problem with a single site, and we designate T-matrix by t.

The representation of the angular momentum is diagonal and its elements are related to the dispersion phase shifts $\delta_l(E)$ via

$$t_l = -\frac{1}{\sqrt{E}}\sin(\delta_l(E))e^{i\delta_l(E)} \qquad \text{(II.59)}$$

In this case, the equation (II.58) becomes:

$$\Delta N(E)=\frac{1}{\pi}\sum_l(2l+1)\delta_l(E) \qquad \text{(II.60)}$$

II.2.4 Scattering of a single site

Now, we discuss the problem of scattering of an integrated atomic spherical potential in free space (a constant potential environment). The reference system is a system with N free electrons (where the Hamiltonian contains only the kinetic energy term, and the proper functions are plane waves). Green's function of a free electron system is:

$$g(\vec{r},\vec{r'},E) = -\frac{1}{4\pi}\frac{e^{ik|\vec{r}-\vec{r'}|}}{|\vec{r}-\vec{r'}|} \qquad \text{(II.61)}$$

With k=$\sqrt{E}$. In the case of scattering by a central potential, it is useful to work in the representation of the angular momentum.

So we figured as a clear incident wave:

$$\psi_{\vec{k}}^{inc}(\vec{r}) = e^{i\vec{k}\vec{r}} = \sum_l 4\pi\, i^l j_l(\sqrt{E}r)Y_L(\vec{r})Y_L(\vec{k}) \qquad \text{(II.62)}$$

In which j_l is the spherical Bessel function, while Y_L is the real spherical harmonics. We use the index L=(l,m) combined, where l and m are the indices of the angular momentum. On the other hand, the Green's function of the free space (II.61) can be developed as :

$g(\vec{r}, \overrightarrow{r'}, E) = \sum_L Y_L(\vec{r})\ g_l(r, r', E) Y_L(\overrightarrow{r'})$ (II.63)

with :

$g_l(r, r', E) = -i\sqrt{E} j_l(\sqrt{E} r_<) h_l(\sqrt{E} r_>)$ (II.64)

In which $h_l = j_l + i n_l$ is the spherical Hankel functions, n_l are the spherical Neumann functions, whereas $r_<(r_>)$ is the smallest of the rays r and r'. Bessel functions $j_l(x)$ are finite when

$(x \to 0)$, whereas h_l (x) and $n_l(x)$ diverge when $(x \to 0)$. Let's suppose now that there is a diffusion potential for a finite field of the form:

$$V(\vec{r}) = \begin{cases} V(r) & r \le S \\ 0 & r > S \end{cases} \quad \text{(II.65)}$$

The radial wave functions R_l (r, E) satisfy the radial Schrödinger equation:

$$\left[-\frac{1}{r} \frac{\partial^2}{\partial r^2} r + \frac{l(l+1)}{r^2} + V(r) - E \right] R_l(r, E) = 0 \quad \text{(II.66)}$$

The asymptotic form of R_l (r, E) is $(r \to \infty)$.

$$R_l(r, E) \to \frac{A_l}{\sqrt{E} r} \sin\left(\sqrt{E} r - \frac{l\pi}{2} + \delta_l(E) \right) \quad \text{(II.67)}$$

In which A_l is independent of r, and $\delta_l(E)$ is the phase shift relative to the wave function for the zero petential.

For r>S; V(r)=0, the general solution of the radial equation is a sum of two special solutions, linearly independent:

$R_l(r, E) = B_l j_l(\sqrt{E} r) + C_l n_l(\sqrt{E} r)$ (II.68)

Where B_l and C_l are constants.

Using the asymptotic shape of the Bessel functions,

$\lim_{x \to \infty} j_l(x) = \frac{1}{x} \sin\left(x - \frac{l\pi}{2} \right)$ (II.69)

$\lim_{x \to \infty} n_l(x) = \frac{1}{x} \cos\left(x - \frac{l\pi}{2} \right)$ (II.70)

with the equations (II.66) and (II.67) we find :

R_l (r, E) = A_l $\left(j_l(\sqrt{E}r)\cos\delta_l + n_l(\sqrt{E}r)\sin\delta_l\right)$ pour r > S (II.71)

On the other hand, the Lippmann-Schwinger equation gives:

R_l (r, E) = $j_l(\sqrt{E}r) + \int_0^S g_l(\mathrm{r}, r', \mathrm{E})\mathrm{V}(\mathrm{r}')R_l(r', \mathrm{E})\, r'^2 \mathrm{dr}'$ (II.72)

Using a previous equation where r > S, we get:

R_l (r, E) = $j_l(\sqrt{E}r) - \mathrm{i}\, h_l(\sqrt{E}r)\sqrt{E}\int_0^S j_l(\sqrt{E}\, r')\mathrm{V}(\mathrm{r}')R_l(r', \mathrm{E})\, r'^2 \mathrm{dr}'$ (II.73)

The integral is simply the T-matrix element in the representation of the angular momentum,

t_l(E) = $\int_0^S j_l(\sqrt{E}\, r)\mathrm{V}(\mathrm{r})R_l(r, \mathrm{E})\, r^2 \mathrm{dr}$ (II.74)

Whereas we get:

R_l (r, E) = $j_l(\sqrt{E}r) - \mathrm{i}\sqrt{E}t_l(\mathrm{E})\, h_l(\sqrt{E}\, r')$ (r > S) (II.75)

With the T-matrix related to the phase shift, we get:

t_l(E) = - $\frac{1}{\sqrt{E}}$ sin $\delta_l(E)e^{i\delta_l(E)}$ (II.76)

An incident wave developed of Bessel functions and spherical harmonic of the equations (II.62) is :

$\psi_{\vec{k}}^{inc}(\vec{r})$ = $\sum_l a_{\vec{k}L}^0\, j_l(\sqrt{E}r)\mathrm{Y_L}(\vec{r})$ (r > S) (II.77)

By analogy the scattered wave can be written as follows:

$\psi_{\vec{k}}^{sc}(\vec{r})$ = $\sum_l a_{\vec{k}L}^{sc}\, j_l(\sqrt{E}r)\mathrm{Y_L}(\vec{r})$ (r > S) (II.78)

When r is closer to S, its written :

$\psi(\vec{r})$ = $\sum_l a_{\vec{k}L} R_l(r, \mathrm{E})\mathrm{Y_L}(\vec{r})$ (II.79)

with boundary conditions of R_l given by the equation (II.75). Continuity of the wave function at r = S, we obtain :

$a_{\vec{k}L}^{sc}$ = $-\mathrm{i}\sqrt{E}t_l(\mathrm{E})\, a_{\vec{k}L}^0$ (II.80)

Green's function is given for the problem of scattering by a central potential.

It can be written as the product of two linearly independent solutions R_l (regular, i.e.: converting $(r \to 0)$) and H_l (irregular, i.e., differing in $(r \to 0)$ of the radial equation.

$$G(\vec{r}, \vec{r'}, E) = -i\sqrt{E} \sum_L R_l(r_<, E) H_l(r_>, E) Y_L(\vec{r}) Y_L(\vec{r'}) \quad \text{(II.81)}$$

$$= \sum_L G_l(r, r', E) Y_L(\vec{r}) Y_L(\vec{r'})$$

The boundary conditions R_l are given by the equation (II.75). In order to find the boundary conditions of H_l, we use the identity $G_l = g_l + g_l t_l g_l$ (g_l *is* given by the equation (II.64), then we find:

$$H_l(r, E) = h_l(\sqrt{E}r) \quad (r > S) \quad \text{(II .82)}$$

2.4 Multiple diffusion theory

We discussed above, the solution of the scattering problem for a single isolated diffusion potential. In the following, we will discuss a set of broadcasters. at this point, we assume the approximation Muffin Tin (MT) of the potential scattering according to which the potential is spherically symmetric around each diffusion center (atomic site) in a sphere radius r. The theory presented here is based on the accounts of scattering amplitudes in a periodic array of diffusers, so that old equation relates the amplitudes of the incoming and outgoing waves emerges. The procedure leads to KKR equations for the periodic crystal band structure. Although the procedure is not necessary for the theory of the Green's function KKR, it gives a physical insight to the finding idea of multiple scattering theory, and it is used in many problems of broadcast waves even when a Green function is not introduced.

Suppose we have a periodic structure of MT potential, centered on the network of sites $\vec{R}^n$

The constant potential in the interstitial can be considered as equal to zero. An outgoing wave $\vec{R}^n$ site can be widened in the incoming waves $\vec{R}^{n'}$ using a theorem for the transformation of Hankel functions:

$$h_l(\vec{r'} + \vec{R}^{n'} - \vec{R}^n, E) = \frac{i}{\sqrt{E}} \sum_{L'} g_{LL'}^{nn'}(E)\ j_{L'}(\vec{r'}, E) \quad \text{(II.83)}$$

Using the abbreviations:

$$j_{L'}(\vec{r'}, E) = j_l(\sqrt{E}r)\, Y_L(\vec{r}) \quad \text{and} \quad h_L(\vec{r'}, E) = h_l(\sqrt{E}r)\, Y_L(\vec{r}) \quad \text{(II.84)}$$

The expansion coefficients, also called structure constants are given by :

$$g_{LL'}^{nn'}(\mathrm{E}) = -(1-\delta_{nn'})\, 4\pi i\sqrt{E}\, \sum_{L"} i^{l-l'+l"}\, C_{LL'L"}\, h_{L"}(\vec{R}^n - \vec{R}^{n'}, E) \qquad \text{(II.85)}$$

With :

$$C_{LL'L"} = \int d\Omega\, \mathrm{Y_L}(\vec{r})\, Y_{L'}\,(\vec{r})\, Y_{L"}\,(\vec{r}) \qquad \text{(II.86)}$$

The coefficients in equation (II.86) were introduced in the summation to include a finite number of terms, since the coefficients cancel for $l" > l' + l$. Using the above extensions, the Green's function for N free electrons can be expressed as following :

$$\mathrm{g}(\vec{r} + \vec{R}^n, \overrightarrow{r'} + \vec{R}^{n'}, \mathrm{E}) = -\frac{1}{4\pi}\frac{e^{ik\left|\vec{r}+\vec{R}^n-\overrightarrow{r'}-\vec{R}^{n'}\right|}}{|\vec{r}+\vec{R}^n-\overrightarrow{r'}-\vec{R}^{n'}|} \qquad \text{(II.87)}$$

$$= -i\sqrt{E}\sum_L\ j_L\,(\vec{r}_<, E)\, h_L\,(\vec{r}_>, \mathrm{E}) + \sum_{LL'} j_L\,(\vec{r}\,, E)\, g_{LL'}^{nn'}(\mathrm{E})\, j_{L'}(\overrightarrow{r'}, \mathrm{E})$$

The multiple scattering theory can be expressed by the following figure:

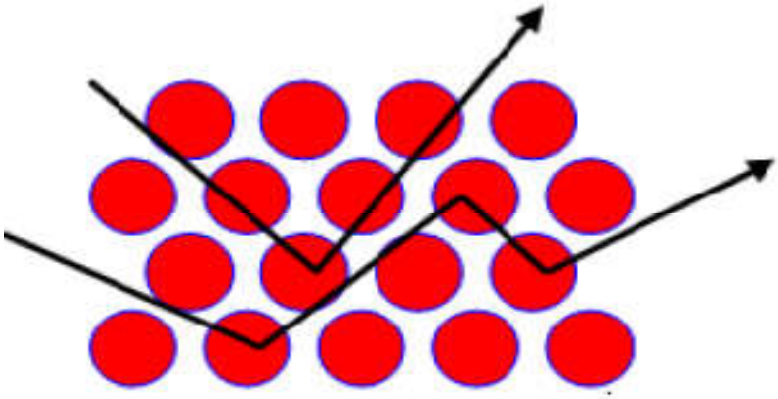

Figure II.3: schematic representation of a Multiple scattering theory.

We consider that outgoing wave of interstitial after a broadcast by a potential event $\vec{R}^n$.

$$\psi_{\vec{k}}^{sc(n)}\,(\vec{r}) = \sum_L\ b_{\vec{k}L}^{sc(n)}\, h_L\,(\vec{r}\,, E) \qquad \text{(II.88)}$$

The same wave can be resolved as an incident wave at different center $\vec{R}^{n'}$

$$\psi_{\vec{k}}^{inc(n')}(\overrightarrow{r'}) = \sum_L b_{\vec{k}L}^{inc(n')} j_L(\overrightarrow{r'}, E) \quad \text{(II.89)}$$

Thus, a scattered wave on the site n can be expressed as entering on the site n':

$$\sum_L b_{\vec{k}L}^{sc(n)} h_L(\overrightarrow{r'} + \vec{R}^{n'} - \vec{R}^{n}, E) = \sum_L b_{\vec{k}L}^{inc(n')} j_L(\overrightarrow{r'}, E) \quad \text{(II.90)}$$

Using the identity in equation (II.83), we get:

$$b_{\vec{k}L}^{(n')} = \frac{i}{\sqrt{E}} \sum_{L'} g_{LL'}^{nn'} b_{\vec{k}L'}^{sc(n')} \quad \text{(II.91)}$$

In view of the periodicity of the crystal lattice, we use the Bloch condition: the amplitude of a scattered wave at the position $\vec{R}^n$ is different from the amplitude of the scattered wave in the position $\vec{R}^{n'}$ by a phase factor $e^{i\vec{k}(\vec{R}^n - \vec{R}^{n'})}$. The total amplitude of the incoming wave $\vec{R}^{n'}$ diffuser originating from all other identical diffusers can be written as:

$$C_{\vec{k}L}^{(n')} = \frac{i}{\sqrt{E}} \sum_{L'} \sum_{n \neq n'} g_{LL'}^{nn'} e^{i\vec{k}(\vec{R}^n - \vec{R}^{n'})} C_{\vec{k}L'}^{sc(n')} = \frac{i}{\sqrt{E}} \sum_{L'} g_{LL'}(\vec{k}, E)\, C_{\vec{k}L'}^{sc(n')} \quad \text{(II.92)}$$

$g_{LL'}^{nn'}$ is the Fourier transform.

The structure constants KKR $g_{LL'}(\vec{k}, \mathrm{E})$ and $g_{LL'}^{nn'}(E)$ depend only on the geometry of the network not the diffusion potential.

The total wave broadcast by a broadcaster in the network site is connected to the total incoming wave at this site via T-matrix with elements t_l(E).

The total incoming wave at a site consists of the external wave, the waves scattered by all network sites are :

$$C_{\vec{k}L}^{sc(n')} = \mathrm{i}\sqrt{E} t_l(\mathrm{E})\left(a_{\vec{k}L}^{0} + C_{\vec{k}L}^{(n')}\right) \quad \text{(II.93)}$$

Combining equations (II.92) and (II.93) we get the following system of equations:

$$a_{\vec{k}L}^{0} = \sum_{L'}\left(\delta_{LL'} - g_{LL'}(\vec{k}, E)\, t_{l'}(\mathrm{E})\right) \frac{i}{\sqrt{E}}\, t_{l'}^{-1}(\mathrm{E})\, C_{\vec{k}L'}^{sc(n')} \quad \text{(II.94)}$$

When there is no incoming external wave, we have :

$$\sum_{L'}\left(\delta_{LL'} - g_{LL'}(\vec{k}, E)\, t_{l'}(\mathrm{E})\right) C_{\vec{k}L'}^{(n')} = 0 \quad \text{(II.95)}$$

The electronic proper values in a crystal are given by solutions of the equation (II.95), that means in the absence of an external wave. In order to have non-trivial solutions of the system it is necessary and sufficient to cancel the determinant :

$$\text{Det}\left[\delta_{LL'} - g_{LL'}(\vec{k},E)\, t_{l'}\,(\text{E})\right] = 0 \qquad \text{(II.96)}$$

It is the old equation of KKR, giving the band energy structure E($\vec{k}$) for periodic crystals.

The total wave function into the interstitial around a diffuser n is given by the sum of the equation of the incident and dispersed wave (II.88) and (II.89). Using the equation (II.93) and (II.95) we end up with the form:

$$\psi_{\vec{k}}\,(\vec{r} + \vec{R}^n) = \sum_L C_{\vec{k}L}^{(n)} R_L(\vec{r},E) \qquad \text{(II.97)}$$

The Bloch theorem gives:

$$C_{\vec{k}L}^{(n)} = e^{i\vec{k}.\vec{R}^n}\, C_{\vec{k}L}^{(0)} \qquad \text{(II.98)}$$

The coefficients $C_{\vec{k}L}^{(n)}$ can be considered as elements of the matrix of a unitary transformation between $\vec{k}$ and (L,n) representations. It implies the orthogonality of the bases:

$$\sum_{n,L} C_{\vec{k}L}^{(n)*}\, C_{\vec{k}'L}^{(n)} = \delta_{\vec{k}\vec{k}'} \qquad \text{(II.99)}$$

$$\sum_{\vec{k}} C_{\vec{k}L}^{(n)*}\, C_{\vec{k}L'}^{(n')} = \delta_{nn'}\delta_{LL'} \qquad \text{(II.100)}$$

II.2.5 Representation of KKR method

To describe the KKR method, we will introduce the representation of the Green's function and Dyson equation. We consider the Green's function of a periodic array of spherical symmetry, without overlapping potentials. The potential is given by:

$$\text{V}\,(\vec{r} + \vec{R}^n) = \text{V}^{\text{n}}\,(\text{r}) \qquad \text{(II.101)}$$

While the Green's function is defined by:

$$(-\nabla^2 + \text{V}^{\text{n}}\,(\text{r}) - \text{E})\ \text{G}\ (\vec{r} + \vec{R}^n\ ,\ \overrightarrow{r'} + \vec{R}^{n'}\ , E\ ) = -\ \delta_{nn'}\,\delta(\vec{r} - \overrightarrow{r'}) \qquad \text{(II.102)}$$

For n≠n', the Green's function satisfies the homogeneous Schrödinger equation and can be developed in the regular solutions of the Schrödinger equation. In the Muffin-Tin

approximation (see equation (II.64)) we have $R_L^n(\vec{r}, E) = R_L^n(r, E)\, Y_L(\vec{r})$, (see equation (II.66)).

For n=n' we have the Green function for a central potential as in equation (II.81), but with a boundary condition of the backscatter, all other potentials in the crystal are taken into consideration.

Green's function is a sum of the general solution of the homogeneous equation corresponding to equation (II.102), plus a particular solution to the inhomogeneous equation (II.102). In the mixture of the angular momentum of representation to the site, the final formula of the Green's function is defined by:

$$G(\vec{r}+\vec{R}^n, \vec{r'}+\vec{R}^{n'}, E) = -i\sqrt{E}\sum_L R_L^n(\vec{r}_<, E) H_L^n(\vec{r}_>, E)\,\delta_{nn'} + \sum_{LL'} R_L^n(\vec{r}, E) G_{LL'}^{nn'}(E)\, R_{L'}^{n'}(\vec{r'}, E) \quad \text{(II.103)}$$

When we use the abbreviation $H_L^n(\vec{r}, E) = H_L^n(r, E)\, Y_L(\vec{r})$, for the irregular solution of the radial equation for the atomic cell n, the coefficients $G_{LL'}^{nn'}(E)$ are called structural Green's functions, and still unknown yet, they can be calculated using the Dyson equation.

Based on the free space of a disturbed system, we have:

$$G(\vec{r}+\vec{R}^n, \vec{r'}+\vec{R}^{n'}, E) = g(\vec{r}+\vec{R}^n, \vec{r'}+\vec{R}^{n'}, E) + \sum_{n''} \int dr''\; g(\vec{r}+\vec{R}^n, \vec{r'}+\vec{R}^{n'}, E)\; V^{n''}(r'')\, G(\vec{r''}+\vec{R}^{n''}, \vec{r'}+\vec{R}^{n'}, E) \quad \text{(II.104)}$$

Substituting equations (II.87) and (II.103) in equation (II.104), we can arrive at the following algebraic Dyson equation which determines the structural Green's function:

$$G_{LL'}^{nn'}(E) = g_{LL'}^{nn'}(E) + \sum_{n'',L''} g_{LL''}^{nn''}(E)\, t_{L''}^{n''}(E)\, G_{L''L'}^{n''n'}(E) \quad \text{(II.105)}$$

When the T-matrix penetrates, instead of the potential that appears in the normal equation of Dyson, the physical meaning of this equation becomes clear if we enlarge the sum on the right side, then we get :

$$G_{LL'}^{nn'}(E) = g_{LL'}^{nn'}(E) + \sum_{n'',L''} g_{LL''}^{nn''}\, t_{L''}^{n''}\, g_{L''L'}^{n''n'} + \sum_{n'',L''}\sum_{n''',L'''} g_{LL''}^{nn''}\, t_{L''}^{n''}\, g_{L''L'''}^{n''n'''}\, t_{L'''}^{n'''}\, g_{L'''L'}^{n'''n'} + \ldots \quad \text{(II.106)}$$

This means that one of the electrons can move from n' to n, directly or after being dispersed once by any site or two sites, etc.

II.2.6 Coherent potential approximation (CPA)

Considering a random alloy system that consists of n components, A_1, A_2...A_n. With their concentrations X_1, X_2,...X_n.

Suppose that the atom A_i is at the center of the effective environment. Green's function that starts from the origin and returns to the origin is:

$$G^{i}_{LL"}(E) = \sum_{L"} G_{LL"} \left[1 - (t_i - T)G\right]^{-1}_{L'L"} \quad \text{(II.107)}$$

$G_{LL"}$ and T are respectively the Greens's function and T-effective environment matrix. CPA is an effective approximation to determine T.

We use the self-coherent equation:

$$\sum_{i=1}^{n} x_i \; G^{i}_{LL'} = G_{LL'} \quad \text{(II.108)}$$

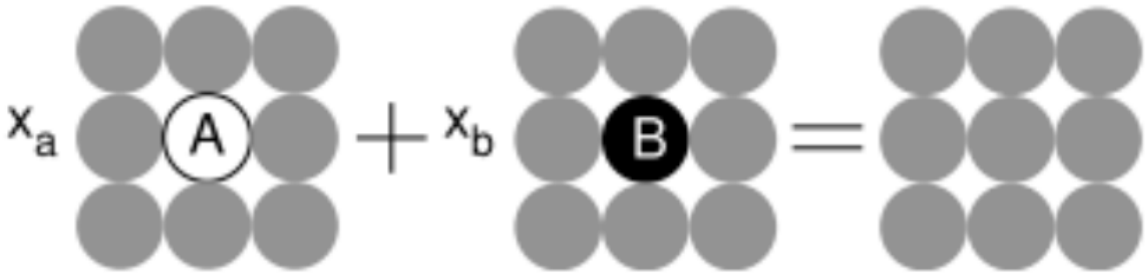

Figure II.4: The process of CPA

Resolving the Kohn sham equations for points of symmetry in the first Brillouin zone can be done iteratively using a self-coherent iterations cycle, besides to the calculation of an initial electron density. That can be the superposition of electron densities of isolated atoms for example. We do this at each cycle, then we have to solve the Kohn and Sham equation $H_{KS}\ \psi_i(r) = E_i\ \psi_i(r)$ with potential determined from the electronic density calculated at the previous iteration. For this, we express the wave functions $\psi_i(r)$ calculated on a finite basis of functions $\Phi_P(r)$. The larger the size of this basis is, the better is the precision of the calculation which is more accurate but it will require in return a greater computing time and more information to be stored in memory. The development of the function of Kohn and Sham $\psi_i(r)$ on the basis of $\Phi_P(r)$ is given by:

$$\psi_i(r) = \sum_{P=1}^{P} C^{i}_{P} \Phi_P(r) \quad \text{(II.109)}$$

Substituting this equation into the equation of Kohn and Sham, we obtain a system of equations allowing to determine the wave functions of Kohn and Sham $\psi_i(r)$ of E_i energy. Then, we have to choose a relevant basis wave functions for the calculation.

III. FPLAPW method implemented in Wien2k

III.1 The basic of Augmented Plane Wave (APW)

The APW method was first proposed by slater to describe the character almost free of the electrons when they are far from the nuclei, as well as the atomic behavior near the nuclei. The system is described as a Muffin Tin potential. In the scheme of the APW, the unit cell of the crystal is divided into two types of areas[69].

- atomic spheres(MT) centered on the nuclei

-The interstitial space (remaining) between atomic spheres.

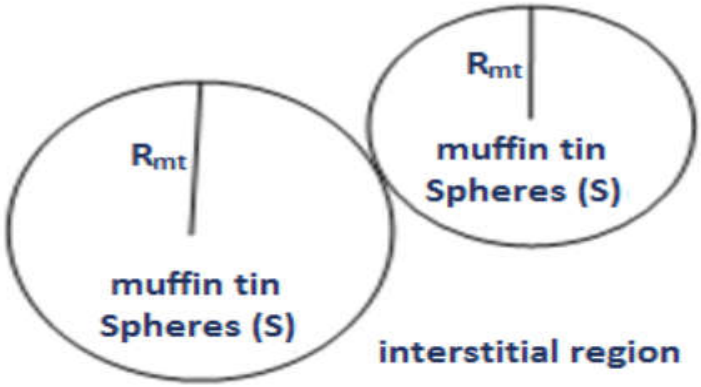

Figure II.5 : Dividing of chemical unit cells into muffin tin spheres (S) with a radius Rmt and an interstitial region (I) adopted in the APW method

At the neighborhood of atomic nucleus, the potential and wave functions have the form "Muffin-Tin" (MT) presenting a spherical symmetry inside the sphere. While between atoms the potential and the wave functions can be considered smooth. Accordingly, the crystal wave functions are developed on a different basis according to the area concerned:

Radial solutions of the Schrödinger equation inside the MT sphere and plane waves in the interstitial region.

So the basic functions, called APW are then Bloch wave functions of Bloch wave vector k(vector of the first Brillouin zone) whose shape is given by:

$$\Phi_K^k(r,E)=\begin{cases} \frac{1}{\sqrt{V}}\, e^{i(k+K)r} & in\ the\ interstitial\ space \\ \sum_{l,m} A_{lm}^{\alpha,k+K} u_l^{\alpha}(r',E) Y_{lm}(r') & in\ the\ atomic\ sphere\ \alpha \end{cases} \quad \text{(II.110)}$$

V is the elementary crystal volume

K is the reciprocal lattice vector

r is the position vector of the electron

r' is the position vector of the electron relative to the center of the atomic-sphere α and Y_{lm} spherical harmonics.

The coefficients $A_{lm}^{\alpha,k+K}$ are parameters to be determined in such a way to ensure the continuity condition of $\Phi_K^k(r,E)$ on the surface of the atomic sphere α. Therefore they must be developed according to the coefficients of the plane waves existing in the interstitial regions.

In practice, the calculation is truncated to a value of L_{max} and will also limit the development of plane wave in the interstitial zone to reciprocal lattice vectors such as $||K|| \leq K_{max}$. The function $u_l^{\alpha}(r',E)$ is a solution of the radial part of the Kohn and Sham equation in the isolated α atomic-sphere and for the energy E.

There remains the problem of the energy parameter E which is to be determined. It would be ideal to take E = ε_k where ε_k is the energy of the state of Kohn and Sham ψ_k. However we do not know the energy. Therefore, it is needed to implement a method "by trial" in order to determine it . An initial value of E is used for the calculation. Once the Kohn and Sham equations resolved, the value of final energy ε_k is compared to E and the calculation must be repeated with a different value of E if they differ. This method seems to be long and and not very effective. Thus, it is better to use an other method that uses linear augmented plane wave (LAPW).

III.2 The basic of linear augmented plane wave (LAPW)

Using a LAPW base prevents the determination of the parameter E by trial. The basic functions in Mt spheres are linear combinations of radial functions $u_l^\alpha(r',E)Y_{lm}(r')$ and their derivatives $\dot{u}_l^\alpha(r',E)Y_{lm}(r')$ compared to energy.

We assume that the function $u_l^\alpha(r',E)$ was calculated for a particular energy E_0. The Taylor development is then achieved around E_0 neglecting the higher order terms in the first order:

$$u_l^\alpha(r',\varepsilon_k) = u_l^\alpha(r',E_0) + (E_0-\varepsilon_k)\left[\frac{\partial u_l^\alpha(r',E)}{\partial E}\right]_{E-E_0} \qquad \text{(II.111)}$$

And we use the notation:

$$\left[\frac{\partial u_l^\alpha(r',E)}{\partial E}\right]_{E-E_0} = \dot{u}_l^\alpha(r',E) \qquad \text{(II.112)}$$

By including this development in the equation augmented plane wave (II.109), we obtain the expression of LAPW : (II.113)

$$\Phi_K^k(r,E)=\begin{cases} \frac{1}{\sqrt{V}}\, e^{i(k+K)r} & \textit{in the interstitial space} \\ \sum_{l,m}[A_{lm}^{\alpha,k+K}u_l^\alpha(r',E_0)+B_{lm}^{\alpha,k+K}\,\dot{u}_l^\alpha(r',E_0)]\,Y_{lm}(r') & \textit{in the atomic sphere } \alpha \end{cases}$$

The coefficients $A_{lm}^{\alpha,k+K}$ and $B_{lm}^{\alpha,k+K}$ are determined from the conditions of continuity in value and spatial derivative functions $\Phi_K^k(r,E)$ on the surface of atomic sphere α. The energy E_0, called pivot energy, is generally chosen near to the center of the energy band to which we are interested. In practice, a different energy pivot is chosen for bands having a strong character (E_{0s}), a strong character p (E_{0p}), and a strong character d (E_{0d}). This choice makes it possible to reduce errors achieved when neglecting the terms of order 2 in the Taylor development of the function $u_l^\alpha(r',E)$.

The Resolution of the Kohn and Sham equations is done by a finite base which allows varying the size via $R_{min}K_{max}$ parameter. R_{min} corresponds to the smallest atomic radius spheres and K_{max} has the maximum value taken ||K||. The parameter $R_{min}K_{max}$ is generally selected between 7 and 9 but the energy of the fundamental state of convergence tests are necessary to verify that the selected value $R_{min}K_{max}$ is large enough. Once solving the equations of Kohn and Sham achieved through self-coherent way and Bloch wave functions $\psi_k^{\uparrow\downarrow}(r)$ calculated, the electron density for the two spin can be calculated by integrating the square of the wave functions module on the first Brillouin zone (this numerical integral is actually a discrete sum and the first Brillouin zone must be sampled). Taking into account the symmetries of the

system, we can limit ourselves to sampling the irreducible part of the first Brillouin zone and also reduce the computation time. The inclusion of spin-orbit coupling breaks certain symmetries in the orientation of the magnetization and thereby increases significantly the number of k vectors which must be taken into account in the first Brillouin zone for the calculation to be accurate enough. The time required for calculating the electron density will also increase [70].

III.3 GW approximation

In 1965, Lars Hedin has proposed a system of equations that leads to self-exact electron energy. These equations are based on two fundamental tools, which are the Green's functions G5 and the screened Coulomb interactions W [71]. Along with its self-consistent equations, Hedin proposed an approximation to the exact self-energy, called GW approximation. This approximation has been published by Hybertsen and Louie [72] and by Godby, Schluter and Sham[73] and has since then shown its great quality in the description of the electronic structure of the quasi-particle. Unlike the DFT, the GW approximation provides access to excited properties of the system, and the Green function G can extract all observable of the system. GW approximation has proved particularly in the calculation of gaps in a very wide range of materials. It allows almost quasi-systematic improvement of gaps calculated by DFT

III.4 Modified Becke and Johnson potential (mBJ)

A new version of the exchange potential, proposed for the first time by Becke and Johnson [74], was recently published by Tran and Blaha [75]. It is about the potential mBJ "modified Becke Johnson potential", which was implemented later, in WIEN2k (ab-intio simulation code).

Tran and Blaha [76] have tested the potential exchange proposed by Becke and Johnson (BJ) which has been designed for the reproduction of the exact form of the exchange potential, the optimized effective potential (OEP). They found using the combined potential BJ to the correlation potential of the LDA may give an understand gap energy. In order to improve results, Tran and Blaha introduced a simple modification to the original potential BJ and have obtained a good agreement with other more costly approaches (because of their high self-coherence) such as hybrid functional [77-79] and GW method [80-82].

Part two:

Results and discussion of magnetic and magneto-optical properties of DMSs (CdTe, ZnSe)

Chapter I:

Results and discussion of the compound CdTe doped with different impurities

Journal of Magnetism and Magnetic Materials 385 (2015) 295–301

Contents lists available at ScienceDirect

Journal of Magnetism and Magnetic Materials

journal homepage: www.elsevier.com/locate/jmmm

Magnetic and magneto-optical properties of doped and co-doped CdTe with (Mn, Fe): Ab-initio study

A. Ait Raiss [a], Y. Sbai [a], L. Bahmad [a,*], A. Benyoussef [a,b,c]

[a] Laboratory of Magnetism and high-energy physics (LMPHE), Faculty of Sciences, University Mohammed-V, Av. Ibn Batouta, B. P. 1014 Rabat, Morocco
[b] Institute of Nanomaterials and Nanotechnologies, MAScIR, Rabat, Morocco
[c] Hassan II Academy of Science and Technology, Rabat, Morocco

ARTICLE INFO

Article history:
Received 20 December 2014
Received in revised form
14 February 2015
Accepted 27 February 2015
Available online 2 March 2015

Keywords:
Diluted magnetic semiconductors (DMS)
Doped and co-doped CdTe
Ab-initio study
Akai-KKR-CPA method
Density functional theory (DFT)
Density of state (DOS)

ABSTRACT

On the basis of ab-initio calculations performed by the Akai-KKR-CPA method within the spin polarized density functional theory (DFT) and local density approximation (LDA). The magnetic and magneto-optical properties of CdTe doped with Mn and Fe, and co-doped with transitions metals (TM), have been investigated. Moreover, the density of state (DOS) have been calculated and plotted with the energy diagram, for different dopants concentrations. In this work we study, these compounds and compare our theoretical results with the experimental works concerning the doped CdTe. Then we determine which one, Mn or Fe, is responsible of the appearing magnetic and/or optical properties. We also investigate the effect of the co-doping with these elements: Mn and Fe. We show that the iron Fe does not contribute strongly in the magnetism, but it affects the optical properties of the co-doped materials. When comparing our results with the existing experimental works, we found that a low concentration of Fe improves well the magneto-optical properties such as the Faraday rotation. On the other hand, we have investigated the microscopic behavior of electrons by studying their electronic structure and density of states (DOS).

© 2015 Elsevier B.V. All rights reserved.

1. Introduction

The diluted magnetic semiconductors (DMS) are the basis materials for new electronic devices, because of their spintronics due to the electron's spin in addition to its charge. In order to enhance the performance of electronic devices, these new materials are obtained by the substitution of some classical semiconductors, by magnetic elements, and transition metals (TM), such as Co, Ni, Mn and Fe [1]. The doped CdTe is a semiconductor with a wide range of applications in spintronics as reported in Ref. [26]. It is used in Infra-Red detectors, solar cells, visible and Infra-Red lasers [2,3]. The compound CdTe is one of the most studied DMSs in solar cells, and it is distinguished by its high solubility for Mn atoms (as high as 77%) [4,5].

The CdTe is a ferromagnetic material at room temperature, and its high thermal equilibrium stability is motiving a lot of works in this field. So far a lot of works were focused on (Ga,Mn)As, see for example Ref. [6] and references therein, also for ZnO-based diluted magnetic semiconductors, see Refs. [24,25]. But the solubility of 3d transition metals in III–V based DMS is extremely lower than (7–8%) with a Curie temperature up to 160 K. On the other hand and since the solubility of 3D-transiotion metal impurity is lower in semiconductors, we can conclude that the clustering by spinodal nano-decomposition with high-blocking temperature (TB) in the super-paramagnetism Refs. [28,30] and the possibility of controlling the localized spins make them highly appreciated for fundamental studies [7,8]. This is relevant for the magneto-optical materials [9,10]. For the (Cd,Mn)Te system, the heavy hole-related PL spectra were perfectly polarized even at low magnetic field values in the RCP due to the giant Zeeman splitting and were red-shifted with the magnetic field [11]. The Faraday effect was enhanced in the paramagnetic CdMnFeTe film by 10 times to the CdMnTe film at room temperature, and the Faraday-rotation spectrum was found to shift to higher photon energies with decreasing temperature values. In addition, the transparency decreases with the co-doping of $Cd_{1-x}Mn_xTe$ with iron Fe atoms [12]. Theoretical and experimental studies concerning this material were discussed and published [13,14]. As reported in [13], the calculations of total and local magnetic moments have shown that every Mn impurity adds no hole carriers to the perfect ZnTe and CdTe crystals, so that the total magnetic moment is found to be equal at 5 μ_B.

In this paper we will present our calculations about this material doped with Mn, Fe separately and co-doped with both these two elements, for different concentrations. In one hand, we will investigate the role and effect of these doping materials, and

* Corresponding author.
E-mail address: bahmad@fsr.ac.ma (L. Bahmad).

http://dx.doi.org/10.1016/j.jmmm.2015.02.077
0304-8853/© 2015 Elsevier B.V. All rights reserved.

Part two : Results and discussion of magnetic properties and Faraday rotation of CdTe and ZnSe doped with different impurities besides to the vacancy defects

I. Magnetic and Magneto-optical properties of doped and co-doped CdTe with (Mn, Fe): Ab-initio study

1. Introduction

The diluted magnetic semiconductors (DMS) are the basic materials for new electronic devices, because of their spintronics due to the electron's spin in addition to its charge. In order to enhance the performance of electronic devices, these new materials are obtained by the substitution of some classical semiconductors, by magnetic elements, and transition metals (TM), such as Co, Ni, Mn and Fe[83]. The doped CdTe is a semiconductor with a wide range of applications in spintronics.It is used in Infra-Red detectors, solar cells, visible and Infra-Red lasers[84,85]. The compound CdTe is one of the most studied DMSs in solar cells, and it is distinguished by its high solubility for Mn atoms (as high as 77%)[86,87]. The CdTe is a ferromagnetic material at room temperature, and its high thermal equilibrium stability is motiving a lot of works in this field. So far a lot of works were focused on (Ga, Mn), see for example Ref.[88] and references therein. But the solubility of 3d transition metals in III-V based DMS is extremely lower than (7-8%) with Curie temperature up to 160 K, so that the high solubility in II-VI DMS and the possibility of controlling the localized spins make them highly appreciated for fundamental studies[89,90].This is relevant for the magneto-optical materials[91,92]. For the (Cd, Mn)Te system, the heavy hole-related PL spectra were perfectly polarized even at low magnetic field values in the RCP due to the giant Zeeman splitting and were red-shifted with the magnetic field [93]. The Faraday effect was enhanced in the paramagnetic CdMnFeTe film by 10 times to the CdMnTe film at room temperature, and the Faraday-rotation spectrum was found to shift to higher photon energies with decreasing temperature values. In addition, the transparency decreases with the co-doping of $Cd_{1-x}Mn_xTe$ with iron Featoms [94].Theoretical and experimental studies concerning this material were discussed and published[95,96].As reported in [95], the calculations of total and local magnetic moments have shown that every Mn impurity adds no hole carriers to the perfect ZnTe and CdTe crystals, so that the total magnetic moment is found to be equal at $5\mu_B$.

In section I of this chapter, we will present our calculations about CdTe compound doped with Mn,Fe separately then co-doped with both for different concentrations. In one hand, we will investigate the role and effect of these doping materials, and compare with the published results. On the other hand, we will study the effect of the co-doping, giving rise to magneto-optical properties, such as the Faraday rotation, which can be well enhanced by co-doping CdMnTe with Fe. The Faraday rotation is found to be increasing when increasing the

concentration of the iron (Fe)[97]. As said before we performed our calculation whith KKR-CPA method for multiple doping concentrations: $Cd_{1-x}Mn_xTe(x=0.02,0.05,0.07,0.1,0.15,0.2)$, $Cd_{1-y}Fe_yTe(y=0.01,0.02,0.05,0.1,0.2,0.25)andCd_{0.96}Mn_{0.02}Fe_{0.02}Te$,$Cd_{0.93}Mn_{0.02}Fe_{0.05}Te$,$Cd_{0.91}Mn_{0.02}Fe_{0.07}Te$,$Cd_{0.83}Mn_{0.02}Fe_{0.15}Te$, $Cd_{0.93}Mn_{0.05}Fe_{0.02}Te$, $Cd_{0.90}Mn_{0.05}Fe_{0.05}Te$, $Cd_{0.603}Mn_{0.38}Fe_{0.017}Te$,$Cd_{0.582}Mn_{0.38}Fe_{0.038}Te$,$Cd_{0.562}Mn_{0.38}Fe_{0.058}Te$.

2. **Computational method :**

Our calculations were done relying on the density functional theory (DFT) using the KKR-CPA method, which is developed by Akai and Dederichs in treating transition metal alloys [98], with the parametrization of Vosko, Wilk, and Nusair (VWN) [99]. The CPA approximations allow this method to take into consideration the random configurations of the impurity elements during the calculations, which make it one of the most useful in the calculation of magnetic properties and electronic structure. For the ordered and disordered systems, we used the KKR-CPA code MACHIKANEYAMA2002V08 package produced by H. Akai of Osaka University [100]. This code uses the(DFT) combined with the coherent potential approximation(CPA), including the (KKR-CPA-LDA). The Local Density Approximation (LDA) is based on the parameterization given by Moruzzi, Janak and Williams (MJW)[101].The most widely used approximation, in density functional theory(DFT), is the local density approximation LDA. We have used k-points up to 200, so we create our input file with the Zinc-Blende structure of CdTe Cd(48), Te(52). The lattice parameters a=6.48 A^o[102]. $\alpha=\beta=\gamma= 90^o$. with no external magnetic field in each site and taken relativistic effect in consideration by employing the scalar relativistic approximation, the crystal potential is approximated by a muffin-tin potential. The following figure illustrates the unit cell of the studied compound:

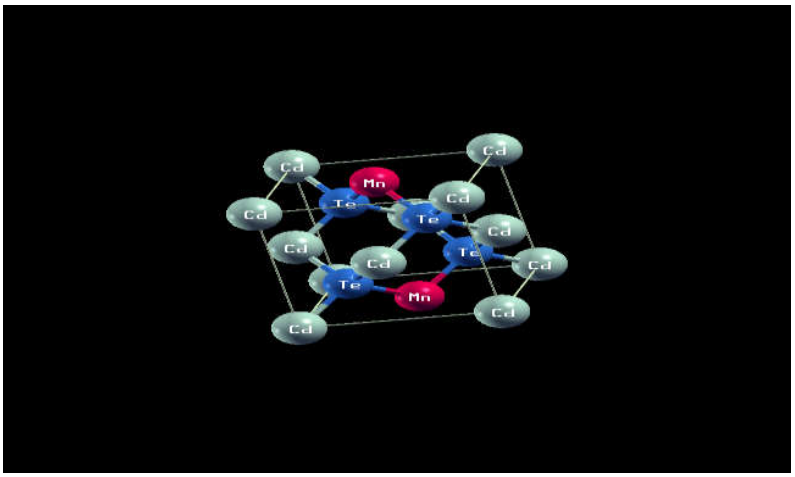

Figure II/I.I.1: The unit cell of CdTe, where the Cd atoms are in (green-grey color) and The Te atoms are in (blue color).

3. **Results and discussion:**

On the basis of the indicated method above, we have determined the electronic structure, and calculate the magnetic moment in order to discuss the magnetic properties. Also, the density of states was plotted for different doping concentrations. First of all, we started our calculation by discussing the pure CdTe. The geometry of the unit cell of CdTe, where the Cd atoms are substituted with magnetic impurities such as Mn, is illustrated above, in Figure II/I.I.1. The atoms of the element (Te) are not substituted in this doping case. From Figure II/I.I.2, when examining the DOS of this pure compound, we found that there is no magnetism appearing in this case. So the doping with magnetic impurities is needed. While, there is a symmetry between the spin up and spin down states, in both valence and conduction bands. the studied material is n-type because the Fermi level is closer to the conduction band which is on the right side. We have found that the band gap is Eg =1.31eV, which is not far from the value found in the literature: Eg=1.45 eV[103], see Figure II/I.I.2.

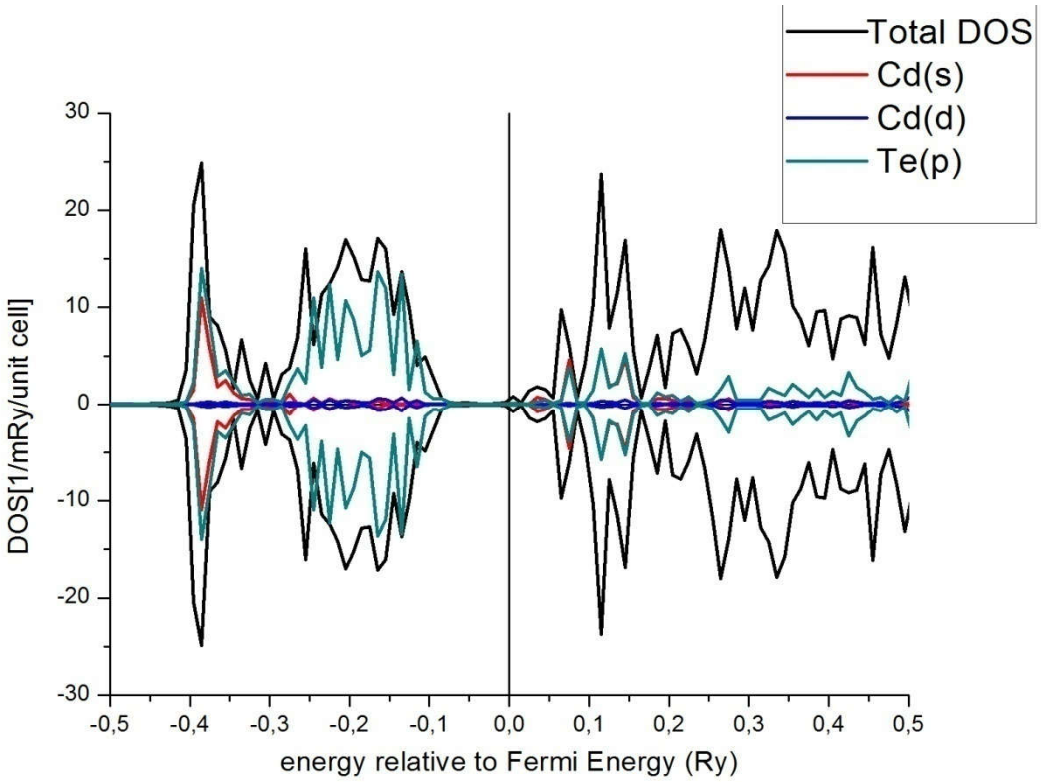

Figure II/I.I.2: The Total DOS and Partial DOS of the pure compound CdTe

Moreover, the diagram of electronic band structure indicates that the gap found by our calculations is a direct one as illustrated in Figure II/I.3:

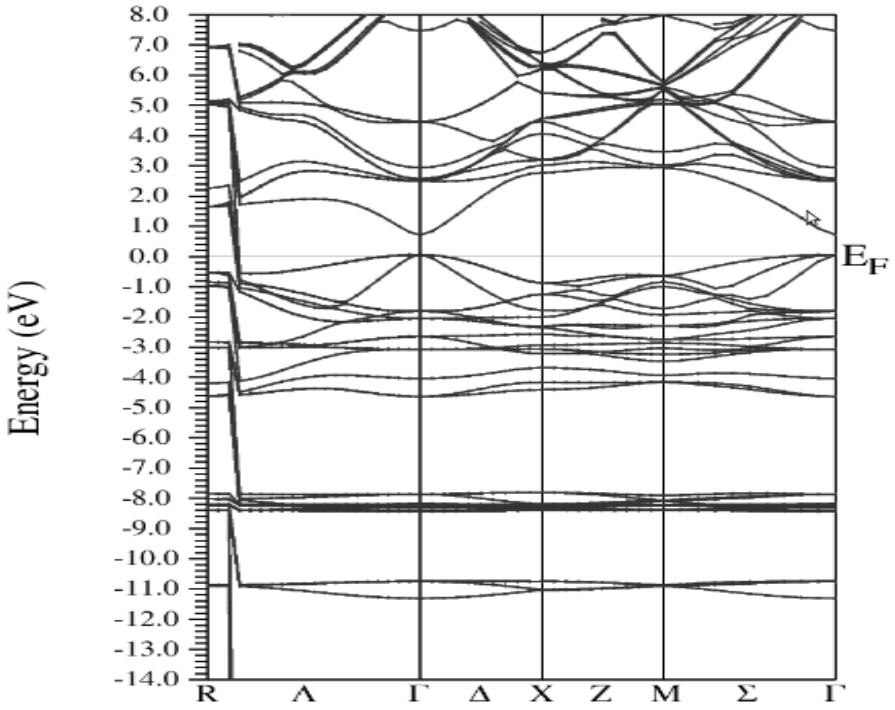

Figure II/I.I.3: The electronic band structure of CdTe.

3.a- CdTe doped with Mn impurity

According to the results of CdTe doped with Mn, see (Figure II/I.I.4), it is found that the substitution of Cd by Mn atoms introduces a magnetic local moment which is due to half-filled d-band. The filled part in the d-band is located in the spin up region, while d-band spin down is completely empty. This finding leads to a ferromagnetic behavior in this alloy, which is stable for all concentrations except for 20% of Mn concentration(Figure II/I.I.4.f). This stability was confirmed by calculating the difference between DLM and ferromagnetic Energy, as illustrated in table II/I.2.The ferromagnetic state is stable when we have ($E_{Ferro} < E_{DLM}$), else the DLM is the stable one. We also observe that there is no spin splitting either in the valence or the conduction band, until 20% of Mn doping, which induces a law spin splitting. Hence, this spin splitting is responsible for the exchange interactions ($N_{0\alpha}$ and $N_{0\beta}$), by referring to the equation given in Ref. [104]:

$$\left(N_{0\alpha} = \frac{\Delta Ec}{x.<S>},\ N_{0\beta} = \frac{\Delta Ev}{x.<S>}\right) \qquad \text{(II/I.I.1)}$$

Where, ΔEc and ΔEv represent the spin splitting of the difference between spin up and spin down in the conduction and valence bands, respectively. While $N_{0\alpha}$ and $N_{0\beta}$), represent the exchange constants in conduction and valence bands, respectively. In addition, it is found that our DMS compound still n-type with Mn doping.

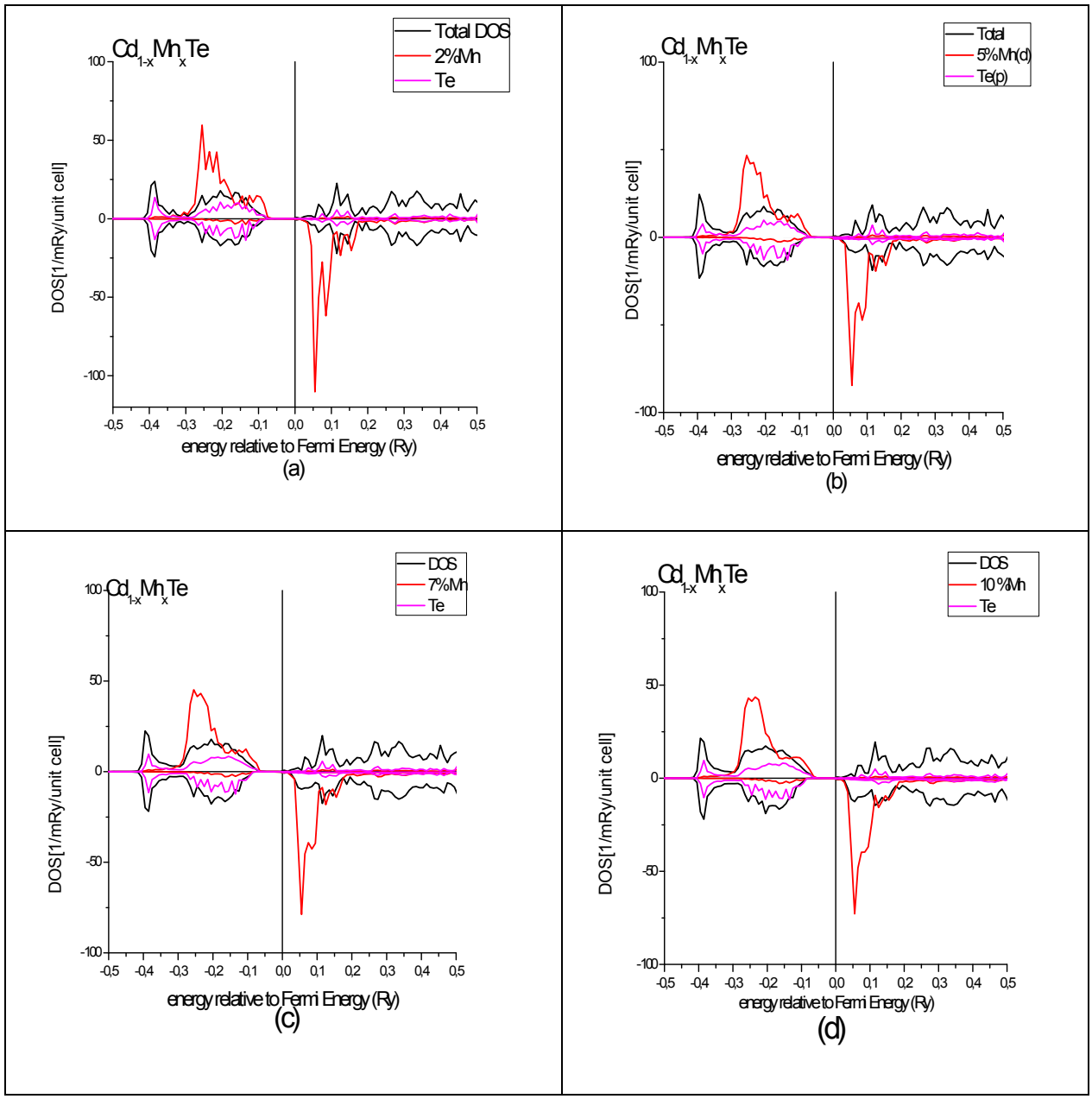

Figure II/I.I.4:Partial DOS of Mn(d) and Te(p) sites in $Cd_{1-x}Mn_xTe$ for different concentrations x.

3.b- CdTe doped with Fe impurity

When doping the CdTe with Fe impurities, we find that the magnetic moment is null until the concentration rate of 25% of Fe (see table II/I.I.1). For other concentrations, our calculations show that the d-band of Fe is located in the valence band, see Figure II/I.I.5(a,b,c,d). So it is filled but not completely filled for (b) case, while some states are unfilled for both spin up and spin down cases. We found that the DMS with Fe doping becomes p-type with high p-d hybridization in the top of the valence band, which means that the exchange interaction, in this case, is a p-d exchange. In Figure II/I.I.5e, we observe that the d-Fe band is moved to the conduction band, so it is completely empty, which can be explained by the transition of electrons to another band. Also, the top of the valence band has shifted to the conduction band which can be explained by the presence of holes in this band, so there is a transition of electrons from this band edge, which let their places as free hole carriers.

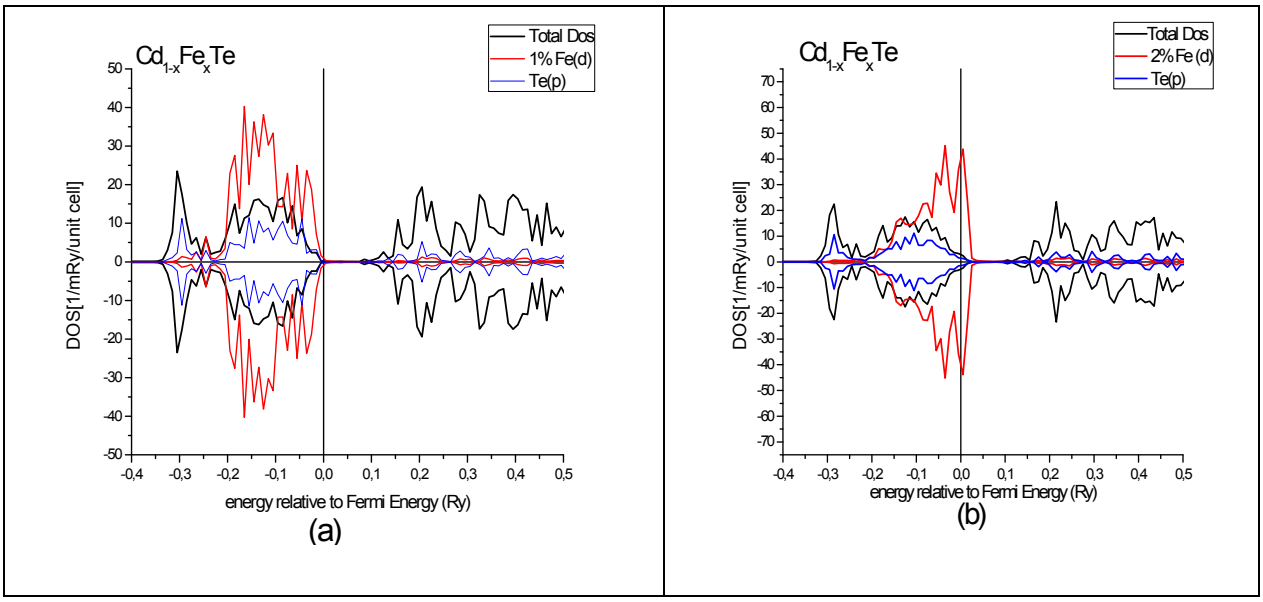

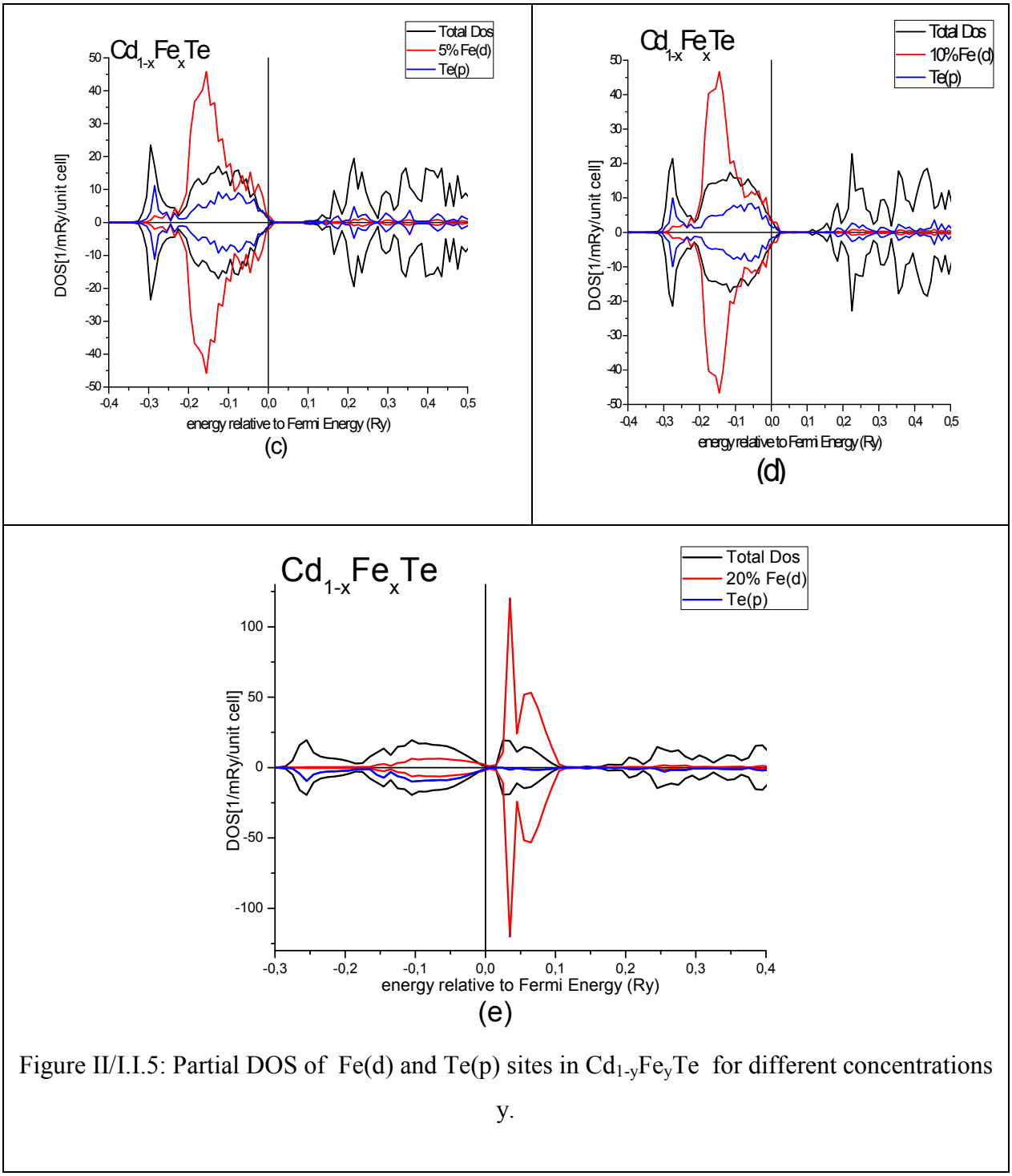

Figure II/I.I.5: Partial DOS of Fe(d) and Te(p) sites in $Cd_{1-y}Fe_yTe$ for different concentrations y.

3.c- CdTe codoped with Mn and Fe impurities

From the Figure II/I.I.6, it is seen that for $Cd_{0.96}Mn_{0.02}Fe_{0.02}Te$ (Figure II/I.I.6.a) and $Cd_{0.93}Mn_{0.02}Fe_{0.05}Te$ (Figure II/I.I.6.b) the Fe band is hybridized with the valence band, also both of spin up and spin down states are filled. While for Mn d-band, the spins up states are

filled and the spins down states are empty. A large gap is shown for this n-type DMS, with no spin splitting, in this case, Figure II/I.I.6.(a,b).

From Figure II/I.I.6.c: ($Cd_{0.83}Mn_{0.02}Fe_{0.15}Te$); Figure II/I.I.6.d : ($Cd_{0.93}Mn_{0.05}Fe_{0.02}Te$); Figure II/I.I.6.f: ($Cd_{0.91}Mn_{0.02}Fe_{0.07}Te$), we observe that the Fe band was shifted to the conduction band. Therefore all of its spin states become empty, and the band gap was decreased, where a strong hybridization between Fe and Mn bands is observed, while the spin splitting is null. In the case of Figure II/I.I.6.e: ($Cd_{0.9}Mn_{0.05}Fe_{0.05}Te$), we observe that Fe d-band still symmetric and lies in the Fermi level, so the majority of spin up states for this band are filled while the minority are empty, and vice-versa for the spin down states. Moreover, a splitting in the conduction band was observed which ensure that there is an interaction in this band which can be estimated by the calculation of exchange constants $N_0\alpha$, using the equation (II/I.I.1).

For the last three cases, in Figure II/I.I.6.g: ($Cd_{0.603}$ $Mn_{0.38}$ $Fe_{0.017}Te$), Figure II/I.I.6.h: ($Cd_{0.582}$ $Mn_{0.38}$ $Fe_{0.038}Te$); Figure II/I.I.6.i: ($Cd_{0.562}$ $Mn_{0.38}$ $Fe_{0.058}Te$), where we choose the same concentrations as an experimental study about magneto-optical properties, especially Faraday rotation [97], we find from those figures that the p-d hybridization is so important between (Te, Mn, Fe). Moreover, we observe that the gap has decreased, which mimics a half-metallic behavior. Furthermore, we observe an important spin splitting which is getting larger with the increase of the concentration. Therefore, we conclude that the large spin splitting, is responsible for the enhancement of the Faraday rotation, according to the equation (II/I.I.2) which is valid for large gap DMSs [105].

$$\theta_F = \frac{\sqrt{\mathrm{F0}}\,\mathrm{d}}{2\pi\mathrm{c}} . \frac{E^2}{(E_0^2 - E^2)^{3/2}} . N_0(\alpha - \beta).\mathrm{x}. < Sz > \quad \text{(II/I.I.2)}$$

Furthermore, we have found that most of the doping cases are anti-ferromagnetic, see table II/I.I.3. In the disordered local moment (DLM), we forced the half of spins to be up and the other half to be down.

Finally, referring to table II/I.I.2, we can deduce that the ferromagnetic state is not stable in the case of Figure II/I.I.6.(a,b,c,d,e,h), Therefore an anti-ferromagnetic state which takes place. While we observe a stable ferromagnetic state in the case of Figure II/I.I.6.(f,g, i).

Besides this, in the experimental study it is confirmed by the XRD spectrum, that the crystal structure which is stable in the case of Figure II/I.I.6.(g,h,i) is Zinc blende with the concentration ($Cd_{0.562}$ $Mn_{0.38}$ $Fe_{0.058}Te$), so it is stable also for lower concentrations. Moreover, it was found that the lattice parameter decreases with the increasing of Fe concentration, and the minimal value of the lattice parameter is about 6.417A^{o}, so these results are given in Ref. [97]. From this reference, the Verdet constant variation is calculated for 300K. It is found that if the photon energy increases, the CdTe Verdet constant takes small and positive values. While, the Verdet constant increases when increasing the rate of Fe co-doping, and takes negative values. The Faraday rotation increases with the increasing of Fe concentration, therefore the Verdet constant is responsible for the Faraday rotation behavior. The peak of Faraday rotation for the CdMnFeTe film increases with the decreasing of the temperature, which is reported in another experimental study[106].

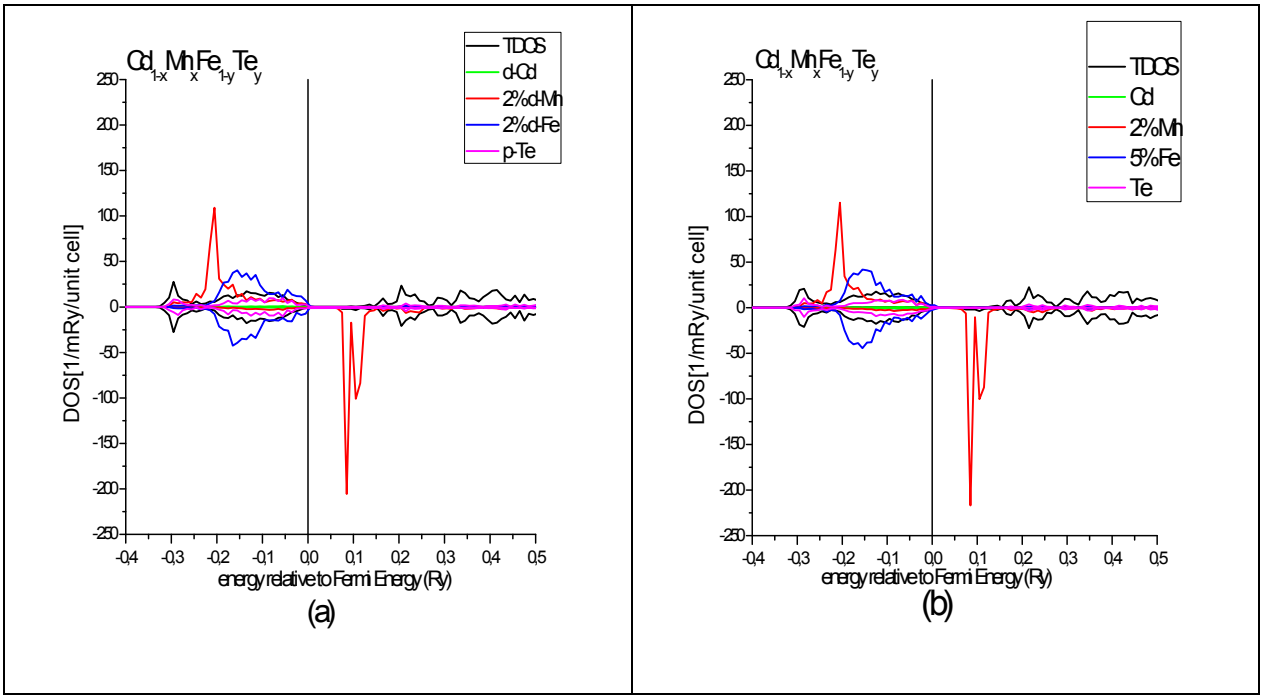

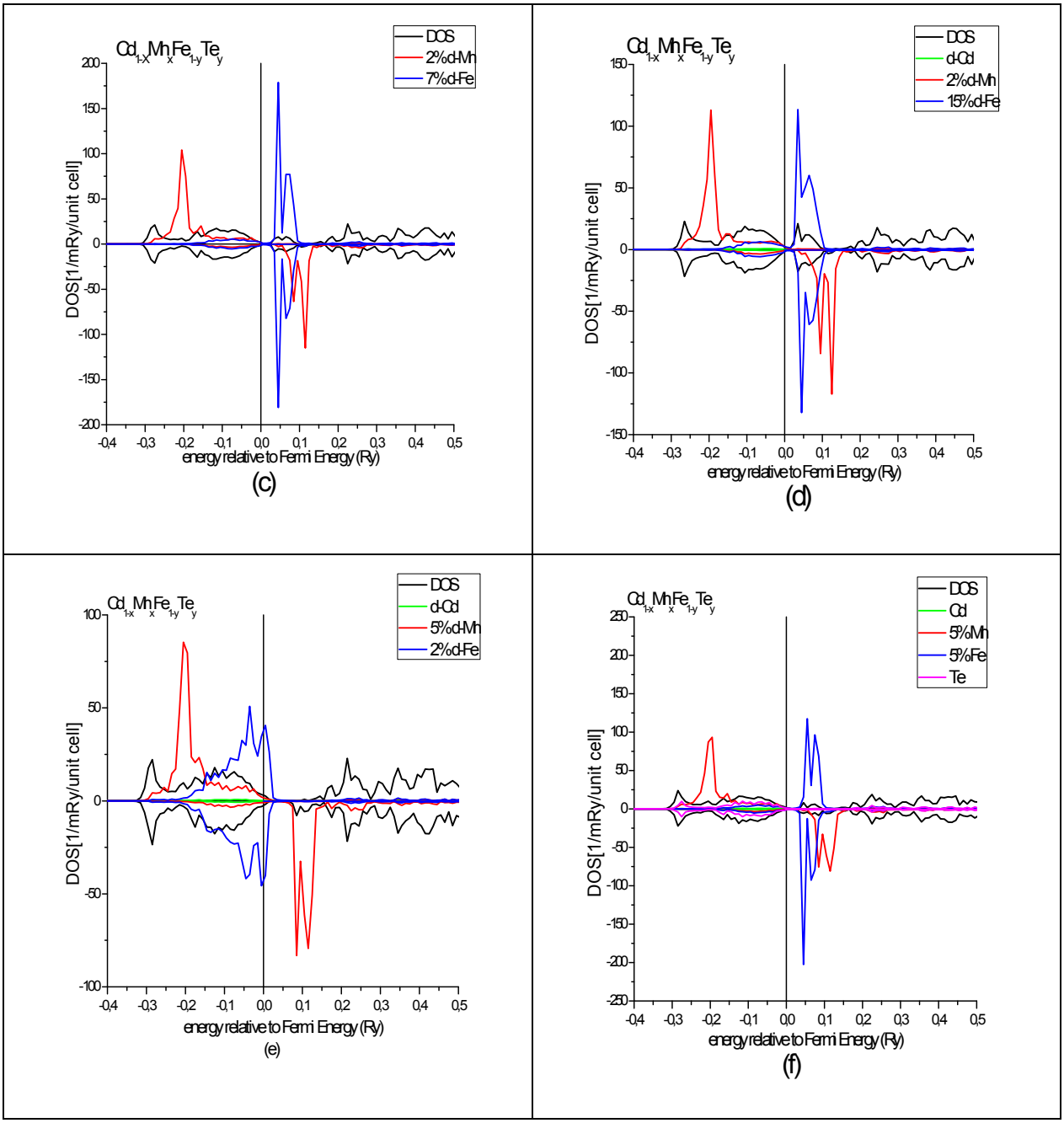
Cd1-xMnxFe1-yTey
DOS
2%d-Mn
7%d-Fe
DOS[1/mRy/unit cell]
energy relative to Fermi Energy (Ry)
(c)
Cd1-xMnxFe1-yTey
DOS
d-Cd
2%d-Mn
15%d-Fe
DOS[1/mRy/unit cell]
energy relative to Fermi Energy (Ry)
(d)
Cd1-xMnxFe1-yTey
DOS
d-Cd
5%d-Mn
2%d-Fe
DOS[1/mRy/unit cell]
energy relative to Fermi Energy (Ry)
(e)
Cd1-xMnxFe1-yTey
DOS
Cd
5%Mn
5%Fe
Te
DOS[1/mRy/unit cell]
energy relative to Fermi Energy (Ry)
(f)

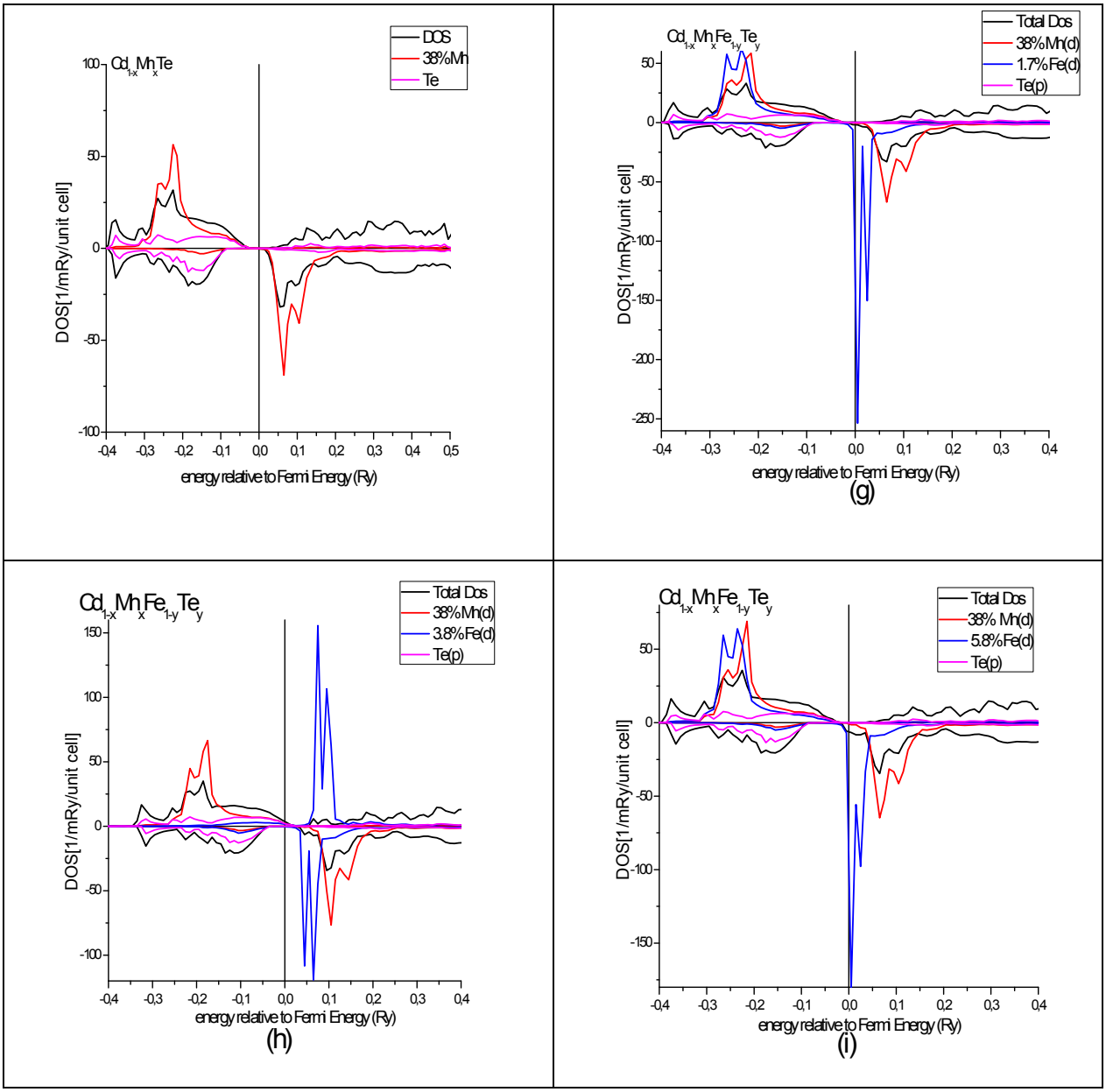

Figure II/I.I.6: Partial DOS of Mn(d), Fe(d) and Te(p) sites in $Cd_{1-x-y}Mn_xFe_yTe$ for different concentrations x and y.

The following table represents the magnetic moment for each site either in the doped or the codoped compound CdTe.

Moment(μ_B) / $Cd_{1-x-y}Mn_xFe_yTe$	Cd	Mn	Fe	Te
$Cd_{0.98}Mn_{0.02}Te$	-0.00094	-4.51187	-	-0.00162
$Cd_{0.95}Mn_{0.05}Te$	0.00223	4.51074	-	0.00453
$Cd_{0.93}Mn_{0.07}Te$	-0.00336	-4.50994	-	-0.00678
$Cd_{0.9}Mn_{0.1}Te$	-0.00486	-4.50844	-	-0.00991

$Cd_{0.85}$ Mn $_{0.15}$Te	0.00730	4.50530	-	0.01531
$Cd_{0.8}Mn_{0.2}$Te	-0.00941	-4.40662	-	-0.03413
$Cd_{0.99}Fe_{0.01}$Te	0	-	0	0
$Cd_{0.98}Fe_{0.02}$Te	0	-	0	0
$Cd_{0.95}Fe_{0.05}$Te	0	-	0	0
$Cd_{0.9}Fe_{0.1}$Te	0	-	0	0
$Cd_{0.8}Fe_{0.2}$Te	0	-	0	0
$Cd_{0.75}Fe_{0.25}$Te	-0.00476	-	-3.61645	-0.04606
$Cd_{0.96}Mn_{0.02}Fe_{0.02}$e	-0.00050	-4.35444	0.01299	0.00037
$Cd_{0.93}Mn_{0.02}Fe_{0.05}$Te	0.00167	-4.29879	0.07886	0.02042
$Cd_{0.83}Mn_{0.02}Fe_{0.15}$Te	-0.00389	-4.36874	-0.10391	-0.02019
$Cd_{0.93}Mn_{0.05}Fe_{0.02}$Te	-0.00205	-4.34599	0.17723	-0.00166
$Cd_{0.9}Mn_{0.05}Fe_{0.05}$Te	-0.00844	-4.40023	-0.02260	-0.04374
$Cd_{0.91}Mn_{0.02}Fe_{0.07}$Te	0.00370	4.36415	0.02196	0.01792
$Cd_{0.603}$ $Mn_{0.38}$ $Fe_{0.017}$Te	0.01779	4.47956	3.59766	0.04773
$Cd_{0.582}$ $Mn_{0.38}$ $Fe_{0.038}$Te	0.02089	4.48075	0.06182	0.10106
$Cd_{0.562}$ $Mn_{0.38}$ $Fe_{0.058}$Te	0.01812	4.47165	3.59783	0.05675

Table II/I.I.1: The magnetic moment of different sites in $Cd_{1-x-y}Mn_xFe_yTe$.

The following tables II/I.I.2 and II/I.I.3, represent the difference in Energy for $Cd_{1-x}Mn_xTe$ and $Cd_{1-x-y}Mn_xFe_yTe$ doping cases.

$Cd_{1-x}Mn_xTe$	E_{Ferro}(Ry)	E_{DLM}(Ry)	E_{DLM}- E_{Ferro} (Ry)
Cd0.98Mn0.02Te	-24579.0802618	-24579.0796799	0.0005819 (FM)
Cd0.95Mn0.05Te	-24313.0954975	-24313.0949768	0.0005207 (FM)
Cd0.93Mn0.07Te	-24135.7725001	-24135.7718558	0.0006443 (FM)
Cd0.9Mn0.1Te	-23869.7880623	-23869.7872243	0.000838 (FM)
Cd0.85Mn0.15Te	-23426.4808804	-23426.4797694	0.001111 (FM)
	-22983.1931535	-22983.1945520	-0.0013985 (DLM)

Cd0.8Mn0.2Te			
Cd0.62Mn0.38Te	-21387.2670222	-21387.2665341	0.0004881 (FM)

Table II/I.I.2: Values of ferromagnetic and DLM energy for different Mn doping concentrations.

$Cd_{1-x-y}Mn_xFe_yTe$	E_{Ferro}(Ry)	E_{DLM}(Ry)	E_{DLM}- E_{Ferro} (Ry)
Cd0.98Mn0.02Fe0.02Te	-24406.3357603	-24406.3365293	-0.000769 (DLM)
Cd0.93Mn0.02Fe0.05Te	-24147.1869812	-24147.1871636	-0.0001824 (DLM)
Cd0.91Mn0.02Fe0.07Te	-23974.4231493	-23974.4232636	-0.0001143 (DLM)
Cd0.83Mn0.02Fe0.15Te	-23283.3690751	-23283.3694046	-0.0003295 (DLM)
Cd0.93Mn0.05Fe0.02Te	-24140.3508671	-24140.3513463	-0.0004792 (DLM)
Cd0.9Mn0.05Fe0.05Te	-23881.2033017	-23881.2032779	0.0000238 (FM)
Cd0.603Mn0.38Fe0.017Te	-21240.4182822	-21240.4177941	0.0004881 (FM)
Cd0.582Mn0.38Fe0.038Te	-21059.0151302	-21059.0162480	-0.0011178 (DLM)
Cd0.562Mn0.38Fe0.058Te	-20886.2532010	-20886.2528125	0.0003885 (FM)

Table II/I.I.3: Values of ferromagnetic and DLM energy for different (Mn, Fe) co-doping concentrations.

J Supercond Nov Magn
DOI 10.1007/s10948-015-3179-2

ORIGINAL PAPER

Study of the Magnetic Properties of $CdMnTe_{1-y}N_y$ and CdMnTe with Defects by Ab Initio Calculations

A. Ait Raiss[1] · Y. Sbai[1] · Z. Zarhri[1] · L. Bahmad[1] · A. Benyoussef[1,2,3]

Received: 11 June 2015 / Accepted: 23 July 2015
© Springer Science+Business Media New York 2015

Abstract We performed ab initio calculations to investigate the effect of the doping in $CdMnTe_{1-y}N_y$ and also of the defects in CdMnTe alloy. Moreover, we studied the magnetic properties in the both cases. Our calculations were carried out using the Akai-Korringa-Kohn-Rostoker method combined with coherent potential approximation (KKR-CPA) within the spin-polarized density functional theory (DFT) and local density approximation (LDA). The density of state (DOS) has also been calculated for different dopants and defect concentrations. The compound $Cd_{1-x}Mn_{x=0.38}Te$ is the diluted magnetic semiconductor (DMS) we studied in one of our earlier works (Ait Raiss, A. et al., doi:10.1016/j.jmmm.2015.02.077). The p-band of the doping with nitrogen (N) atoms lies in the Fermi level, which is similar to the half-metallic behavior. The stabilized magnetic state in all these concentrations is the disordered local moment (DLM) state. The defect effect depends on their positions, either these defects are in the Cd sites or in telluride (Te) sites. In the both cases, we obtained different stable magnetic states. These states are either ferromagnetic or DLM ones. We also examined the effect of the N doping atoms on the Faraday rotation as a magneto-optical property of CdMnTe.

Keywords Ab initio study · Akai-KKR-CPA method · CdMnTe doping · Magnetic properties · DFT · DOS

1 Introduction

Recently, the spintronic is one of the most interesting fields of research; so, it covers the relation between the electron and its charge, for developing and inventing new electronic devices, based on diluted magnetic semiconductors (DMSs), in order to enhance the efficiency and the capacity of different electronic materials [1]. So, those DMSs are obtained by substituting some elements of the host material by magnetic impurities, such as:

Mn, Ni, Fe, Co, etc. [2]. So, the host material of our alloy is CdTe, which is used in a wide range of applications in spintronics and also in optic solar cells, infrared detectors, and magneto-optical devices [3–5]. The CdTe compound is characterized by its belonging to the II–IV DMS group, which makes it one of the most studied and used materials in the domain of solar cells, thanks to its high solubility for Mn impurities which is close to an important value (as higher as 77 %) for II–IV DMSs [6, 7].

The CdTe-based DMS doped with Mn impurities is presented in a lot of works to be a ferromagnetic material, and it is characterized by its high thermal equilibrium stability, which makes it one of the most studied materials in different fields, so a lot of works were focused on this material especially in the field of solar cells. We can also find that a lot of works were interested in III–V DMSs

✉ A. Ait Raiss
aitraiss.abderrahim@gmail.com

[1] Laboratory of Magnetism and High-Energy Physics (LMPHE-URAC 12), Faculty of Sciences, University Mohammed V, Av. Ibn Batouta, 1014 Rabat, Morocco

[2] Institute of Nanomaterials and Nanotechnologies, MAScIR, Rabat, Morocco

[3] Hassan II Academy of Science and Technology, Rabat, Morocco

Published online: 13 August 2015

II. Study of the magnetic properties of $CdMnTe_{1-y}N_y$ and CdMnTe with defects by Ab initio calculations

II.1. Introduction

In this section, we will present our calculations about the CdTe material doped with a fixed concentration of Mn ($Cd_{0.062}Mn_{0.38}Te$), and we will dope it by substituting Te atoms by Nitrogen atoms (N) for different concentrations, and we will observe the effect of this doping and discuss the results. Then, we will introduce defects in this material, by creating vacancy defects either in Ga sites or Te sites, after that we will discuss the results, and investigate the effect of these defects on the magnetic properties and electronic structure. So as said before, our calculations were performed by KKR-CPA method for multiple doping and defects concentrations, which is illustrated below, in the plotted graphs of the density of states (DOS).

II.2. Results and discussion

II.2.a- case of $Cd_{0.62}Mn_{0.38}Te$

First of all, we start by presenting the host material of our work which is $Cd_{0.62}Mn_{0.38}Te$, we found that its magnetic state is ferromagnetic stable (E_{DLM}-E_{ferro}=-21387.2665341-(-21387.2670222) = 0.0004881 Ry>0). The plotted DOSs are illustrated in Figure II/I.II.1, where the spins up are filled, while the spins down are empty, with a spin splitting in the valence band ($\Delta Ev \neq 0$). This means that there is a Faraday effect appearing. Moreover, we have a strong hybridization between the magnetic spin up d-band and the edge of the valence band. The crystal filled is null because e and t_2 bands are not split. Furthermore, the gap for spin up was decreased because of the shifting of the valence band spins up towards the conduction band. This is due to the strong p-d hybridization between the valence band and the magnetic impurities.

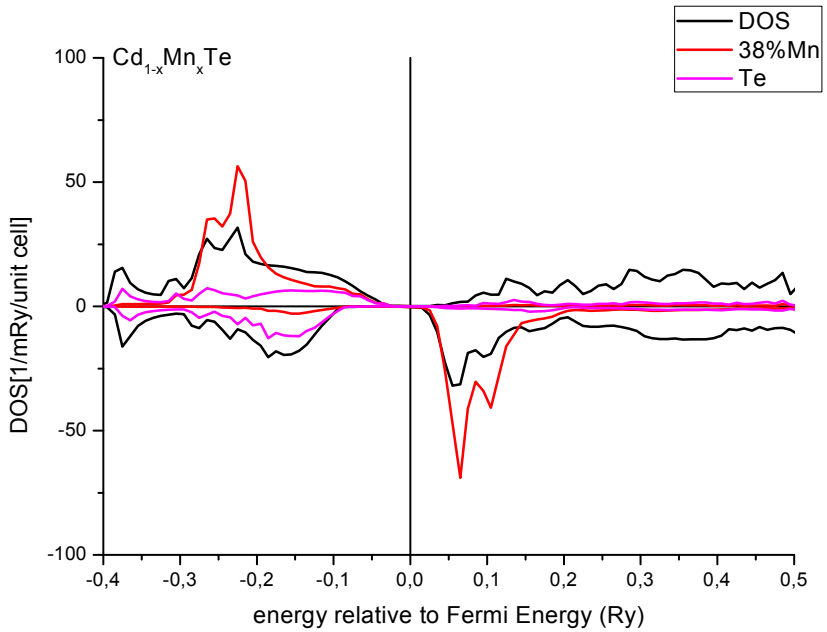

Figure II/I.II.1: Partial DOS of Mn(d) and Te(p) sites for $Cd_{1-x}Mn_x$ Te ,with x=0.38.

II.2.b- case of $Cd_{0.62}Mn_{0.38}Te$ co-doped with Nitrogen (N)

Concerning the co-doping with N atoms instead of Te atoms, there is no spin splitting in the valence and the conduction bands, so $N_{0\alpha} = N_{0\beta}=0$, refering to the equation (II/I.I.1), Ref.[107] Therefore, the Faraday rotation is null, according to the equation (II/I.2), Ref[108]. Thus, we have investigated that the magneto-optical property which is Faraday rotation is negatively affected by this type doping. In addition, the Nitrogen p-band lies around the Fermi level, so it shows a peak in it. This peak gives a half-metallic caracter to the studied compound, which make it as a conductor for spin up electrons, and as an insulator for spin down electrons. in addition, the peaks of magnetic impurities (Mn) decreases then increases when N concentration becomes higher, when we increase the N concentration, the splitting between e and t_2 becomes weak and the peak of N decreases and gets larger, which means that we have a double exchange interactions in this case . We also find that all the concentrations studied for this N doping are not ferromagnetic stable according to the difference in energies, see Table II/II.2. Moreover, we observe that the gap in this co-doping is almost canceled, without an important splitting neither in valance band nor in conduction band, see Figure II/I.II.2.

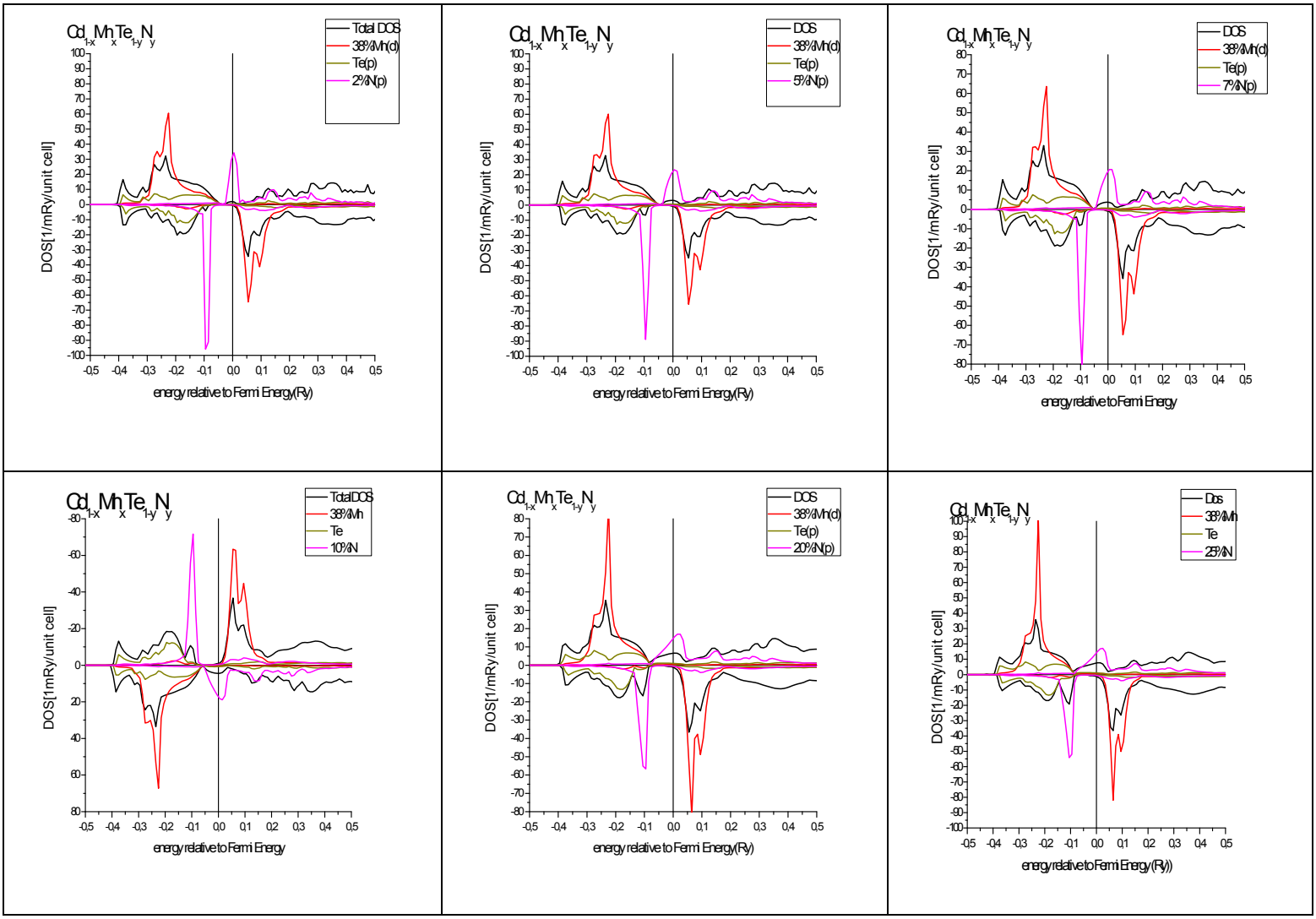

Figure II/I.II.2: Partial DOS of Mn(d) ,Te(p) and N(p) sites for $Cd_{0.62-y}Mn_{0.38}N_y$ for different concentrations of y.

Moment(μ_B) / $Cd_{0.62}Mn_{0.038}Te_{1-y}N_y$	Cd	Mn	Te	N
$Cd_{0.62}Mn_{0.38}Te_{0.98}N_{0.02}$	-0.02028	-4.49306	-0.04273	1.35474
$Cd_{0.62}Mn_{0.38}Te_{0.95}N_{0.05}$	-0.02378	-4.50170	-0.04202	1.37655
$Cd_{0.62}Mn_{0.38}Te_{0.93}N_{0.07}$	-0.02605	-4.50260	-0.04141	1.38032
$Cd_{0.62}Mn_{0.38}Te_{0.9}N_{0.1}$	-0.02954	-4.51179	-0.04156	1.39647
$Cd_{0.62}Mn_{0.38}Te_{0.8}N_{0.2}$	-0.04087	-4.54239	-0.04358	1.39889
$Cd_{0.62}Mn_{0.38}Te_{0.75}N_{0.25}$	-0.04576	-4.55746	-0.04479	1.39650

Table II/I.II.1: magnetic moments for different sites of $Cd_{0.62}Mn_{0.038}Te_{1-y}N_y$

$Cd_{0.62}Mn_{0.38}Te_{1-y}N_y$	E_{Ferro}(Ry)	E_{DLM}(Ry)	E_{DLM}- E_{Ferro} (Ry)
$Cd_{0.62}Mn_{0.38}Te_{0.98}N_{0.02}$	-21117.8732341	-21117.8752797	-0.0020456
$Cd_{0.62}Mn_{0.38}Te_{0.95}N_{0.05}$	-20713.7865282	-20713.7883450	-0.0018168
$Cd_{0.62}Mn_{0.38}Te_{0.93}N_{0.07}$	-20444.3961499	-20444.3976805	-0.0015306
$Cd_{0.62}Mn_{0.38}Te_{0.9}N_{0.1}$	-20040.3113196	-20040.3126798	-0.0013602
$Cd_{0.62}Mn_{0.38}Te_{0.8}N_{0.2}$	-18693.3687421	-18693.3694369	-0.0006948
$Cd_{0.62}Mn_{0.38}Te_{0.75}N_{0.25}$	-18019.9012054	-18019.9015430	-0.0003376

Table II/I.II.2: Energy Ferro and Energy DLM for different concentrations of $Cd_{0.62}Mn_{0.38}Te_{1-y}N_y$

II.2.c- case of vacancy defects in Te sites of $Cd_{0.62}Mn_{0.38}Te$

For the defects results, we start by discussing the Figure II/I.II.3, according to the plotted results we observe that it is an n-type DMS, and the d-band (spin up) of Mn becomes completely filled for 0.05 of a vacancy in Te sites. Furthermore, the conduction band is moving to the Fermi level with the increase of the concentration, which means that there is a transition of electrons to this band. Concerning the magnetic behavior, we found that the ferromagnetic behavior is stable just for 0.05 and 0.07, while it is not stable for the rest of concentrations presented in this work, see Table II/I.II.3. Moreover, we can observe that the Mn d-band (spin up) is hybridized with the valence band for all the studied concentrations, as well as the Mn d-band (spin down) with the conduction band. This means that the mechanism of interaction, in this case, is a p-d exchange.

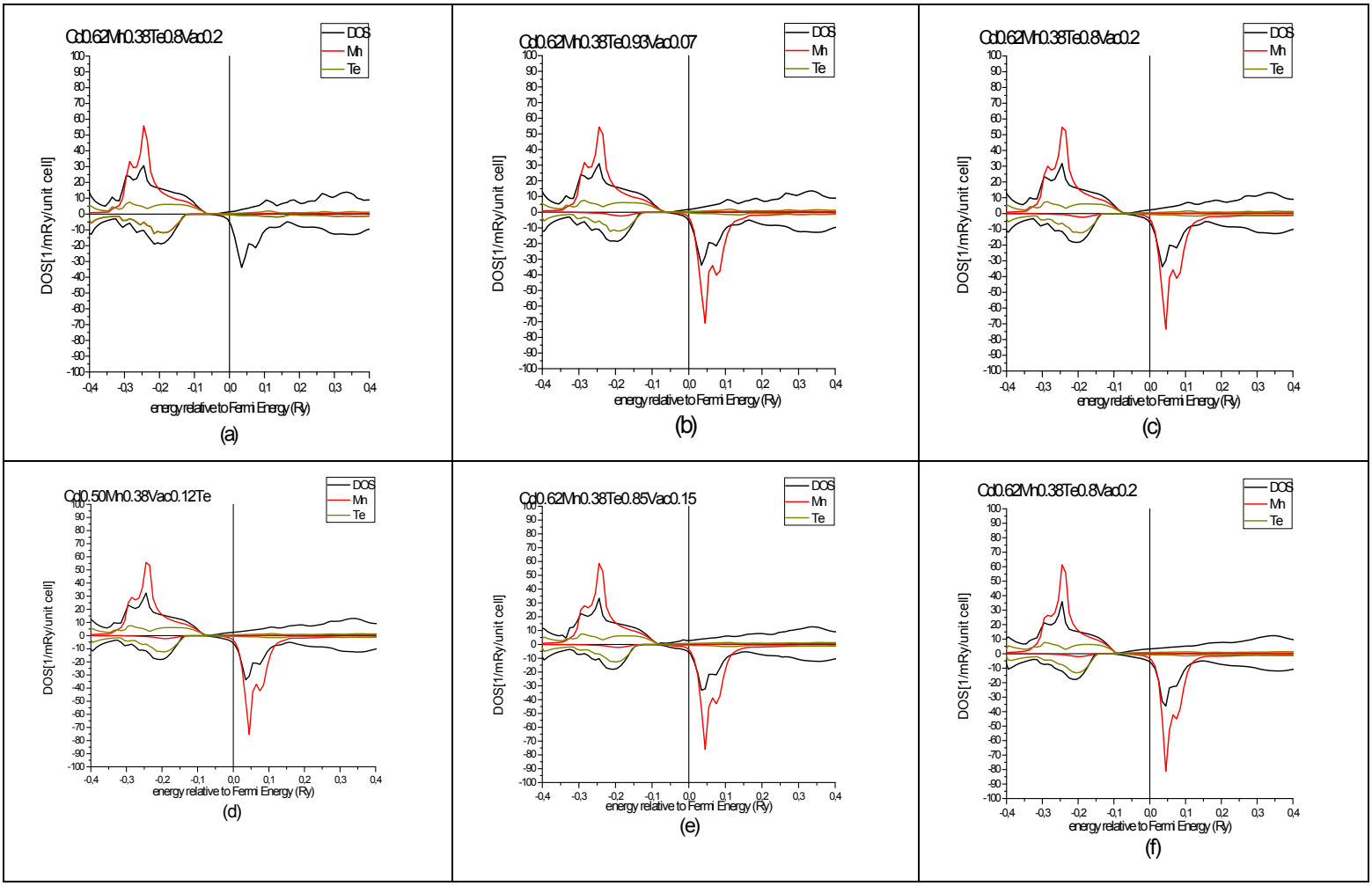

Figure II/I.II.3: Partial DOS of Mn(d) and Te(p) sites for $Cd_{0.62}Mn_{0.38}Te$ with vacancies in Te sites for different concentrations.

$Cd_{0.62}Mn_{0.38}Te_{1-y}Vac_y$	E_{Ferro}(Ry)	E_{DLM}(Ry)	E_{DLM}- E_{Ferro} (Ry)
$Cd_{0.62}Mn_{0.38}Te_{0.95}Vac_{0.05}$	-20708.3533394	-20708.3533379	0.0000015
$Cd_{0.62}Mn_{0.38}Te_{0.93}Vac_{0.07}$	-20436.7906357	-20436.7905706	0.0000651
$Cd_{0.62}Mn_{0.38}Te_{0.90}Vac_{0.10}$	-20029.4470148	-20029.4470424	-0.0000276

$Cd_{0.62}Mn_{0.38}Te_{0.88}Vac_{0.12}$	-19757.8848210	-19757.8849036	-0.0000826
$Cd_{0.62}Mn_{0.38}Te_{0.85}Vac_{0.15}$	-19350.5418350	-19350.5419515	-0.0001165
$Cd_{0.62}Mn_{0.38}Te_{0.80}Vac_{0.20}$	-18671.6374787	-18671.6376194	-0.0001407

Table II/I.II.3: Energy Ferro and Energy DLM for different concentrations of $Cd_{0.62}Mn_{0.38}Te_{1-y}Vac_y$

II.2.d- case of vacancy defects in Cd sites of $Cd_{0.62}Mn_{0.38}Te$

In the case of defects introduced by vacancies in Cd sites (Figure II/I.II.4), we observe that the type of the semiconductor has changed from n to p-type, which mean that the majority carriers, in this case, are the holes. In addition, an important splitting in both of the valence and the conduction band is appearing and increases when increasing the concentration. Besides that, the magnetic behavior in this system is not ferromagnetic for the small concentrations, see Table II/I.II.4. This ferromagnetic state becomes stable since 0.12 of Cd vacant sites. Furthermore, the p-d exchange mechanism is the responsible for the exchange interactions, because there is a strong hybridization between the Mn d-band and the valence band, as well as the conduction band.

For the magnetic moments, we can deduce according to the tables Table II/I.II.1, Table II/I.II.5, Table II/I.II.6 that the other sites are influenced by the magnetic moment of the Mn atoms, which create small magnetic moments in those sites. However, for N codoping, we have investigated and observed that the created moment in N sites is very important, according to Table II/I.II.1.

As a further information, LDA approximation seems to be weak to determine the correct electronic structure, SIC-LDA is very good compared to the photoemission experiments without any adjustable parameters. Ref. [109,110], also the Curie temperature is calculated by LDA and SIC-LDA and there is no much difference between the two approximations as investigated by Toyoda et al.[111].

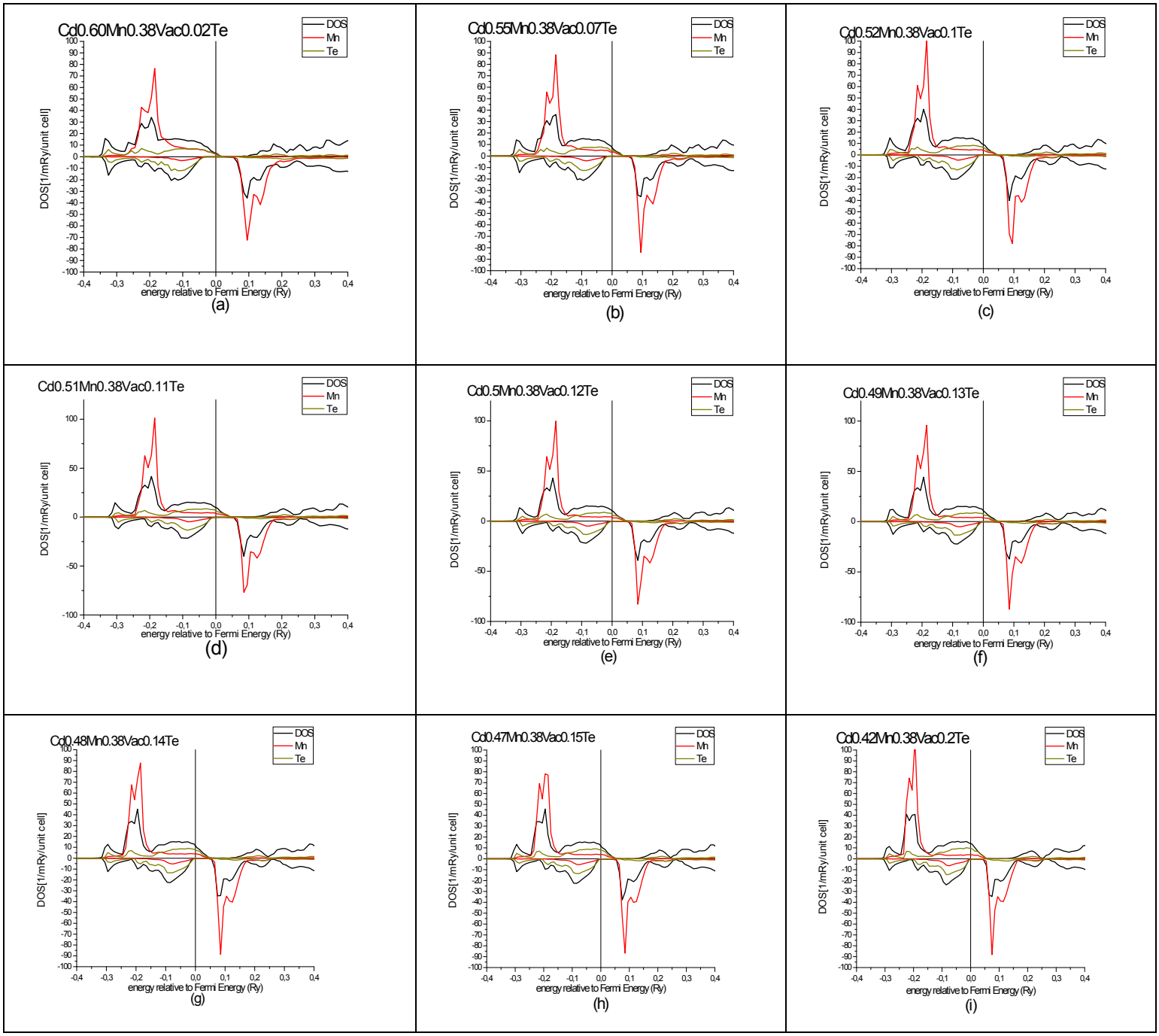

Figure II/I.II.4: Partial DOS of Mn(d) and Te(p) sites for $Cd_{0.62}Mn_{0.38}Te$ with vacancies in Cd sites for different concentrations.

$Cd_{0.62-x}Mn_{0.38}Vac_xTe$	E_{Ferro}(Ry)	E_{DLM}(Ry)	E_{DLM}- E_{Ferro} (Ry)
$Cd_{0.60}Mn_{0.38}Vac_{0.02}Te$	-21163.6715292	-21163.6756741	-0.0041449
$Cd_{0.55}Mn_{0.38}Vac_{0.07}Te$	-20604.6550067	-20604.6561629	-0.0011562
$Cd_{0.52}Mn_{0.38}Vac_{0.1}Te$	-20269.2438950	-20269.2443399	-0.0004449
$Cd_{0.51}Mn_{0.38}Vac_{0.11}Te$	-20157.4403153	-20157.4405137	-0.0001984
$Cd_{0.50}Mn_{0.38}Vac_{0.12}Te$	-20045.6368320	-20045.6367640	0.0000680
$Cd_{0.49}Mn_{0.38}Vac_{0.13}Te$	-19933.8334039	-19933.8331010	0.0003029
$Cd_{0.48}Mn_{0.38}Vac_{0.14}Te$	-19822.0300224	-19822.0295362	0.0004862
$Cd_{0.47}Mn_{0.38}Vac_{0.15}Te$	-19710.2267158	-19710.2260778	0.0006380
$Cd_{0.42}Mn_{0.38}Vac_{0.2}Te$	-19151.2112886	-19151.2099925	0.0012961

Table II/I.II.4: Energy Ferro and Energy DLM for different concentrations of $Cd_{0.62-x}Mn_{0.38}Vac_xTe$

Moment(μ_B) / $Cd_{0.62}Mn_{0.38}Te_{1-y}Vac_y$	Cd	Mn	Te	y=VacTe
$Cd_{0.62}Mn_{0.38}Te_{0.95}Vac_{0.05}$	0.00885	4.48611	0.02791	0.00652
$Cd_{0.62}Mn_{0.38}Te_{0.95}Vac_{0.07}$	-0.00648	-4.48682	-0.02419	-0.00764
$Cd_{0.62}Mn_{0.38}Te_{0.95}Vac_{0.1}$	-0.00385	-4.50114	-0.02009	-0.00871
$Cd_{0.62}Mn_{0.38}Te_{0.95}Vac_{0.12}$	-0.00252	-4.51255	-0.01771	-0.00921
$Cd_{0.62}Mn_{0.38}Te_{0.95}Vac_{0.15}$	-0.00102	-4.53175	-0.01455	-0.00978
$Cd_{0.62}Mn_{0.38}Te_{0.95}Vac_{0.2}$	0.00056	-4.55909	-0.00992	-0.01051

Table II/I.II.5: magnetic moments for different sites of $Cd_{0.62}Mn_{0.38}Te_{1-y}Vac_y$

Moment(μ_B) / $Cd_{0.62-x}Mn_{0.38}\ Vac_xTe$	Cd	Mn	x=VacCd	Te
$Cd_{0.60}Mn_{0.38}Vac_{0.02}Te$	-0.01575	-4.41075	-0.00296	-0.03318
$Cd_{0.55}Mn_{0.38}Vac_{0.07}Te$	- 0.01442	-4.30329	-0.00217	0.01042
$Cd_{0.52}Mn_{0.38}Vac_{0.1}Te$	-0.01375	-4.24921	-0.00157	0.03762
$Cd_{0.52}Mn_{0.38}Vac_{0.11}Te$	0.01351	4.23187	0.00136	-0.04699
$Cd_{0.52}Mn_{0.38}Vac_{0.12}Te$	0.01329	4.21420	0.00116	-0.05662
$Cd_{0.52}Mn_{0.38}Vac_{0.13}Te$	0.01310	4.19619	0.00095	-0.06602
$Cd_{0.52}Mn_{0.38}Vac_{0.14}Te$	0.01293	4.17845	0.00074	-0.07546
$Cd_{0.52}Mn_{0.38}Vac_{0.15}Te$	0.01275	4.16144	0.00054	-0.08494
$Cd_{0.52}Mn_{0.38}Vac_{0.2}Te$	-0.01159	-4.07732	0.00029	0.13418

Table II/I.II.6: magnetic moments for different sites of $Cd_{0.62-x}Mn_{0.38}\ Vac_xTe$

J Supercond Nov Magn
DOI 10.1007/s10948-017-4135-0

ORIGINAL PAPER

Ab Initio Study of the Electronic Structure and Magnetic Properties of Vanadium-Doped CdTe with Vacancy Defects

Abderrahim Ait Raiss[1] · Younes Sbai[1] · Lahoucine Bahmad[1] · Abdelilah Benyoussef[1,2]

Received: 6 April 2017 / Accepted: 12 April 2017
© Springer Science+Business Media New York 2017

Abstract In this paper, we aimed to investigate the effect of vanadium doping on the CdTe compound and also the effect of introducing vacancies in Cd sites, as a type of structural defect. For this purpose, we used the Akai-KKR-CPA method within the spin polarized density functional theory (DFT) with local density approximation (LDA). We performed our calculations on doping CdTe with different concentrations of vanadium, which are 0.05, 0.07, 0.09, and 0.11. Then, we added to each one of them 0.03 and 0.05 of vacancies in Cd sites, in order to examine the effect of the defects on the electronic structure and magnetic properties of the alloy CdTe. We also aimed to check if doping and vacancy defects have any effect on the Faraday rotation and the critical temperature of this material. We have also found that all the studied cases show a half-metallic behavior and have a stable ferromagnetic state. In addition, the critical temperature increases with the increasing of vacancies in Cd sites, especially in the case of adding 0.03 of vacancies. This improves well the ferromagnetic state and ensures its stability up to higher temperatures.

Keywords $Cd_{1-x-y}V_xVac_yTe$ · Ab initio study · Akai-KKR-CPA method · Density functional theory (DFT) · Density of states (DOS)

✉ Abderrahim Ait Raiss
aitraiss.abderrahim@gmail.com

[1] Laboratory of Magnetism and High-Energy Physics (LMPHE), Faculty of Sciences, University Mohammed-V, Av. Ibn Battouta, B. P. 1014, Rabat, Morocco

[2] Hassan II Academy of Science and Technology, Rabat, Morocco

1 Introduction

Diluted magnetic semiconductors (DMS) still have a huge interest from condensed matter physicists, especially in the field of spintronics. The spin electronic is a new electronic which deals with the electron's spin besides its charge. This is to improve and develop a new kind of electronic device, for example the stockage memories. This kind of materials (DMS) can be obtained by substituting some cations of the host material, with magnetic impurities, which are in general, the transition metals (TM), such as Fe, Ni, Mn, and Co [1–4]. The doped CdTe semiconductors have a wide range of applications in the spintronic field [5]. They still remain the most natural candidates for red, blue, and green lasers besides the light-emitting diodes (LED), which are widely used for the production of full color visible optical devices [3, 4]. This material is also used in solar cells, infrared detectors, and visible and infrared lasers [6, 10]. It is considered as one of the most studied DMSs in solar cells, while it is distinguished by its high solubility, especially for Mn atoms (as high as 77%) [7, 8]. CdTe alloy is a wide direct band gap belonging to the group of II–VI semiconductors which is a large family of compounds that have suitable physical properties, for developing electronic and opto-electronic devices. The II–VI semiconductors remain the most natural candidates for red, blue, and green lasers and light-emitting diodes (LED). Furthermore, a lot of studies were focused on (Ga,Mn)As; see for example ref. [9] and references therein. But the solubility of 3d transition metals in III–V-based DMS is found to be extremely lower than 7–8% with a Curie temperature up to 160 K, while the solubility in II–VI DMS and the possibility of controlling the localized spins make them much appreciated for fundamental studies [10, 11]. The studied compound is considered as one of the interesting magneto-optical materials [12–15].

Published online: 24 April 2017

III. Study of electronic structure and magnetic properties of Vanadium doped CdTe with vacancy defects: Ab initio approach

III.1. Introduction

In this section, we will present our calculation on CdTe doped with Vanadium impurity as well as the vacancy defects. Then we will discuss their effect on the magnetic state and the critical temperature of the studied material. So we have doped our material with Vanadium atoms for different concentrations (x). Then we have introduced some vacancies (y) as defects on Cd sites. Therefore, we will discuss the effect of that on the magnetic state and Faraday rotation of the doped CdTe. Then we will compare our results with the published ones. In some works Faraday rotation is found to be improved when doping with Mn and co-doping with Fe impurities, where it is found to be weak and positive, then it changes the sense and increases well when doping with Mn. Where the adding of a weak concentration of Fe atoms, improves this Faraday effect until ten times as reported in first section. Based on the equation(II.I.I.1) and equation(II.I.I.2), cited before, we will study the Faraday rotation while observing the evolution of the spin splitting in the valence and conduction band, which is due to the mobility of carriers between those bands. As said above, our calculations were performed with KKR-CPA method for different doping concentrations:

$Cd_{1-x-y}V_xVac_yTe$ (x= 0.05, 0.07, 0.09, 0.11); (y= 0; 0.03; 0.05) ; Vac(vacancies)

III.2. Results and discussion

III.2.a- case of Vanadium doped CdTe

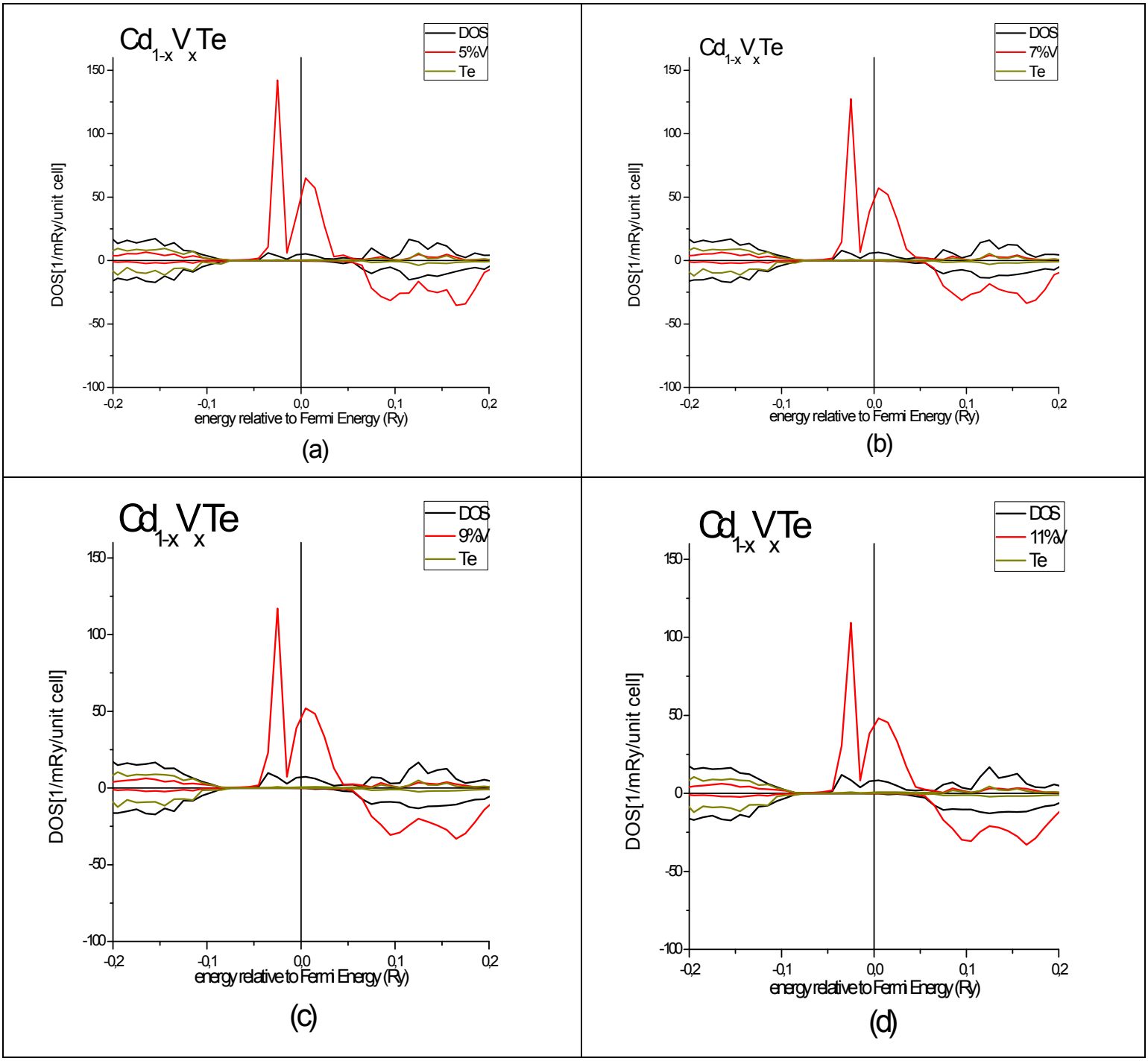

Figure II/I.III.1: Total and Partial DOS of V(d) and Te(p) sites in $Cd_{1-x}V_xTe$ for different concentrations x.

As a result of doping with Vanadium impurity, as illustrated by the Figure II/I.III.1, we have investigated that there is a magnetism appearing when doping with Vanadium atoms (V). This is due to the semi-filled d-bands of the introduced impurity (V) and its location in the band

gap of the material. We can see from the Figure II/I.III.1, that the d-band spins up are separated into two bands, one is called e, which is completely filled, that's why it is located in the valence band. The second band is called t_2 (higher in energy) and it is approximately one third filled, that's why it is located in the gap, which makes from it a bridge between the valence and the conduction band. This gives birth to the half-metallic behavior in our material. For the d-band spin down, we observe that it is empty, while it is located in the conduction band and hybridized with it. In addition, the separation of the d-band spin up into two bands (e and t_2) is due to the crystal field induced in the studied system. We found that when the Vanadium concentrations increases, the e, and t_2 bands are getting wider and shorter, which means that there is a double exchange interaction mechanism between the magnetic elements (Vanadium). Furthermore, after the calculation of the ferromagnetic (FM) and the (disordered local moment) DLM energies, we have found that all those doping cases have a stable ferromagnetic state because the FM energy is lower comparing to DLM energy. The FM and the DLM energies are available in the table Table II/I.III.1, besides to the difference between them. The critical temperatures are given in the same table as well. The semiconductor is still conserving it's n-type, while we observe that there is a splitting between the spins up and spins down in the conduction band (for the total DOS). A part of the split spins up are shifted to the valence band, which means that there are filled. So we have some free electrons in the conduction band, which ensures the n-type of the semiconductor. It's clear from the graphs (Figure II/I.III.1.a, Figure II/I.III.1.b, Figure II/I.III.1.c, and Figure II/I.III.1.d), that the shifting is increasing with the increase of the doping concentration.

$Cd_{1-x}V_xTe$	E_{Ferro}(Ry)	E_{DLM}(Ry)	E_{DLM}- E_{Ferro} (mev)	Tc (K)
$Cd_{0.95}V_{0.05}Te$	-24292.1852682	-24292.1849788	3.93584	608
$Cd_{0.93}V_{0.07}Te$	-24106.4974141	-24106.4970217	5.33664	589
$Cd_{0.91}V_{0.09}Te$	-23920.8095426	-23920.8090276	7.004	602
$Cd_{0.89}V_{0.11}Te$	-23735.1216718	-23735.1210216	8.84272	621

Table II/I.III.1: Values of ferromagnetic and DLM energies for different Vanadium doping concentrations.

III.2.b- case of vacancy defects in Cd sites of Vanadium doped CdTe

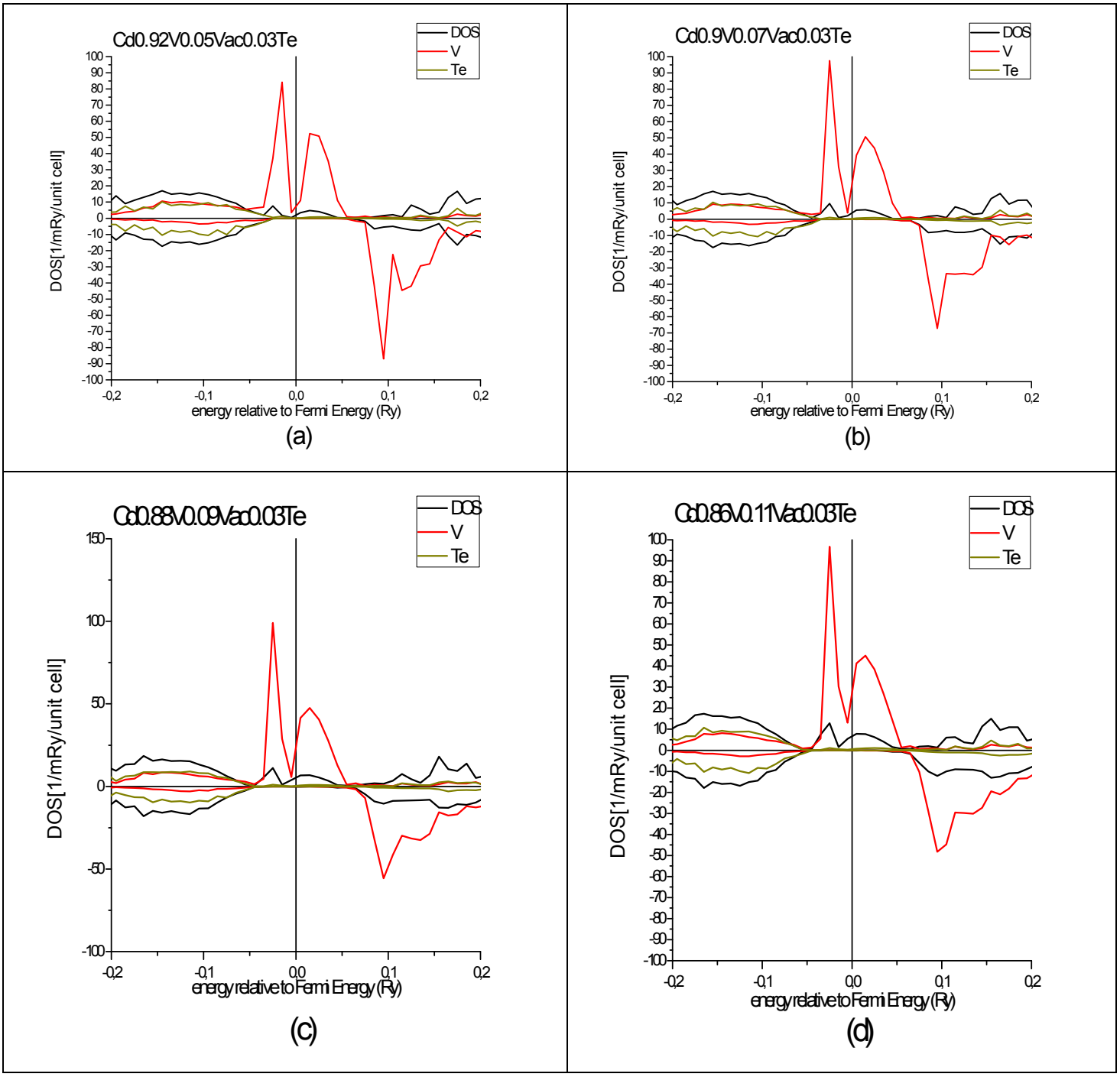

Figure II/I.III.3 : Total and Partial DOS of V(d) and Te(p) sites in $Cd_{1-x-0.03}V_xVac_{0.03}Te$ for different concentrations x.

Concerning the introduction of vacancies as a type of defects in the Cd sites, we move to discuss the Figure II/I.III.3. So in this case, we have investigated that the defects affect the type of the semiconductor, which becomes p-type because the Fermi level is now located near to the valence band. In this case, the free charge carriers are the holes, which can be the responsible for the stability of the ferromagnetic behavior. The part of the valence band spin up, which is shifted to the conduction band, means that the spin up electrons who left their places are the source of the free hole carriers in this case. The studied defects do not affect much the half-metallic behavior, except in the case of introducing 0.03 of vacancies to the CdTe doped with 0.05 of Vanadium atoms (Figure II/I.III.3.a), where the t_2 band has shifted to the conduction band, which mean that there was a transition of electrons from this band. Comparing to the doped case without defects, the introduction of 0.03 of vacancy defects, improves well the ferromagnetic behavior, and also the critical temperatures, which mean that the material can keep this behavior until higher temperatures than the doped case, see Table II/I.III.2.

$Cd_{1-x-0.03}V_xVac_{0.03}Te$	E_{ferro}(Ry)	E_{DLM}(Ry)	E_{DLM}- E_{ferro} (mev)	Tc (K)
$Cd_{0.92}V_{0.05}Vac_{0.03}Te$	-23956.7979535	-23956.7966857	17.24208	2670
$Cd_{0.90}V_{0.07}Vac_{0.03}Te$	-23771.1057469	-23771.1044679	17.3944	1920
$Cd_{0.88}V_{0.09}Vac_{0.03}Te$	-23585.4152145	-23585.4139045	17.816	1530
$Cd_{0.86}V_{0.11}Vac_{0.03}Te$	-23399.7252357	-23399.7238268	19.16104	1350

Table II/I.III.2: Values of ferromagnetic and DLM energies for different Vanadium doping concentrations with 0.03 of vacancy defects.

The Figure II/I.III.4, illustrates the case of making 0.05 of vacancy defects in Cd sites of the doped compound. The graphs (Figure II/I.III.4.a, Figure II/I.III.4.b, Figure II/I.III.4.c, and Figure II/III.4.d) show that the shifting of the valence band and the d-band has increased compared to the case of 0.03 of vacancy defects. Also, the e band is the responsible of ensuring the half-metallic behavior in the case of $Cd_{0.90}V_{0.05}Vac_{0.05}Te$ and $Cd_{0.88}V_{0.07}Vac_{0.05}Te$ (e lies on Fermi level). While for the case of $Cd_{0.86}V_{0.09}Vac_{0.05}Te$, the e is filled, where the t_2 is empty. So we lose the half-metallic behavior in this case. The ferromagnetic state is not affected, but the critical temperature becomes smaller than the case of 0.03 of vacancy defects, see Table II/I.III.3.

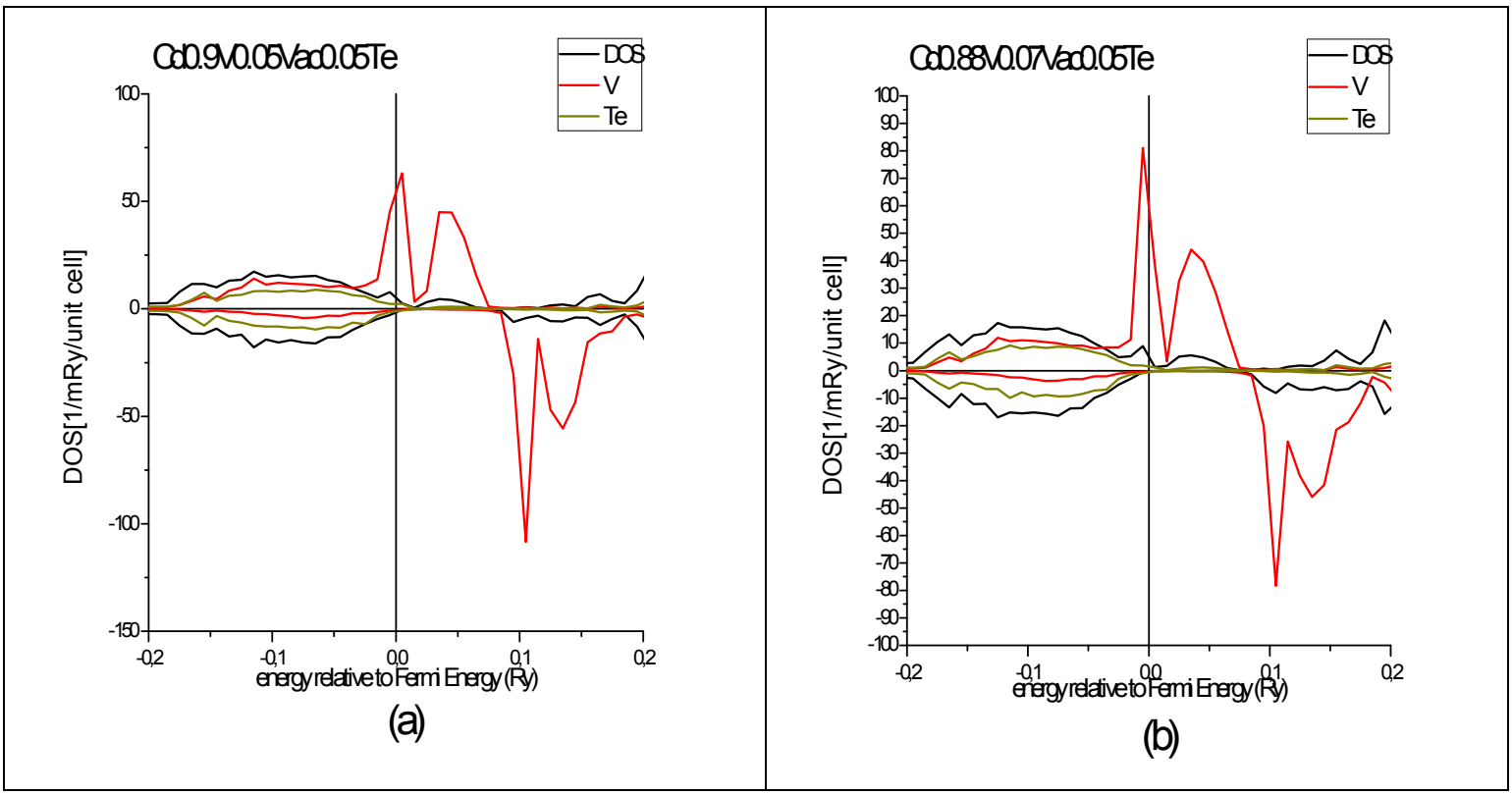

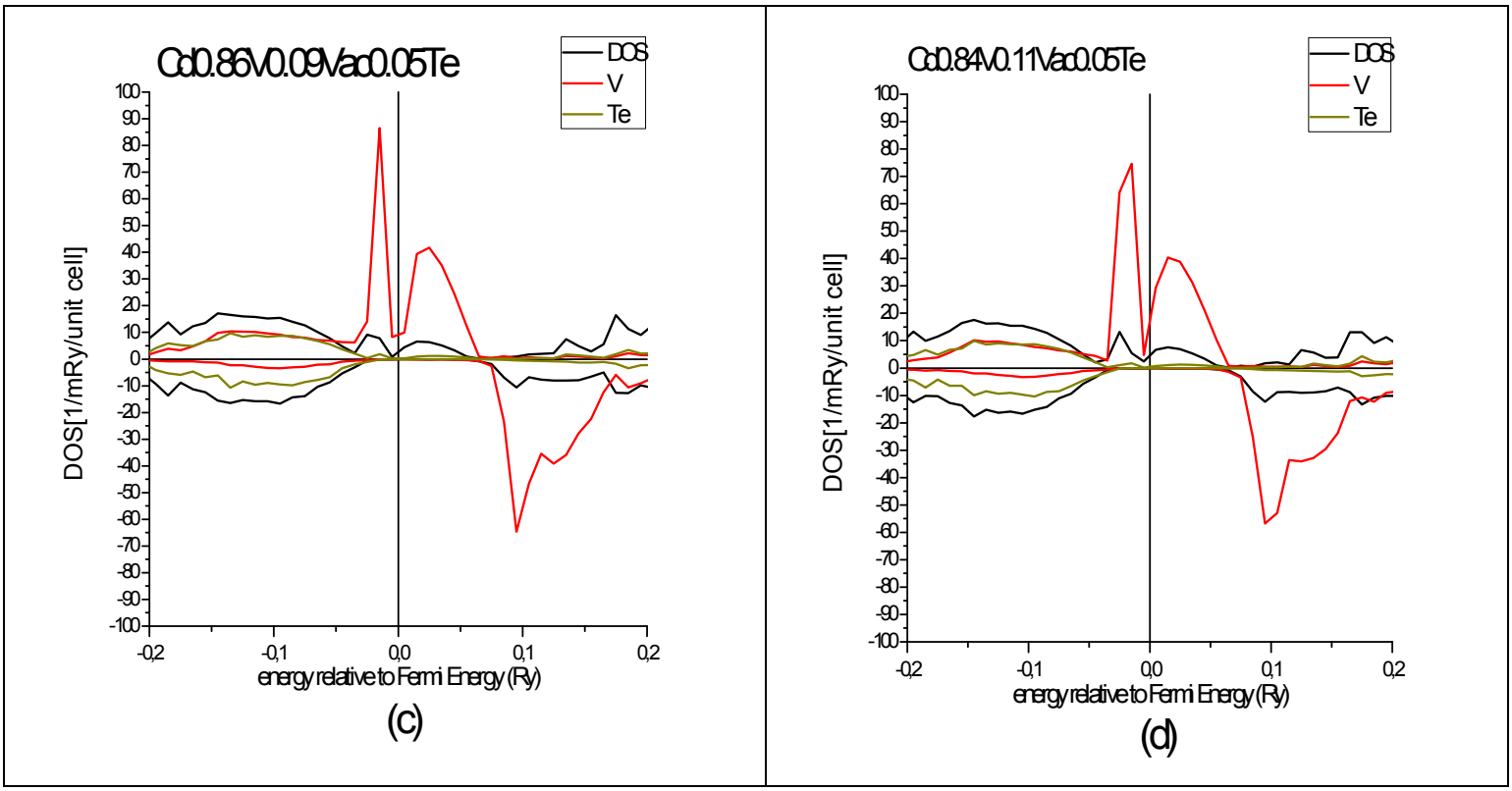

Figure II/III.4 : Total and Partial DOS of V(d) and Te(p) sites in $Cd_{1-x-0.05}V_xVac_{0.05}Te$ for different concentrations x.

$Cd_{1-x-0.05}V_xVac_{0.05}Te$	E_{Ferro}(Ry)	E_{DLM}(Ry)	E_{DLM}- E_{Ferro} (mev)	Tc (K)
$Cd_{0.90}V_{0.05}Vac_{0.05}Te$	-23733.2016813	-23733.2014209	3.54144	547
$Cd_{0.88}V_{0.07}Vac_{0.05}Te$	-23547.5115038	-23547.5109049	8.14504	899
$Cd_{0.86}V_{0.09}Vac_{0.05}Te$	-23361.8172956	-23361.8153209	26.85592	2310
$Cd_{0.84}V_{0.11}Vac_{0.05}Te$	-23176.1262938	-23176.1244636	24.89072	1750

Table II/I.III.3: Values of ferromagnetic and DLM energies for different Vanadium doping concentrations with 0.05 of vacancy defects

III.2.c- discussion of Faraday rotation

To discuss the Faraday rotation property, we will discuss the following equations:

$$\left(N_0\alpha = \frac{\Delta Ec}{x.<S>}, N_0\beta = \frac{\Delta Ev}{x.<S>} \right) \qquad \text{(II/I.I.1)}$$

$$\Theta_F = \frac{\sqrt{F0}\,d}{2\pi c}.\frac{E^2}{(E_0^2-E^2)^{3/2}}.N_0(\alpha-\beta).x.<Sz> \quad \text{(II/I.I.2)}$$

The first one, which is the equation (II/I.I.1), represents the relation between the splitting ΔEc, ΔEv and the exchange interactions $N_0\alpha, N_0\beta$, respectively in the conduction and the valence bands[112].While the equation (II/I.I.2)represents the relation between the Faraday rotation and the exchange interactions constants ($N_0\alpha, N_0\beta$), where F_0, is a constant, E is the photon energy, E_0, is the exciton energy, and d is the sample thickness. So Θ_F, is proportional to the value of the concentrations of doping x, and $N_0(\alpha-\beta)$[113]. To explain the Faraday rotation effect in our case, we will discuss the splitting ΔEc and ΔEv for the pure CdTe, then the doped one, besides to the case of vacancy defects. So for the pure compound, it is evident to see that there is no splitting between the spins up and spins down in both the valence and the conduction bands. For the doped case, see Figure II/I.III.1, we found out that there is a splitting between the spins up and spins down in the conduction band (ΔEc≠0), so the exchange interactions $N_0\alpha$, are the responsibe of the Faraday rotation in this case. While for the case of adding vacancies, see Figure II/I.III.3 and Figure II/I.III.4, we observe that ΔEc is weak, while the splitting in the valence band(ΔEv), appears and becomes higher than ΔEc. This means that the exchange interactions $N_0\beta$, affect the Faraday rotation and improve it, either in the positive or in the negative sense. Therefore, the vacancy defects improve the magnetic state and affect the Faraday rotation , affecting the exchange interactions ($N_0\alpha, N_0\beta$).

IV. Conclusion

In section I of this chapter, we have studied the effect of Mn and Fe in the doped and co-doped CdTe with different concentrations, so we have investigated that Mn-doped CdTe, almost present a stable ferromagnetic state, according to the rate of concentrations, while it conserves the n-type as the pure CdTe. In the other hand, we have found that in the Fe doping case, the DMS present a null moment (table II/I.I.1) for all the studied concentrations. We also found that the Fe doping changes the type of the studied compound, from n-type to p-type. In addition, for the co-doping case we have investigated that the ferromagnetic state is stable for the case of Figure II/I.I.6.(f,g,i), While the Faraday rotation is enhanced by increasing the concentration of Fe keeping the concentration of Mn at (38%). in this case, an important spin splitting was observed, which is due to p-d exchange interactions between spins and ions. it is concluded that the Faraday rotation is enhanced by the exchange interactions between Mn and Fe ions[24]. Furthermore, it is remarked that the local magnetic moment of Mn reduces from its free space charge value of $5\mu_B$[13] to around $\pm 4\ \mu_B$ due to p–d hybridization and produces small local magnetic moments on the nonmagnetic Cd and Te sites.

In section II, we present our calculations about the co-doping with N and the defects by introducing vacancies in Cd and Te sites. we have controlled the vacancy positions, in one hand it's in the cation (Cd sites) and in the other hand it's in the anion (Te sites). We recommend that this kind of co-doping is not suitable in seeking ferromagnetic DMSs, because N doping transforms the ferromagnetic state to a DLM state, for the case of 0.05, 0.07 and 0.1 [116]. We have found out the that all the studied concentrations of N co-doping show a DLM stable state. However, just 0.05 and 0.07 which shows this stability in the case of Te vacancy defects. Furthermore, the ferromagnetic state becomes stable for the case of Cd vacancies from the concentration of 0.12. For Spintronic devices where Ferromagnetic materials are required, CdMnTe with vacancy defects in the cation sites (Cd) can be useful and interesting when the rate of vacancy defects is above 0.12. Therefore, it is recommended to avoid the co-doping with N atoms.

As a conclusion for the section III, we have investigated that doping CdTe with the Vanadium impurity (V) for the concentrations (0.05; 0.07; 0.09; 0.11), shows a half-metallic behavior,

and stabilizes the ferromagnetic state for all those concentrations. Also, we have calculated the critical temperatures, which approximate 621(K). This means that the ferromagnetic state is ensured until this temperature in the case of $Cd_{0.89}V_{0.11}Te$. In addition, we have investigated that adding 0.03 of vacancy defects, improves well the ferromagnetic state, while the critical temperature becomes higher. So the ferromagnetic behavior, in this case, can remain stable up to higher temperatures than the case of doping, or the case of adding 0.05 of vacancy defects (Table II/III.2). Concerning the Faraday rotation, we have found out that the doping improves this property, affecting the exchange interactions N0α. While for the case of adding vacancies, this property is improved, by the contribution of the exchange interactions $N_0\beta$. Moreover, it is found that the gap is decreasing with the increasing of doping concentrations, besides to the vacancy concentrations. Finally, we can say that the finding results may open the door for various applications, especially in the field of storage, detection, and solar cells.

Chapter II:

Magnetic properties and Faraday rotation of doped ZnSe(Cr,Mn)

Magnetic properties and Faraday rotation of Cr doped ZnSe with defects: First principles calculations

Abderrahim Ait Raiss [1,*], Younes Sbai [1], Lahoucine Bahmad [1],

Abdelilah Benyoussef [2]

(1) Laboratory of Condensed Matter and Interdisciplinary Sciences (LaMcSI), Mohammed V University, Faculty of Sciences, Rabat, Morocco

(2) Resident Member in Hassan II Academy of Sciences and Technology, Rabat, Morocco

Abstract:

Using KKR-CPA method within the spin-polarized Density Functional Theory (DFT) with the Local Density Approximation (LDA), we have performed our calculations on ZnSe compound, doped with chromium atoms, for different concentrations. This, to study the effect of this magnetic impurity on the magnetic properties and Faraday rotation of the studied alloy. We also have investigated the effect of defects, by introducing vacancies in Zn sites. In one hand we have doped our compound with (0.01; 0.05; 0.1; 0.15; 0.2; 0.25) of chromium atoms, in the other hand, we have introduced (0.01; 0.03;0.05) of vacancy defects in Zn sites, for each state of chromium doping. We have investigated that there is a magnetism appearing when doping with chromium atoms. In addition, the adding of vacancy defects improves the ferromagnetic state. The density of states (DOS) illustrates the analyzed results. Moreover, the energy of each case has been calculated for both the DLM (Disordered Local Moment) and the ferromagnetic states.

Key Words: $Zn_{1-x-y}Cr_xVac_ySe$; First principle calculations; KKR-CPA method; Density functional theory (DFT); Density of states (DOS).

I. Magnetic properties and Faraday rotation of Cr doped ZnSe with defects: First principles calculations

I.1. Introduction

A lot of research works in Spintronic, have focused on studying the diluted magnetic semiconductors (DMS). This, in order to enhance the performance of electronic devices. To form this new kind of materials, we substitute a part of the host material's cations by magnetic impurities, which are the transition metals (TM) such as Co, Ni, Fe and Mn [114-122]. ZnSe compound is a wide band-gap semiconductor, which represents a large family of alloys that belongs to the II-VI group. We can conclude from the published works that a lot of studies were focused on the III–V family of semiconductors, such as (Ga, Mn)As, see for example Ref.[123] and references therein. But the solubility of 3d transition metals in III-V based DMS was found to be extremely lower than (8 %) with a Curie temperature up to 160 K, whereas the higher solubility in II-VI DMS and the possibility of controlling the localized spins make them much appreciated for fundamental studies [118,124]. ZnSe is considered as a semiconductor that is optically active in the visible region and has some potential use in thin film devices, especially in optoelectronic devices such as light emitters (blue laser diodes), photo detectors and photovoltaic devices. This, due to its wide direct band gap (2.7 eV) and large bonding energy exciton (21 meV) at room temperature [125]. Thanks to its wide band gap, ZnSe is an efficient inorganic sensitizing shell for ZnO to construct heterostructures, aiming to improve the optical properties and to widen the optical region of ZnO crystal. In order to achieve a good quality of ZnSe films, various growth techniques have been employed, such as metal organic chemical vapor deposition (MOCVD) [126,127], molecular beam epitaxy [128] and photochemical deposition [129].

In this section(II.II.I), we are going to present our study of the pure ZnSe compound, then the results of doping with chromium atoms (Cr), for different concentrations. Furthermore, we will introduce some vacancies as defects in Zn sites, in order to study the effect of defects, besides to the effect of chromium doping on the magnetic properties and Faraday rotation for ZnSe compound. We will also observe the evolution of the critical temperature within mean field approximation, using the following formula, for each case of doping:

$$T_C = \frac{2}{3}\frac{E_{DLM}-E_{FM}}{C.K_B} \qquad (II.II.I.1)$$

Where C is the chromium doping concentration, K_B is the Boltzmann constant, and E_{DLM}-E_{Ferro} is the difference in energy between the anti-ferromagnetic and the ferromagnetic state.

Then we will illustrate our results by providing the plotted density of states (DOS) curves with the tables of different values of energies and the critical temperatures. As said above, we performed our calculation with KKR-CPA method for different doping concentrations:

$Zn_{1-x-y}Cr_xVac_ySe$ (x= 0.01; 0.05; 0.1; 0.15; 0.2; 0.25) ; (y= 0; 0.01; 0.03 ; 0.05) ;Vac (vacancies).

In section(II.II.II), we will present the results of doping this material with different concentrations of manganese atoms(Mn). After that, we will introduce some vacancies as defects in Zn sites. This, to check the effect of defects in addition to the effect of Mn doping on the magnetic properties and Faraday rotation of ZnSe. Moreover, we will observe the evolution of the critical temperature within the mean field approximation (MFA), based on the equation (II.II.I.1).

Later, we will illustrate the obtained results by giving the plotted density of states (DOS) curves and the tables of different values of energies besides to the critical temperatures. Our calculations were performed with the KKR-CPA method. The simulations were carried out for the following doping concentrations:

$Zn_{1-x-y}Mn_xVac_ySe$ (x= 0.05; 0.1; 0.15; 0.2) ; (y= 0; 0.03 ; 0.05) ; Vac (vacancies).

I.2. Computational method :

To perform our calculations, we have used the KKR-CPA method, based on DFT. This method was developed by Akai and Dederichs to deal with the disordered transition metal alloys. The coherent potential approximation (CPA) enables this method to cover the random configurations of the impurity elements, during the calculations [130]. The KKR-CPA code MACHIKANEYAMA2002V08 package is produced by H. Akai of Osaka University [131]. This code uses the (DFT) combined with (CPA). We use the local density approximation (LDA) as a potential approximation. (LDA) Is based on the parameterization given by Moruzzi, Janak and Williams (MJW) [132]. This approximation is considered to be the most widely used in (DFT). The external magnetic field in each site of the structure is considered to be null. We took the relativistic effect into account by employing the scalar relativistic approximation. The crystal potential is approximated by a muffin-tin potential. So, we have created the input for the simulation of ZnSe in the zinc blende structure, using the

lattice parameter a=5.66 Å, with $\alpha=\beta=\gamma= 90^{o}$. The Zn atoms occupy the (0,0,0) sites, while the Se atoms occupy the (1/4,1/4,1/4) sites. The following figure illustrates the structure of the studied material.

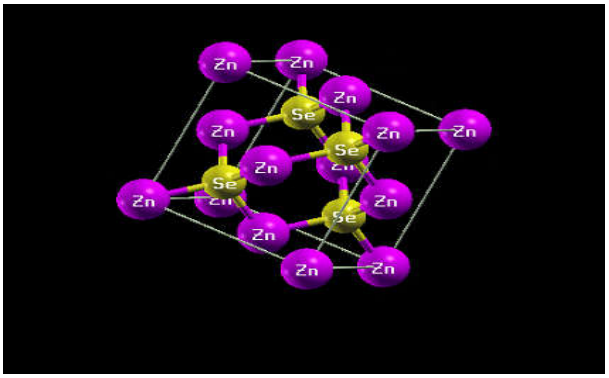

Figure II.II.I.1: A geometry of the studied compound Zn (Cr)Se, The atoms of Zn are with a magenta color, while the Se atoms are with gold color.

I.3. Results and discussion:

As a result of our calculations, performed on ZnSe compound doped with chromium, we have investigated that doping our alloy with Cr impurity induces a magnetic behavior. This behavior depends on the concentration of doping, as well as the defects introduced in the structure.

I.3.a- case of undoped ZnSe

First of all, we will discuss the undoped material ZnSe. Referring to the plotted (DOS), see Figure II.II.I.2.

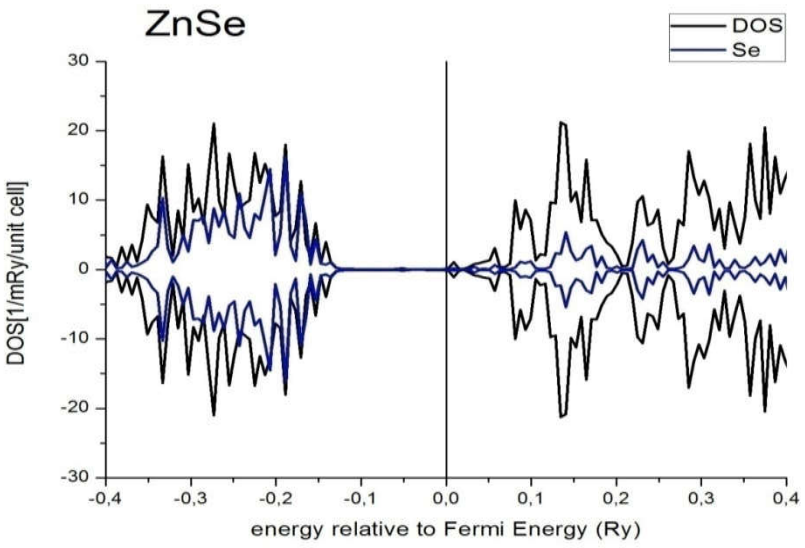

Figure II.II.I.2: The Total and Partial DOS of the pure compound ZnSe

We observe that our material is an n-type semiconductor because the Fermi level is located near to the conduction band. Concerning the magnetic properties, we can see that there is symmetry between the spins up and spins down, in both conduction and valence bands. This means that our host material is not magnetic, that's why we have introduced transition material atoms, as a magnetic impurity. In addition, we have found that the gap between the host material is Eg=2.85 ev, which is near to the known value in the literature.

I.3.b- case of Chromium doped ZnSe

In this part, we move to discuss and explain the results in the doping case without introducing vacancy defects, see Figure II.II.I.3.

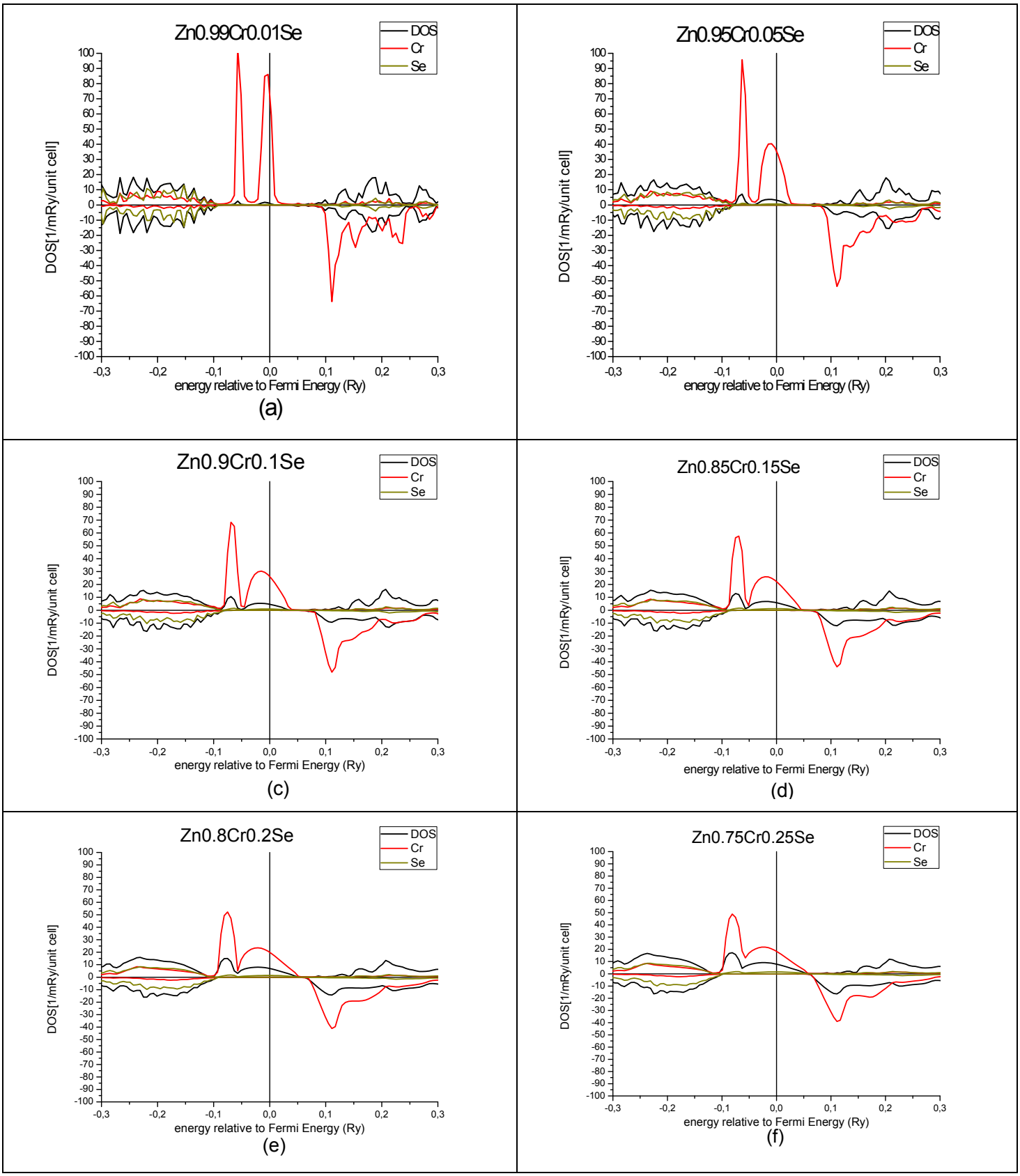

Figure II.II.I.3: Total and Partial DOS of Cr(d) and Se(p) sites in $Zn_{1-x}Cr_xSe$ for different concentrations x.

In this case, we have found out that the doping with chromium atoms gives birth to the magnetic behavior in ZnSe. The magnetism appearing is either in a stable ferromagnetic state or spin glass, according to the evaluation of the energies of each case of doping. When the energy of the FM state is minimal, we have a stable ferromagnetic state, but when the Disordered Local Moment (DLM) Energy is minimal, the DLM state is the stable one, for which the total moment is null, and the half of Cr spins are forced to be up, while the other half is forced to be down. This means that the DLM state is anti-ferromagnetic. The figure (Figure II.II.I.3), shows the plotted (DOS) of the chromium doping with the concentrations (0.01; 0.05; 0.1; 0.15; 0.2; 0.25). So for the case of Figure II.II.I.3.a (0.01), we observe that the doping with chromium introduces a d-band spin up in the gap of the host material, which is divided into two bands e (lower in energy), and t_2 (higher in energy). It is obvious from the graph that e is filled, while t_2 is two third filled, which gives the half-metallic character to our material. This is in agreement with the expectation in Ref.17, in which they expect to have the two orbitals of e filled, besides to two of t_2 orbitals. The half-metallic behavior is very important in the Spintronic field, while this property makes this material suitable for many applications. For example, it can function as a conductor for the spin up electrons, and as an insulator or semiconductor in the case of spin down electrons (spin valve). This, because the spin down d-band is empty and hybridized with the conduction band, so there is a gap between the filled and empty spin down states. The splitting between the e and t_2 spin up d-band means that there is a crystal field in the system, while the degeneration in the spin down d-band, can be explained by the Jahn Teller effect, which results from the distortion of the structure, in order to stabilize the geometry. Afterwards, from the other concentrations, we have investigated that the gap is decreasing, while the d-bands are getting shorter and wider, which means that there is a double exchange interaction, which means that the exchange of electrons between the magnetic ions, is indirectly ensured via the host anions. Concerning the stability of the magnetic states, we have found out that our compound is ferromagnetic stable for all the studied concentrations, except in the case of Figure II.II.I.3.a (0.01) of Cr doping, which has an anti-ferromagnetic state (DLM), see Table II.II.I.1. Where $(E_{DLM} - E_{Ferro})>0$, means that the ferromagnetic state is the stable, else the DLM.

$Zn_{1-x}Cr_xSe$	E_{Ferro}(Ry)	E_{DLM}(Ry)	E_{DLM}- E_{Ferro} (Ry)	Tc (K)
$Zn_{0.99}Cr_{0.01}Se$	-8425.3572366	-8425.3572472	-0.0000106	DLM
$Zn_{0.95}Cr_{0.05}Se$	-8365.7897410	-8365.7895462	0.0001948	410
$Zn_{0.9}Cr_{0.1}Se$	-8291.3315754	-8291.3310621	0.0005133	540
$Zn_{0.85}Cr_{0.15}Se$	-8216.8737439	-8216.8728488	0.0008951	627
$Zn_{0.8}Cr_{0.2}Se$	-8142.4161378	-8142.4148195	0.0013183	693
$Zn_{0.75}Cr_{0.25}Se$	-8067.9587085	-8067.9569339	0.0017746	746

Table II.II.I.1: Values of ferromagnetic, DLM energies and the critical temperature for different Cr doping concentrations x.

I.3.c- introducing vacancy defects in Cd sites of Chromium doped ZnSe

In the case of Figure II.II.I.4, where we have introduced 0.01 of vacancy defects in Zn sites. We discover that this defect changes the state of the compound from the anti-ferromagnetic to the ferromagnetic state, see Figure II.II.I.4.a and Table II.II.I.2.

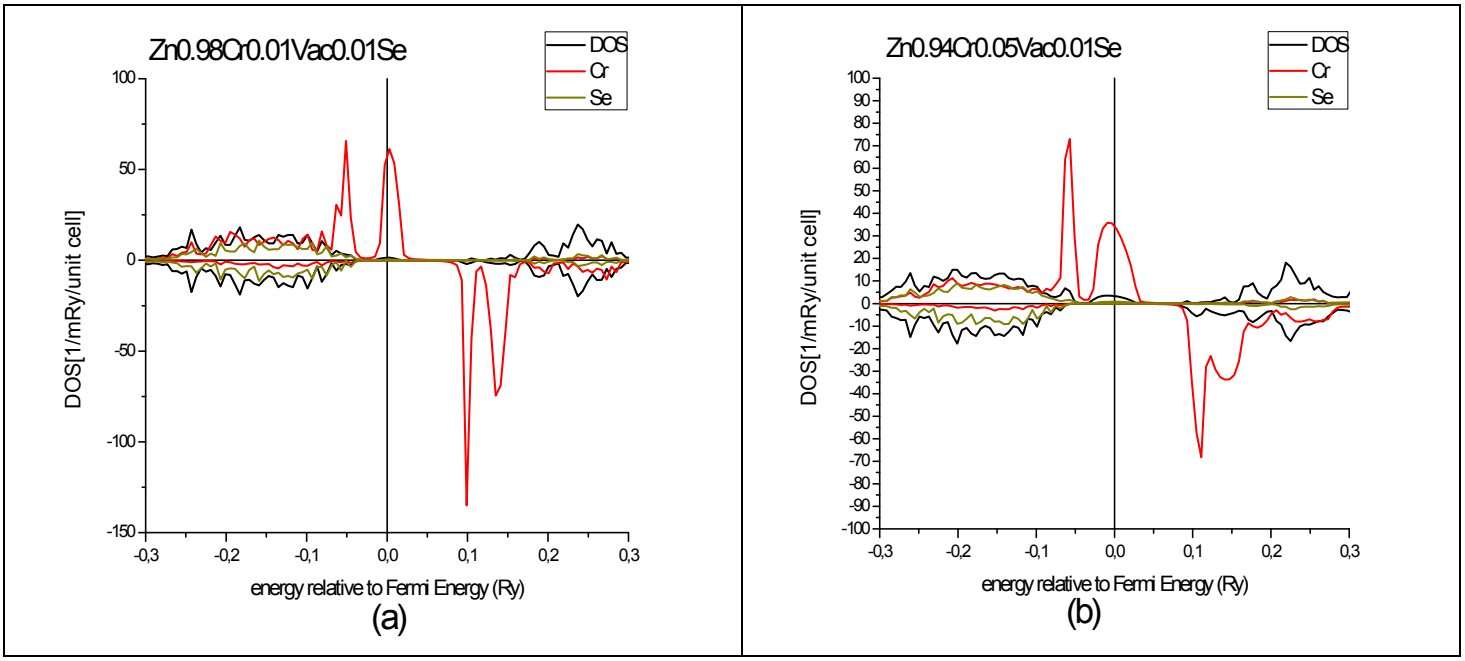

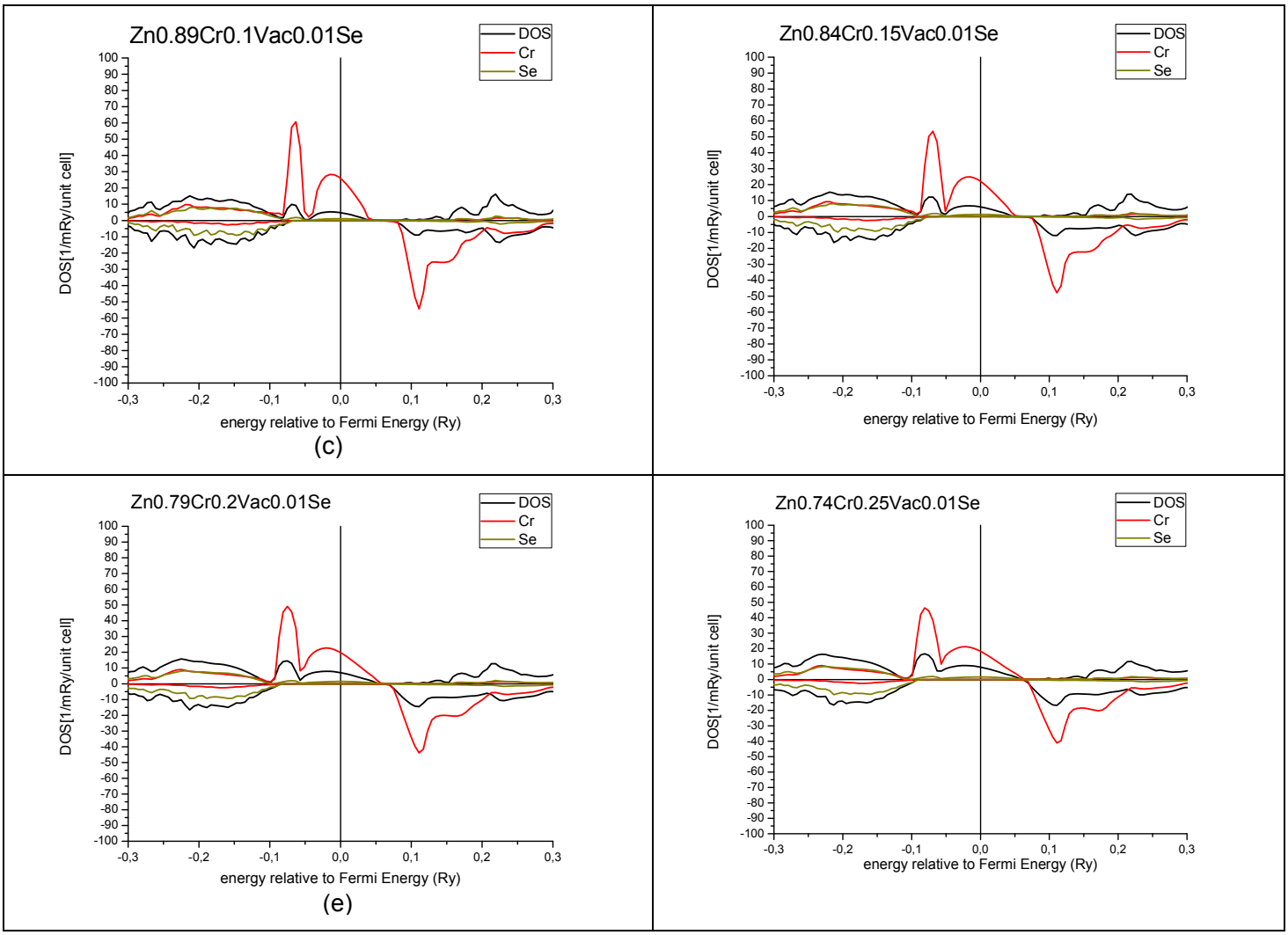

Figure II.II.I.4: Total and Partial DOS of Cr(d) and Se(p) sites in $Zn_{1-x-0.01}Cr_xVac_{0.01}Se$ for different concentrations x.

$Zn_{1-x-0.01}Cr_xVac_{0.01}Se$	E_{ferro}(Ry)	E_{DLM}(Ry)	E_{DLM}- E_{ferro} (Ry)	Tc (K)
$Zn_{0.98}Cr_{0.01}Vac_{0.01}Se$	-8389.4767372	-8389.4766618	0.0000754	793
$Zn_{0.94}Cr_{0.05}Vac_{0.01}Se$	-8329.9095998	-8329.9093813	0.0002185	459
$Zn_{0.89}Cr_{0.1}Vac_{0.01}Se$	-8255.4512315	-8255.4506664	0.0005651	594
$Zn_{0.84}Cr_{0.15}Vac_{0.01}Se$	-8180.9931427	-8180.9921642	0.0009785	686

$Zn_{0.79}Cr_{0.2}Vac_{0.01}Se$	-8106.5352565	-8106.5338231	0.0014334	753
$Zn_{0.74}Cr_{0.25}Vac_{0.01}Se$	-8032.0775321	-8032.0756154	0.0019167	806

Table II.II.I.2: Values of ferromagnetic, DLM energies and the critical temperature for different Cr doping concentrations x with 0.01 of vacancy defects.

In addition, this vacancy defects improves the stability of the ferromagnetic state for the other concentrations of chromium doping. While it decreases the degeneration of the spin down d-band and increases the double exchange interaction. In the case of introducing 0.03 and 0.05 of vacancy defects, see Figure II.II.I.5 and Figure II.II.I.6, respectively. For 0.01 of Cr doping (Figure II.II.I.4.a and Figure II.II.I.5.a), the t_2 spin up band is shifted to the conduction band, so it becomes empty, which means that there is a transition of electrons from this band to another one. While for the case of 0.05 Cr doping (Figure II.II.I.4.b and Figure II.II.I.5.b), we can see that t_2 spin up band is approximately one third filled, which can be explained by the transition of electrons, caused by the vacancy defects. In another way, we can see that the d-bands are becoming shorter and wider with the increasing of the vacancy defects, which improves the double exchange interaction. This increasing of vacancies improves also the stability of the ferromagnetic state, and the critical temperature, which increases with the increasing of vacancies, see tables II.II.I 1, II.II.I 2, II.II.I.3 and II.II.I.4.

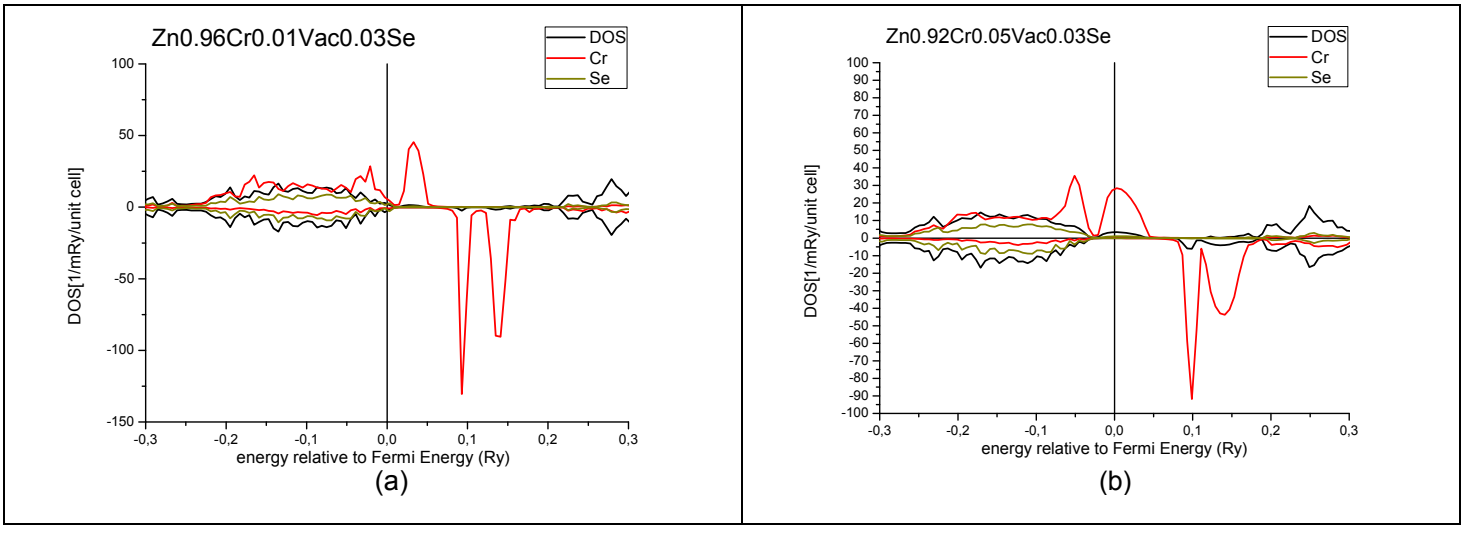

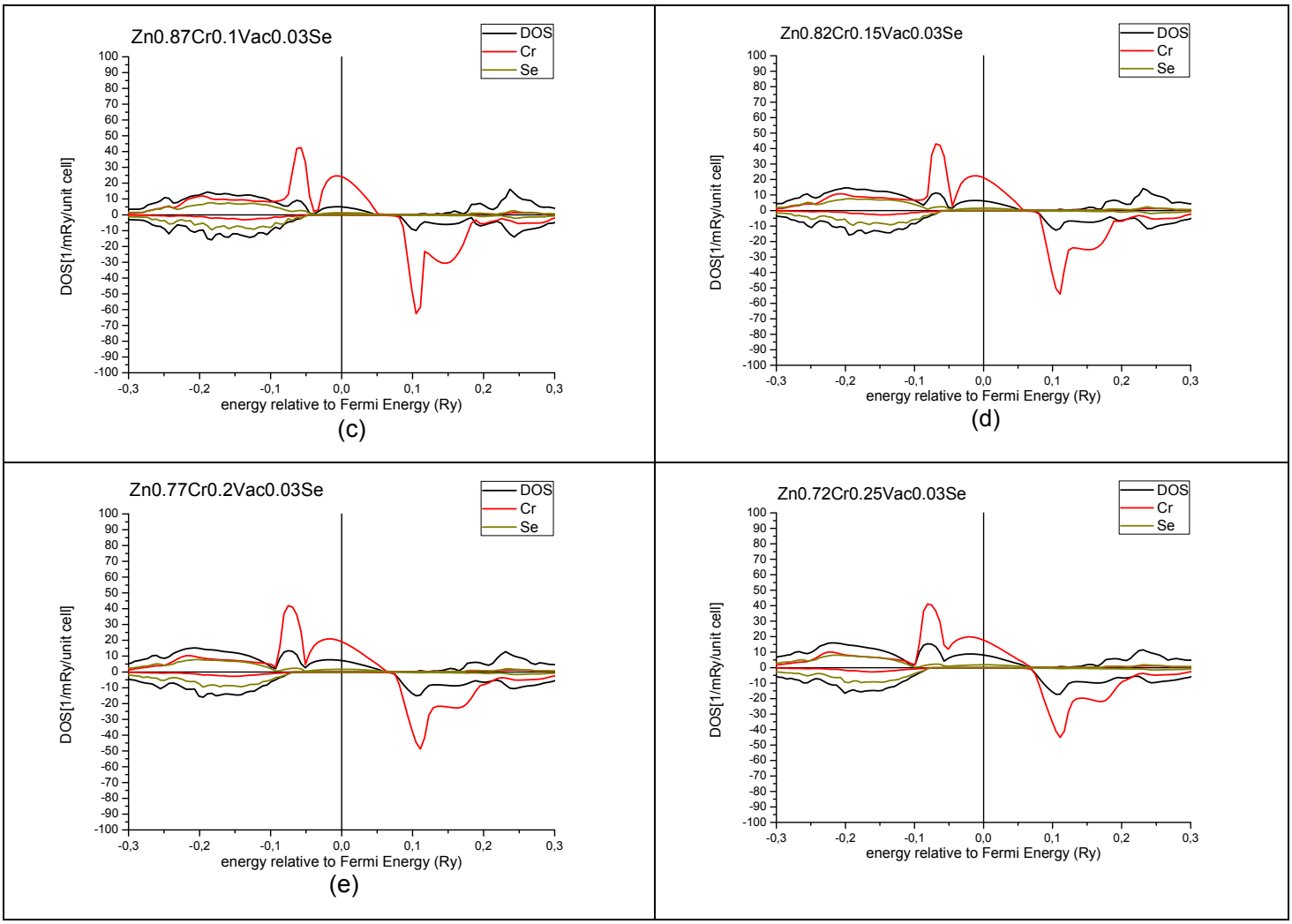

Figure II.II.I.5: Total and Partial DOS of Cr(d) and Se(p) sites in $Zn_{1-x-0.03}Cr_xVac_{0.03}Se$ for different concentrations x.

$Zn_{1-x-0.03}Cr_xVac_{0.03}Se$	E_{Ferro}(Ry)	E_{DLM}(Ry)	E_{DLM}- E_{Ferro} (Ry)	Tc (K)
$Zn_{0.96}Cr_{0.01}Vac_{0.03}Se$	-8317.7150166	-8317.7150103	0.0000063	66
$Zn_{0.92}Cr_{0.05}Vac_{0.03}Se$	-8258.1486256	-8258.1483822	0.0002434	512
$Zn_{0.87}Cr_{0.1}Vac_{0.03}Se$	-8183.6901365	-8183.6894798	0.0006567	690
	-8109.2316998	-8109.2305684		793

$Zn_{0.82}Cr_{0.15}Vac_{0.03}Se$			0.0011314	
$Zn_{0.77}Cr_{0.2}Vac_{0.03}Se$	-8034.7733612	-8034.7717160	0.0016452	865
$Zn_{0.72}Cr_{0.25}Vac_{0.03}Se$	-7960.3151185	-7960.3129336	0.0021849	919

Table II.II.I.3: Values of ferromagnetic, DLM energies and the critical temperature for different Cr doping concentrations x with 0.03 of vacancy defects.

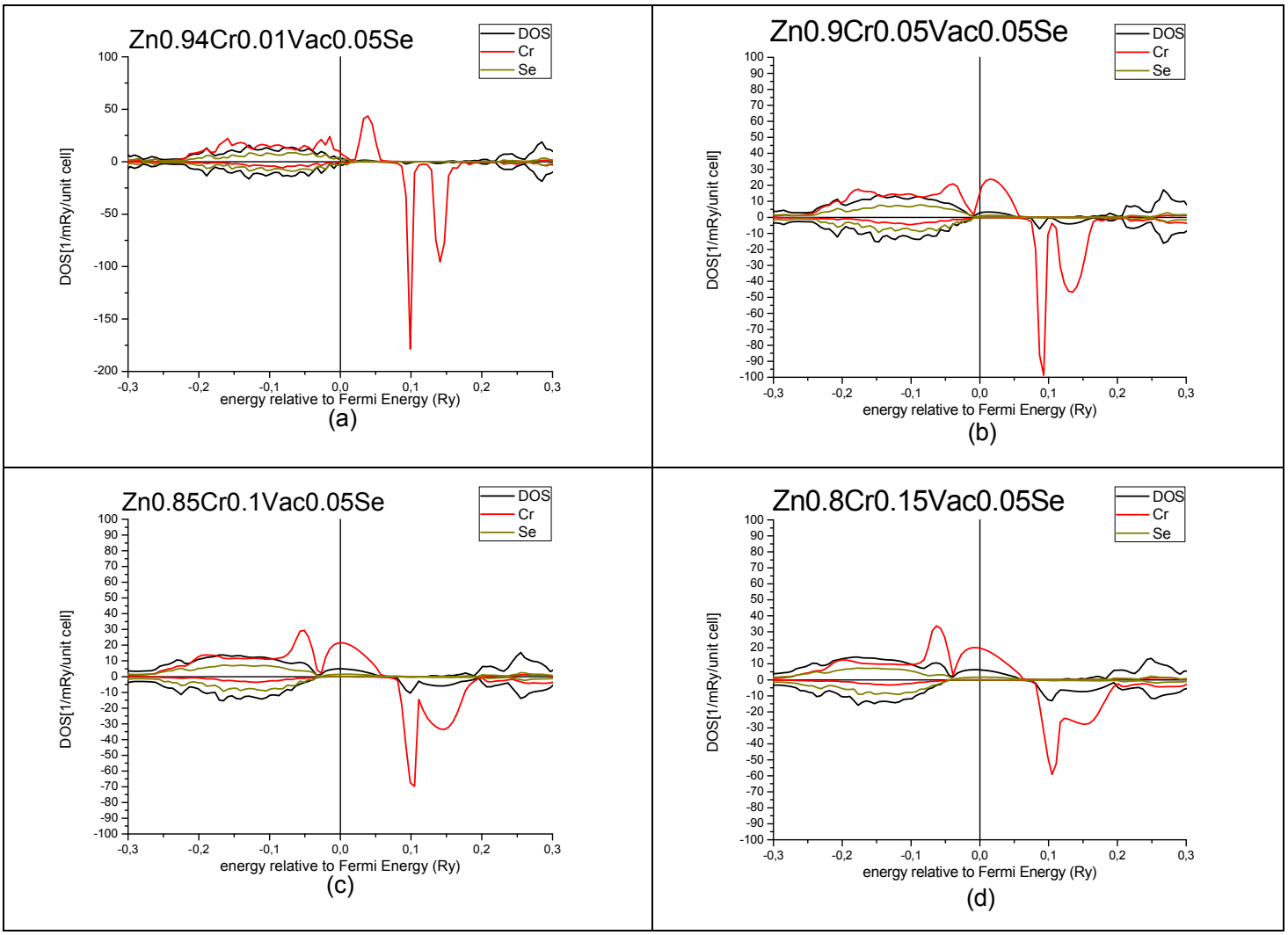

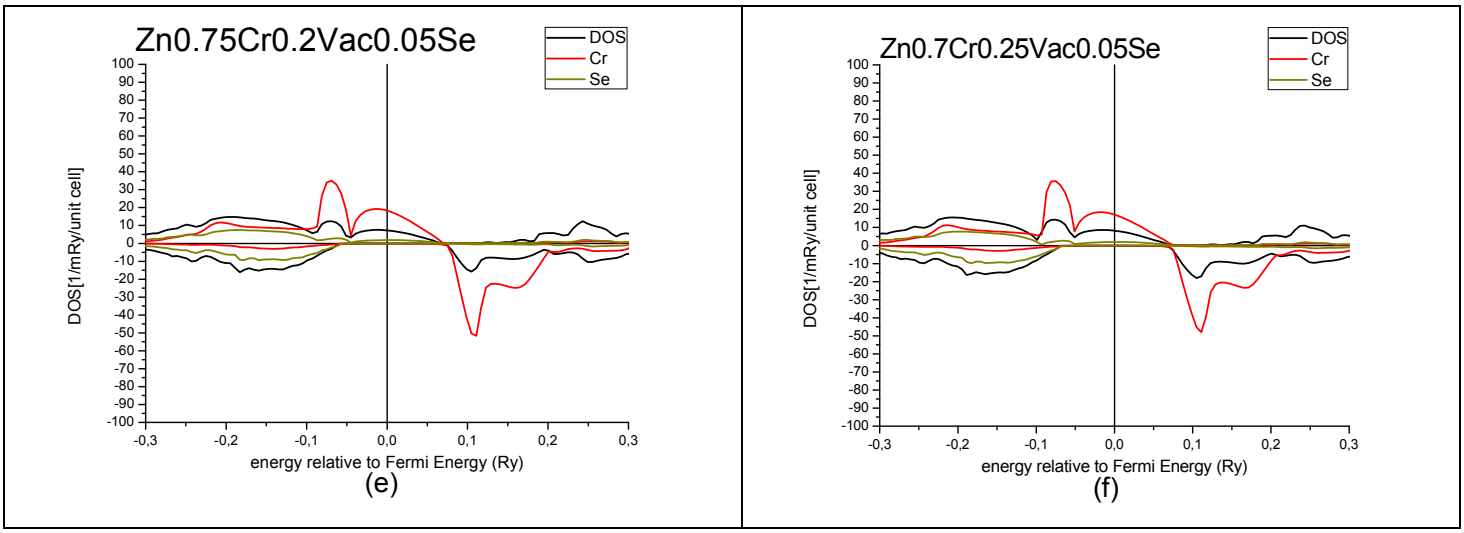

Figure II.II.I.6: Total and Partial DOS of Cr(d) and Se(p) sites in $Zn_{1-x-0.05}Cr_xVac_{0.05}Se$ for different concentrations x.

$Zn_{1-x-0.05}Cr_xVac_{0.05}Se$	E_{Ferro}(Ry)	E_{DLM}(Ry)	E_{DLM}- E_{Ferro} (Ry)	Tc (K)
$Zn_{0.94}Cr_{0.01}Vac_{0.05}Se$	-8245.9520019	-8245.9519969	0.000005	53
$Zn_{0.9}Cr_{0.05}Vac_{0.05}Se$	-8186.3866411	-8186.3865352	0.0001059	223
$Zn_{0.85}Cr_{0.1}Vac_{0.05}Se$	-8111.9284961	-8111.9278426	0.0006535	687
$Zn_{0.8}Cr_{0.15}Vac_{0.05}Se$	-8037.4699455	-8037.4687240	0.0012215	856
$Zn_{0.75}Cr_{0.2}Vac_{0.05}Se$	-7963.0112971	-7963.0094902	0.0018069	950
$Zn_{0.7}Cr_{0.25}Vac_{0.05}Se$	-7888.5526348	-7888.5502229	0.0024119	1010

Table II.II.I.4: Values of ferromagnetic, DLM energies and the critical temperature for different Cr doping concentrations x with 0.05 of vacancy defects.

Finally, to discuss the Faraday rotation effect, we will recall the following equations:

$$(N_{0\alpha} = \frac{\Delta Ec}{x.<S>},\ N_{0\beta} = \frac{\Delta Ev}{x.<S>}) \quad \text{(II/I.I.1)}$$

$$\theta_F = \frac{\sqrt{F0}\,d}{2\pi c}.\frac{E^2}{(E_0^2-E^2)^{3/2}}.N_0(\alpha-\beta).x.<Sz> \quad \text{(II/I.I.2)}$$

We have investigated that this rotation is null in the case of the pure ZnSe compound, because there is no splitting between the spin up and spin down for both the valence and the conduction bands ($\Delta Ev = 0, \Delta Ec = 0$), that leads to $N_0(\alpha-\beta) = 0$. But when doping with chromium, it's clear on the DOS graphs that the splitting in the valence band appears in the case of 0.05 of doping concentration, while the splitting in the conduction band starts to appear in the case of 0.1 of Cr doping. Thereafter, as the concentrations of chromium doping increases, the splitting ($\Delta Ev, \Delta Ec$) increases, especially in the valence band (ΔEv). This increasing of the splitting increases the Faraday rotation, sees equations (II/I.I.1)and (II/I.I.2). Concerning the effect of vacancy defects on the Faraday rotation (Figure II.II.I.4, Figure II.II.I.5, Figure II.II.I.6), we don't see any change in the splitting ($\Delta Ev, \Delta Ec$), compared to the case of chromium doping without introducing vacancies. We conclude that the introduction of vacancy defects doesn't affect this magneto-optical property, which is Faraday rotation. this effect can also be experimentally controlled by varying the thickness d of the compound, see equation (II/I.I.2).

The vacancy defects in ZnMnSe induces a half-metallic behavior and stabilizes the ferromagnetic state: Ab initio study

Abderrahim Ait Raiss [1,*], Younes Sbai [1], Lahoucine Bahmad [1],

Abdelilah Benyoussef [2]

(1) Laboratory of Condensed Matter and Interdisciplinary Sciences (LaMcSI), Mohammed V University, Faculty of Sciences, Rabat, Morocco

(2) Resident Member in Hassan II Academy of Sciences and Technology, Rabat, Morocco

Abstract:

Based on Akai-KKR-CPA method within the spin-polarized Density Functional Theory (DFT) with the Local Density Approximation(LDA), we have studied the Compound ZnSe, which we have doped with Mn impurities, then we added some vacancy defects in Zn sites. This study aimed to examine the effect of both Mn doping and vacancy defects on the studied semiconductor. This study aimed to explore the effect of that doping and vacancies on the magnetic and Faraday rotation, comparing to the pure ZnSe. Therefore, we have doped our host material with (0.05; 0.1; 0.15; 0.2) of Manganese impurities, in Zn sites. Then, we have introduced (0.03; 0.05) of vacancy defects in the same type of sites, for each case of Mn doping. Thereby, we have investigated that there is a magnetism appearing when doping with Mn impurity. In addition, the introduced vacancy defects affect the stability of the magnetic states appearing. In our case, we have found out that these defects change the stable magnetic state from the Disordered Local Moment (DLM) to the Ferromagnetic state (FM), this also, gives birth to the half-metallic behavior and affects the electronic structure of the host material.

Key Words: $Zn_{1-x-y}Mn_xVac_ySe$; Ab-initio study; KKR-CPA method; Density functional theory (DFT); Density of states (DOS).

II. The vacancy defects in ZnMnSe induces a half-metallic behavior and stabilizes the ferromagnetic state: Ab initio study

II.1. Results and discussion:

In this section, we will discuss and explain the results obtained after performing our calculations on the doped ZnSe alloy. So we have investigated that there is a magnetism behavior induced when doping ZnSe with Mn impurity. The appearing magnetism depends on the doping concentrations and the vacancy defects in the structure. As reported in the previous section(II.II.I), the host material ZnSe (undoped) is an n-type semiconductor. Moreover, the undoped ZnSe compound is not magnetic. In addition, the gap, in this case, was found to be Eg=2.85 eV.

II.2.a. magnetic properties and Faraday rotation of Mn-doped ZnSe

As follows, we are going to discuss and explain the results of Mn-doped ZnSe, see Figure II.II.II.1.

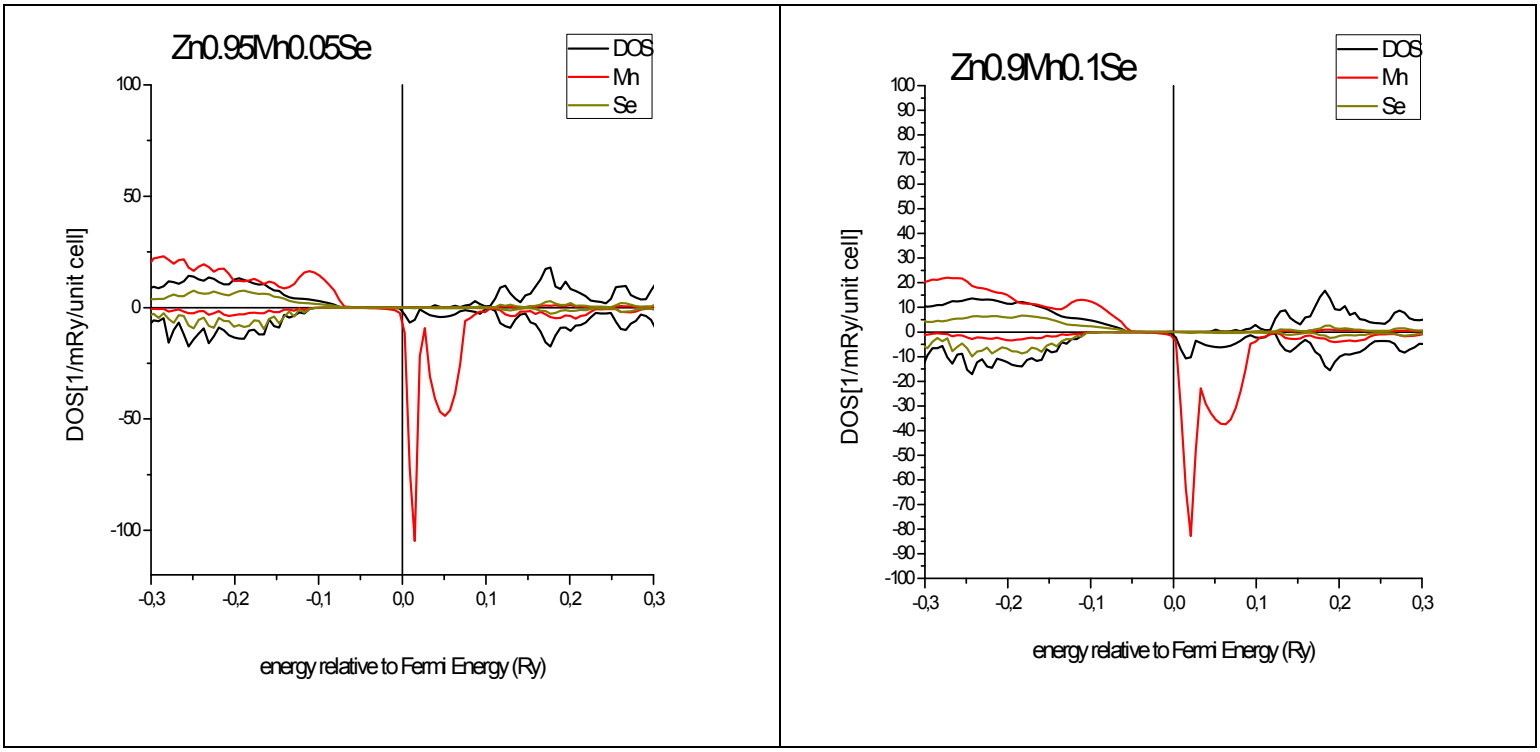

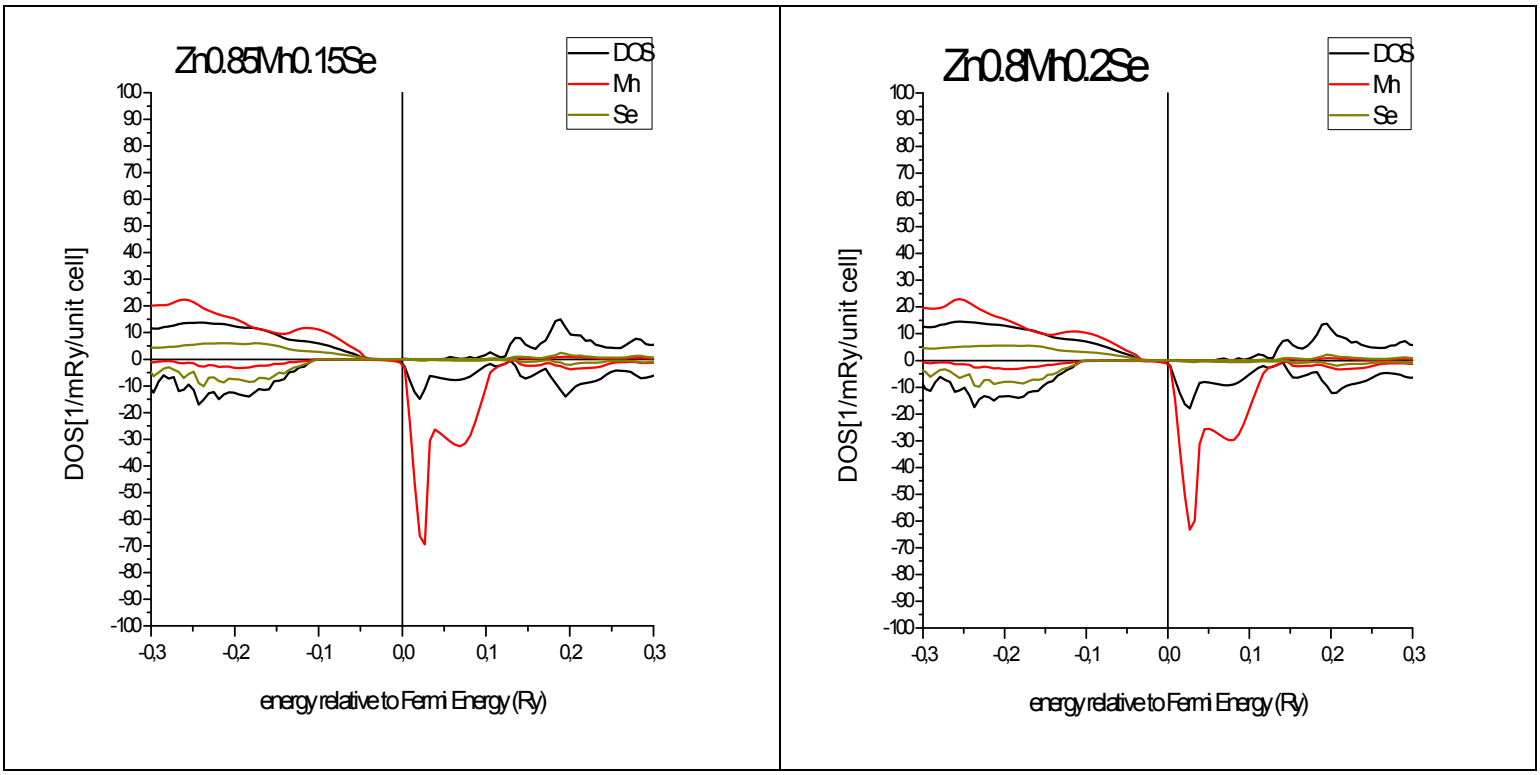

Figure II.II.II.1 : Total and Partial DOS of Mn(d) and Se(p) sites in $Zn_{1-x}Mn_xSe$ for different concentrations x.

In this figure, we observe that Mn doping induces a magnetism behavior in ZnSe because the Mn impurity has introduced an asymmetric d-band in the system. This behavior is either ferromagnetic or anti-ferromagnetic, depending on the difference between the energies of the states. In other words, when the energy of the FM state is minimal, we have a stable ferromagnetic state, while the anti-ferromagnetic state is stable when the energy minimal is that of the Disordered Local Moment (DLM). To calculate the DLM (anti-ferromagnetic) energy, we force the half of the system's spins to be up and the rest to be down. In this case, the magnetic moment becomes null as expected. Return to the Figure II.II.II.1, which illustrates the plotted graphs of the density of state (DOS) of Mn doping with the concentrations (0.05; 0.1; 0.15; 0.2). it's clear to see that the gap is decreasing with the increasing concentrations. Moreover, we conclude that there is no crystal field ($\Delta_t = 0$) in this case, because the e and t_2 bands are not separated, either in the valence or the conduction band. Δ_t is the crystal field of the tetrahedral geometry as the case of our compound, which is expressed by calculating the difference in energy between e and t_2 bands. Furthermore, the spin up d-band is completely filled, while it is located in the valence band, and hybridized with it, which mean that there is an exchange interaction between them. This exchange is an sp-d exchange. The d-band spin down is empty and located in the conduction band, closer to

the Fermi level. The d-bands are getting shorter and wider, with the increasing concentrations. This means that we have a double exchange interactions in this case, which mean that the exchange of electrons between the magnetic ions, is done via the host anions (Se). Furthermore, we observe that the doped ZnSe, keeps its n-type in this case, this means that there is free carriers in the lattice, and these carriers are electrons. About the stability of the magnetic states, we have investigated that the stable magnetic state for the previous case (Mn doped ZnSe), is the anti-ferromagnetic state, where ((E_{DLM}- E_{Ferro})<0). The ferromagnetic state is stable when we have ((E_{DLM}- E_{Ferro})>0), see Table II.II.II.1.

$Zn_{1-x}Mn_xSe$	E_{Ferro}(Ry)	E_{DLM}(Ry)	E_{DLM}- E_{Ferro} (Ry)	Tc (K)
$Zn_{0.95}Mn_{0.05}Se$	-8376.5591779	-8376.5594662	-0.0002883	DLM
$Zn_{0.9}Mn_{0.1}Se$	-8312.8678993	-8312.8683073	-0.000408	DLM
$Zn_{0.85}Mn_{0.15}Se$	-8249.1770019	-8249.1776574	-0.0006555	DLM
$Zn_{0.8}Mn_{0.2}Se$	-8185.4860567	-8185.4870514	-0.0009947	DLM

Table II.II.II.1: Values of ferromagnetic and DLM energies for different Mn doping concentrations x.

II.2.b- case of Mn-doped ZnSe with 0.03 of vacancy defects in Zn sites

For the case of introducing vacancy defects in the compound ZnSe we will discuss the following figure, Figure II.II.II.2:

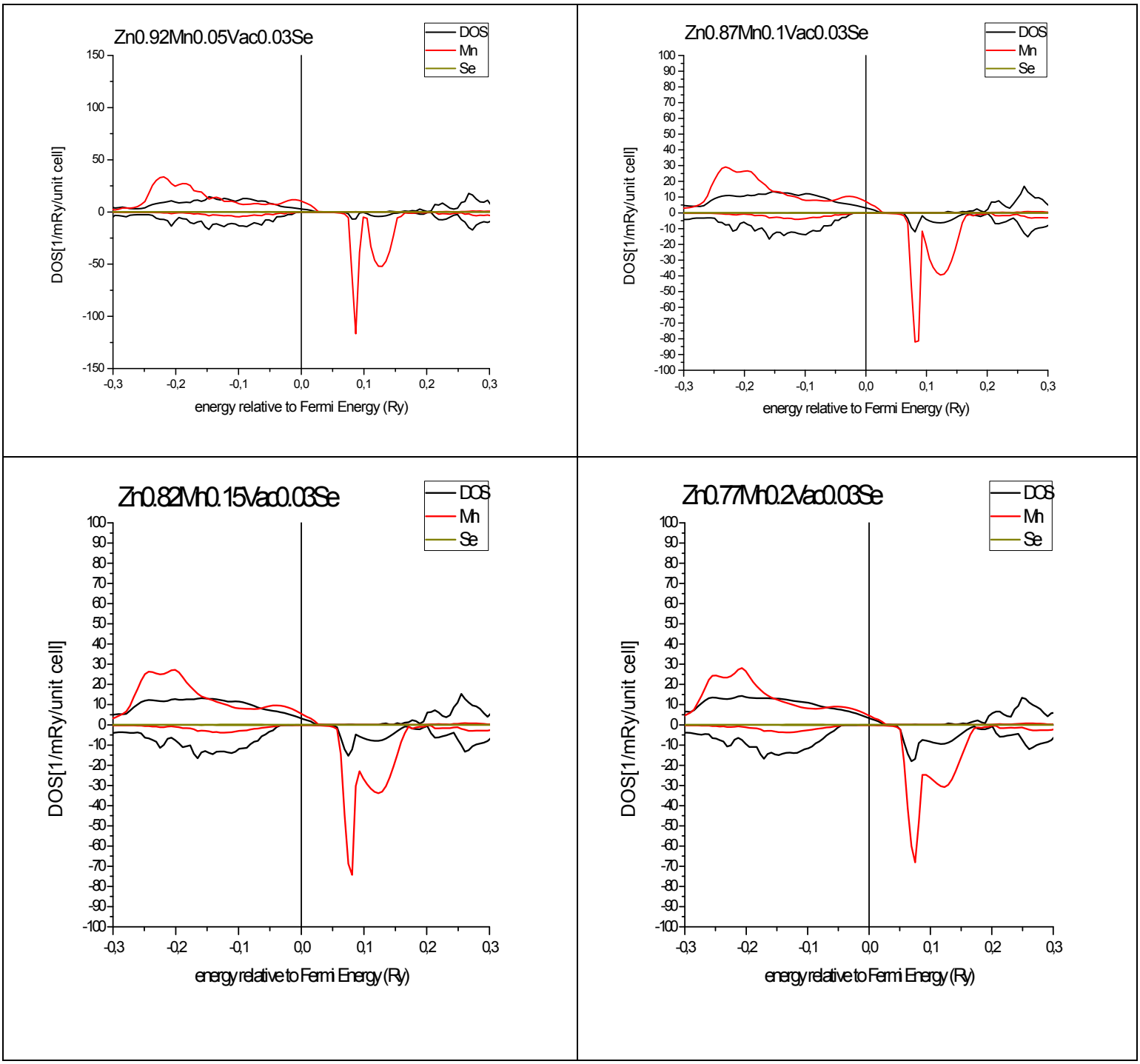

Figure II.II.II.2:Total and Partial DOS of Mn(d) and Se(p) sites in $Zn_{1-x-0.03}Mn_xVac_{0.03}Se$ for different concentrations x.

we can see that the Fermi level becomes closer to the valence band, which means that our compound has changed the type to a p-type semiconductor, so the majority carriers, in this case, are the holes. In addition, the half-metallic behavior appears for all the concentrations, because of the d- band spin up lies at the Fermi level. The half-metallic behavior is a very

important property in the Spintronic field, while it makes this material suitable for many applications. As an example, this material can function as a conductor for the spin up electrons, and as an insulator or semiconductor in the case of spin down electrons (spin valve). Many applications can be based on this spin valve such as the giant magneto-resistance (GMR). The introduced defects affect the magnetic state in the case of 0.05 and 0.1 of Mn doping. So it stabilizes the ferromagnetic state in this case, with a critical temperature up to 250 k for ($Zn_{0.92}Mn_{0.05}Vac_{0.03}Se$), see Table II.II.II.2.

$Zn_{1-x-0.03}Mn_xVac_{0.03}Se$	E_{Ferro}(Ry)	E_{DLM}(Ry)	E_{DLM}- E_{Ferro} (Ry)	Tc (K)
$Zn_{0.92}Mn_{0.05}Vac_{0.03}Se$	-8268.9156385	-8268.9155195	0.000119	250
$Zn_{0.87}Mn_{0.1}Vac_{0.03}Se$	-8205.2246696	-8205.2245579	0.0001117	117
$Zn_{0.82}Mn_{0.15}Vac_{0.03}Se$	-8141.5334692	-8141.5334960	-0.0000268	DLM
$Zn_{0.77}Mn_{0.2}Vac_{0.03}Se$	-8077.8420548	-8077.8423457	-0.0002909	DLM

Table II.II.II.2: Values of ferromagnetic, DLM energies and the critical temperatures for different Mn doping concentrations x with 0.03 of vacancies defects.

II.2.c- case of Mn-doped ZnSe with 0.05 of vacancy defects in Zn sites

The results of introducing 0.05 as vacancy defects in Zn sites are found to be almost similar to the case of 0.03 of vacancy defects, see Figure II.II.II.3. But the important thing, in this case, is that the magnetic state is changed to a stable ferromagnetic state for all the Mn doping concentrations. Also, the critical temperatures are improved and they are higher than those in the case of 0.03 of defects, up to 373 k for ($Zn_{0.85}Mn_{0.1}Vac_{0.05}Se$), see Table II.II.II.3.

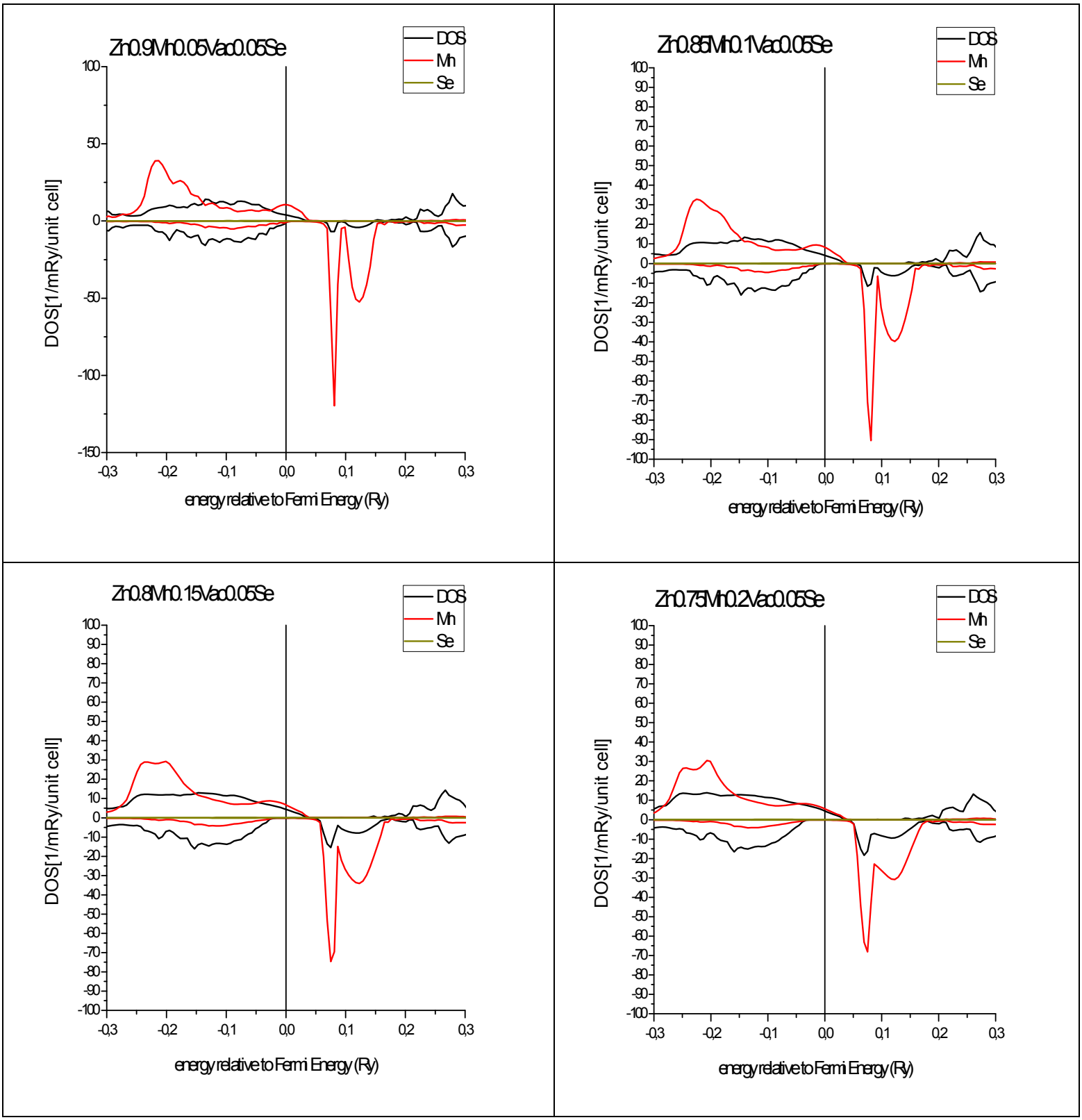

Figure II.II.II.3:Total and Partial DOS of Mn(d) and Se(p) sites in $Zn_{1-x-0.05}Mn_xVac_{0.05}Se$ for different concentrations x.

$Zn_{1-x-0.05}Mn_xVac_{0.05}Se$	E_{Ferro}(Ry)	E_{DLM}(Ry)	E_{DLM}- E_{Ferro} (Ry)	Tc (K)
$Zn_{0.9}Mn_{0.05}Vac_{0.05}Se$	-8197.1526130	-8197.1524711	0.0001419	298
$Zn_{0.85}Mn_{0.1}Vac_{0.05}Se$	-8133.4616305	-8133.4612758	0.0003547	373
$Zn_{0.8}Mn_{0.15}Vac_{0.05}Se$	-8069.7702438	-8069.7698522	0.0003916	274
$Zn_{0.75}Mn_{0.2}Vac_{0.05}Se$	-8006.0785343	-8006.0782614	0.0002729	143

Table II.II.II.3: Values of ferromagnetic, DLM energies and the critical temperatures for different Mn doping concentrations x with 0.05 of vacancy defects.

Later, to discuss the Faraday rotation, we will discuss the previous equations (II.I.I.1; II.I.I.2)

We report again that we have found in the previous section that this rotation is null in the case of the pure ZnSe , because there is no splitting between the spin up and spin down for both the valence and the conduction bands ($\Delta Ev = 0, \Delta Ec = 0$), which leads to $N_0(\alpha - \beta) = 0$. But when doping with Mn impurity, it's obvious to see on the DOS graphs, that the splitting $(\Delta Ev, \Delta Ec)$ in both the valence and the conduction bands appears in the case of 0.05 of doping concentration. Then, the splitting is increasing with the increasing of the concentrations. This increasing of the splitting increases the Faraday rotation, see equations (II.I.I.1) and (II.I.I.2). Concerning the effect of the vacancy defects on the Faraday rotation, we can't observe any change in the splitting $(\Delta Ev, \Delta Ec)$, comparing to the case without introducing vacancy defects. Therefore, we conclude that the introduction of vacancy defects doesn't affect well this magneto-optical property, which is Faraday rotation in this case of doping. This effect can also be controlled by controlling the thickness d of the compound, see equation (II.I.I.2).

III. Conclusion:

In the first section of this chapter, we have studied the magnetic properties and the Faraday rotation of ZnSe doped with chromium. In addition, we have studied the effect of creating vacancies in this material, as a type of defects. Hence, we have found that doping with chromium induces a half-metallic behavior, for all the studied concentrations. This

ferromagnetic half-metallic state is very sought by the researchers. The ferromagnetic behavior is affected when introducing vacancy defects besides to the Cr doping. Also, the critical temperature is found to increase with the increasing of doping concentrations and vacancies. This allows the material (ZnCrSe) to keep the ferromagnetic behavior reaching higher temperatures. As a result, the adding of vacancies as defects improves the ferromagnetic state of the studied alloy (ZnCrSe). However, these vacancies do not affect the Faraday rotation. Thus, this finding pushes one to recommend or to allow creating vacancy defects in this compound in order to improve its magnetic properties.

In the second section, we have investigated that doping ZnSe with Mn impurities, induces a magnetism behavior, which is stable in the anti-ferromagnetic state for all the studied concentrations. While introducing 0.05 of vacancy defects in Zn sites, affect the magnetic state, by changing it to a stable ferromagnetic state. This also gives birth to the half-metallic behavior and improves the critical temperatures, which mean that the ferromagnetic state keeps stable until higher temperatures than the case of 0.03 of vacancy defects. In one hand, introducing vacancies as defects, affect well the studied material (ZnMnSe), in the case of seeking the stability of the ferromagnetic and the half-metallic behavior. On the other hand, this defects doesn't affect the Faraday rotation. So in this case, making vacancies as defects in Zn sites, is recommended in order to improve the ferromagnetic state and to seek the half-metallic behavior. In other words, the vacancy defects play a positive and important role in this case. Finally, we hope that this study can help well in the experimental works. Experimental researchers can also act on the thickness d of the compound, in order to control this magneto-optical property, which is Faraday rotation.

In the present work, we have investigated that doping ZnSe with Mn impurities, induces a magnetism behavior, which is stable in the anti-ferromagnetic state for all the concentrations. While introducing 0.05 of vacancy defects in Zn sites, affect the magnetic state, by changing it to a stable ferromagnetic state. This also gives birth to the half-metallic behavior and improves the critical temperatures, which mean that the ferromagnetic state keeps stable until higher temperatures than the case of 0.03 of vacancy defects. In one hand, introducing vacancies as defects, affect well the studied material (ZnMnSe), in the case of seeking the stability of the ferromagnetic and the half-metallic behavior. On the other hand, this defects doesn't affect the Faraday rotation. So in this case, making vacancies as defects in Zn sites, is recommended in order to improve the ferromagnetic state and to seek the half-metallic behavior. In other words, the vacancy defects play a positive and important role in this case.

Finally, we hope that this study can help well in the experimental works. Experimental researchers can also act on the thickness d of the compound, in order to control this magneto-optical property, which is Faraday rotation.

General conclusion

In this thesis, we aimed to study the magnetic properties as well as the evolution of the Faraday rotation, for both the CdTe and ZnSe compounds. Therefore, we have investigated that those compounds are very interesting due to the results found out when doping them with magnetic impurities. Based on the finding results, we confirm that they can highly participate in the development and promotion of the nanotechnology field, such as in spintronic or photovoltaic applications.

To sum up, we have investigated that Mn-doped CdTe has presented a ferromagnetic state in some cases of doping concentrations. The Fe doped CdTe found to be paramagnetic and changes the type of the semiconductor from n-type to p-type. While in the co-doping case with both Mn and Fe, the most results show an antiferromagnetic state. We have found out that this co-doping doesn't affect the Faraday rotation in small concentrations. But for the case of 38% of Mn with a small rate of Fe, we have investigated that this gives birth to the Faraday rotation and improves it well. We also conclude that the Faraday rotation is enhanced by the exchange interactions between the Mn and Fe ions, as reported in Ref.[24]. Furthermore, it was remarked that the local magnetic moment of Mn reduces from its free space charge value of $5\mu_B$[13] to around $\pm 4\ \mu_B$ due to p–d hybridization and produces small local magnetic moments on the nonmagnetic Cd and Te sites. Moreover, The codoping with N atoms in Te sites affects the magnetic stability. Therefore, this co-doping changes the stability of the compound from ferromagnetic to antiferromagnetic state. Therefore, it is recommended to avoid this co-doping and to be aware of this structural defect. Furthermore, we have investigated that doping CdTe with the Vanadium impurity (V) for the concentrations (0.05; 0.07; 0.09; 0.11), shows a half-metallic behavior, and stabilizes the ferromagnetic state for all those concentrations. We have also calculated the critical temperatures, which approximates 621(K). This means that the ferromagnetic state is ensured until this temperature in the case of $Cd_{0.89}V_{0.11}Te$. In addition, we have investigated that adding 0.03 of vacancy defects, improves well the ferromagnetic state, while the critical temperature becomes higher. So the ferromagnetic behavior, in this case, can remain stable up to higher temperatures than the case of doping, or the case of adding 0.05 of vacancy defects (Table.2). Concerning the Faraday rotation, we have found out that the doping improves this property, affecting the exchange interactions$N_{0\alpha}$. While in the case of adding vacancies, this property is improved, due to the contribution of the exchange interactions $N_{0\beta}$. Moreover, it is

found that the gap is decreasing with the increasing of doping concentrations, besides to the vacancy defects.

In the case of ZnSe, we have investigated that doping with chromium induces a half-metallic behavior, for all the studied concentrations. This ferromagnetic half-metallic state is very sought by the researchers. The ferromagnetic behavior is affected when introducing vacancy defects besides to the Cr doping. Also, the critical temperature was found to increase with the increase of doping concentrations and vacancies. This allows the material to keep the ferromagnetic behavior reaching higher temperatures. The adding of vacancies as defects improves the ferromagnetic state of the studied alloy (increase). However, these vacancies do not affect the Faraday rotation. Thus, this finding pushes one to recommend the adding of vacancies in order to improve the magnetic properties of such compounds. In addition, we have investigated that doping ZnSe with Mn impurities, induces a magnetism behavior, which is stable in the anti-ferromagnetic state for all the concentrations. While introducing 0.05 of vacancy defects in Zn sites, affect the magnetic state, by changing it to a stable ferromagnetic state. this also gives birth to the half-metallic behavior and improves the critical temperatures. In one hand, introducing vacancies as defects, affect well the studied material (ZnMnSe), in the case of seeking the stability of the ferromagnetic and the half-metallic behavior. In the other hand, this defects doesn't affect the Faraday rotation in this case. Therefore, making vacancies as defects in Zn sites is recommended in this case, in order to improve the ferromagnetic state and to seek the half-metallic behavior. In other words, the vacancy defects play a positive and important role in some cases while it is not recommended in other cases depending on the material as well as the doping magnetic impurities. As a comparison between the studied materials, we find that CdTe doped with Vanadium gives the seeked results as ferromagnetism and half metallic behavior with Critical temperature above room temperature. In addition we have investigated in this case that the Faraday rotation is improved in the positive sense due to the exchange splitting in the conduction band. while the adding of vacancy defects to this doping increases the Critical temperature and shows a negative Faraday rotation, which is due to the exchange splitting in the valence band, Moreover, the vacancy defects change the type of the semiconductor from n-type to p- type. For ZnSe, we have found that This compound is ferromagnetic and shows a half metallic behavior when doped with Chromium atoms except in the case of 1% of Cr doping. The Critical temperature was found to be above room temperature (almost similar to the finding one in the case of CdTe doped with Vanadium). The vacancy defects improve the

ferromagnetic state for this compound, but it doesn't affect the Faraday rotation which is negative for both the doping and the vacancy defects. This leads to recommend it to be in the basis of the devices with negative Faraday rotation. Finally, we can say that the finding results may open the door for various applications, especially in the field of Spintronic, storage, detection, and solar cells.

List of publications

1- **A. Ait Raiss**, Y. Sbai, L. Bahmad, A. Benyoussef. Magnetic and magneto-optical properties of doped and co-doped CdTe with (Mn, Fe): Ab-initio study. 2015. Journal of Magnetism and Magnetic Materials. DOI: 10.1016/j.jmmm.2015.02.077 .

2- Y. Sbai **A. Ait Raiss**, E. Salmani, L. Bahmad, A. Benyoussef. Ab-initio study of magnetic properties and phase transitions in Ga (Mn) N with Monte Carlo approach . 2015 Journal of Magnetism and Magnetic Materials. DOI : 10.1016/j.jmmm.2015.08.032.

3- **A. Ait Raiss**, Y. Sbai, Z. Zarhri, L. Bahmad, A. Benyoussef. Study of the Magnetic Properties of CdMnTe1−y N y and CdMnTe with Defects by Ab Initio Calculations. 2015. Journal of Superconductivity and Novel Magnetism. DOI: 10.1007/s10948-015-3179-2.

4- Arejdal, M.,Kadiri, M.,Abbassi, A., **Ait Raiss, A.** ,Bahmad, L.,Benyoussef. A Magnetic Properties of the DoublePerovskite Ba2CoUO6: Ab Initio Method, Mean Field Approximation, and Monte Carlo Study. 2016 Journal of Superconductivity and Novel Magnetism. DOI : 10.1007/s10948-016-3598-8.

5- Ziat, Y., Abbassi, A.,Slassi, A., **Ait Raiss, A.** , Echihi, S.,Kenz, A.E. First principles investigation of the electronic and optical properties of Al-doped FeS2 pyrite for photovoltaic applications. 2016 Optical and Quantum Electronics. DOI : 10.1007/s11082-016-0781-x .

6- Ziat, Y.,Slassi, A.,Zarhri, Z., **Ait Raiss, A**, Kenz, A.E.,Benyoussef, A. First-Principles Study of Magnetic and Electronic Properties of Fluorine-Doped Sn0. 98Mn0.02O_2 System. 2016 Journal of Superconductivity and Novel Magnetism.

7- Sbai, Y., **Ait Raiss, A**., Bahmad, L., Benyoussef, A. Ab initio study of (Fe, Ni) doped GaAs: Magnetic, electronic properties and Faraday rotation. 2017 Superlattices and Microstructures. DOI : 10.1016/j.spmi.2017.03.042.

8- **A. Ait Raiss**, Y. Sbai, L. Bahmad, A. Benyoussef. Ab Initio Study of the Electronic Structure and Magnetic Properties of Vanadium-Doped CdTe with Vacancy Defects. Journal of Superconductivity and Novel Magnetism. DOI: 10.1007/s10948-017-4135-0.

9- **A. Ait Raiss**, Y. Sbai, L. Bahmad, A. Benyoussef. Effect of Cobalt doping and vacancy defects on Magnetic properties and Faraday rotation as a Magneto-optical effect of CdTe compound: Ab initio study. Journal of Superconductivity and Novel Magnetism. DOI: 10.1007/s10948-017-4519-1

10- **A. Ait Raiss**, Y. Sbai, L. Bahmad, A. Benyoussef. Magnetic properties and Faraday rotation of Cr doped ZnSe with defects: First principles calculations. Submitted to Journal.

11- **A. Ait Raiss**, Y. Sbai, L. Bahmad, A. Benyoussef. The vacancy defects in ZnMnSe induces a half-metallic behavior and stabilizes the ferromagnetic state: Ab initio study. Submitted to Journal.

12- **A. Ait Raiss**, Y. Sbai, L. Bahmad, A. Benyoussef. Ab initio calculations of magnetic and magneto-optical properties of GaAs doped with (Mn, Co). Submitted to Journal.

References

[1] M. N. Baibich et al. Phys. Rev. Lett. **61** (1988) 2472.

[2] G. Binasch et al. Phys. Rev. B **7** (1989) 4828.

[3] Levy, Peter M.; Zhang, Shufeng; Fert, Albert. Phys. Rev. Lett. **65** (1990) 1643.

[4] P.M. Tedrow, R. Meservey, Phys. Rev. Lett. **26** (1971) 192.

[5] M. Julliere. Phys. Lett. A, 54 **3** (1975) 225.

[6] Tsymbal, Evgeny Y.; Mryasov, O. N.; and LeCair, P. R., (2003).Evgeny Tsymbal Publications.Paper 19.

[7] J.S. Moodera, L. R. Kinder, T. M. Wong, R. Meservey, Phys. Rev. Lett.**74** (1995) 3273.

[8] Titus, E., Ferreira, A. L., Grácio, J., Singh, M., Krishna, R., & Dias, R. G. (2011). Carbon Nanotube Based Magnetic Tunnel Junctions (MTJs) for Spintronics Application. INTECH Open Access Publisher.

[9] A case study of spintronics: origin of room-temperature ferromagnetism in Co doped ZnO Appl. Phys. Lett. **88**, 242507-24259 (2006).

[10] S. Datta, B. Das, Appl. Phys. Lett. **56**,(1990) 665.

[11] Y. Bychkov and E. L. Rashba, J. Phys. C **17** (1984) 6093.

[12] H. Ohno, et al., Appl. Phys. Lett. **69** (1996) 363.

[13] P.R. Hammar, B.R. Bennett, M.J. Yang, and M. Johnson, Phys. Rev. Lett. **79**, (1999) 1750.

[14] G. Lampel, Phys. Rev. Lett. **10** (1968) 491.

[15] A case study of spintronics: origin of room-temperature ferromagnetism in Co doped ZnO Appl. Phys. Lett. **88**, 242507-24259 (2006).

[16] Y.D. Park, A.T. Hanbicki, J.E. Mattson, B.T. Jonker, , Appl. Phys. Lett. **81** (2002) 1471

[17] R. Goswami, G. Kioseoglou, A.T. Hanbicki, B.T. Jonker, G. Spanos, Acta Materialia **55** (2007) 4625

[18] V. Zestrea, V.Y. Kodash, V. Felea, P. Petrenco, D.V. Quach, Joanna R. Groza ,Vladimir Tsurkan, J Mater Sci **43** (2008) 664.

[19] P.G. Steeneken, L.H. Tjeng, I. Elfimov, G.A. Sawatzky, G. Ghiringhelli, N.B. Brookes, D.J. Huang, Phys. Rev. Lett. **88** (2002) 47201.

[20]J. Stangl, V. Holý, and G. Bauer, Rev. Mod. Phys. **76** (2004) 725.

[21] N. Theodoropoulou, A. F. Hebard, S. N. G. Chu, M. E. Overberg, C. R. Abernathy, S. J. Pearton, R. G. Wilson, J. M. Zavada, and Y. D. Park, J. Vac. Sci. Technol. A, **20** (2002) 579.

[22] A. Haury, A. Wasiela, A. Arnoult, J. Cibert, T. Dietl, Y. M. D'aubigne and S. Tatarenko, Phys. Rev. Lett.,**79** (1997) 511.

[23] H. Munekata, H. Ohno, S. Von Molnar, A. Segmuller, L. L. Chang, and L. Esaki, Phys. Rev. Lett., **63** (1989) 1849.

[24] M. Jain, J.L. Robbins, Material preparation, crystal structure and energy gap of diluted magnetic semiconductors, in: M. Jain (Ed.), Diluted Magnetic Semiconductors, World Science Publishing Co. Pvt. Ltd., Singapore (1991) 13.

[25] K. Sato et al . Advances in Crystal Growth Research, Elsevier, Amsterdam, (2001) 303.

[26] H. Ohno et al. Phys. Rev. Lett., **68** (1992) 2664.

[27] Y. Ohno et al. Nature (London) **402** (1999) 790.

[28] G. Kioseoglou, A. Hanbicki, C. Li, S. Erwin, R. Goswami, and B. Jonker, cond-mat/0302231 (submitted to Appl. Phys. Lett., (2003).

[29] O. Madelung (Ed.), Numerical Data and Functional Relationships in Science and Technology, Landolt Bornstein, New Series, Group III, vol.22, Springer, Berlin, 1987 (Pts.A).

[30] K. Durose et al. Journal of Crystal Growth **197** (1999) 733

[31]V. Fthenakis : National PV EHS Assistance Program; K. Zweibel: National Renewable Energy Laboratory. Presented at the National Center for Photovoltaics and Solar Program Review Meeting Denver, Colorado March (2003) 24.

[32]M. Marwede, A. Reller. Resources, Conservation and Recycling **69** (2012) 35.

[33] G. Grebe, G. Roussos, and H.-J. Schulz. J. Phys. C: Solid State Phys. **9** (1976) 4511.

[34] J. Gutowski, N, Presser and G. Kudlek, Phys. Stat. Sol. (a). 120 (1990) 11.

[35] Filipe Oliveira,"Faraday rotation effect and other magneto-optic effects in semiconductors", MAP-Fis, Universidade do Minho. DOI: 10.13140/RG.2.1.1319.6881.

[36] Taskeya Haider. International Journal of Electromagnetics and Applications **1**(2017) 17.

[37] C. Zener. J. Phys. Rev. **82** (1951) 403.

[38] C. Zener. J. Phys. Rev. **81** (1951) 440.

[39] G. H. Jonker and J. H. van Santen. Physica, **16** (1950) 337.

[40] J. B. Goodenough, A. Wold, R. J. Arnot, and N. Menyuk. Phys. Rev., **124** (1961) 373.

[41] John B. Goodenough. Scholarpedia, 3(10) (2008) 7382.

[42] P.W.Anderson, J. Phys. Rev **79** (1950) 350.

[43] Z. Ben Ayadi et al, Nanotechnology **18** (2007) 445702

[44] M. A. Ruderman, C. Kittel, J. Phys. Rev **96** (1954) 99.

[45] T. Kasuya, Progress of Theoretical Physics **16** (1956) 45.

[46] K. Yosida, J. Phys. Rev **106** (1957) 893.

[47] X. L. Wang et al, EPL, **87** (2009) 47001.

[48] M. Born and J. R. Oppenheimer. Annalen der Physik, **389** (1927) 457.

[49]D.R. Hartree. Mathematical Proceedings of the Cambridge Philosophical Society. **24** (1928) 89.

[50] D. R.Hartree, "the calculation of atomic structures". (Wiley, New York, 1957).

[51] L.H. Thomas. Math. Proc. Cambridge Philos. Soc., **23** (1927) 542.

[52] E. Fermi. Z. Phys., **48** (1928) 73.

[53] P. Hohenberg and W. Kohn.J. Phys. Rev.B, **136** (1964) 864.

[54] W. Kohn and L.J. Sham. J. Phys. Rev. A, **140** (1965) 1133.

[55] R. M. Martin. Cambridge University Press, 2004.

[56] P. Ghosez. First-principle study of the dielectric and dynamical properties of baryum titanate. PhD thesis, University catholique in Louvain, 1997.

[57] W. Kohn L. J. Sham, J. Phys. Rev.B, **136** (1965) 864.

[58] M D Segall et al J. Phys. Cond. Mat. **14** (2002) 2717.

[59] D. M. Ceperley aet al. J. Phys. Rev. Lett. **45** (1980) 566.

[60] A. St-Amant, W. D. Cornell, P. A. Kollman, and T. A. Halgren *J. Comput. Chem.* **16** (1995) 1483.

[61] D. C. Langreth and M. J. Mehl. J. Phys. Rev. B, **28** (1983) 1809.

[62] J. P. Perdew, J. A. Chevary, S. H. Vosko, K. A. Jackson, M. R. Pederson, D. J. Singh and C. Fiolhais. J. Phys. Rev. B **46**, (1992) 6671.

[63] J. Korringa, Physica **13** (1947) 392.

[64] W. Kohn and N. Rostoker. J. Phys. Rev. **94** (1954) 1111.

[65] T. H. Dupree, Ann. Phys. (N. Y.), **15**, 63 (1961); J. L. Beeby, Proc. Roy. Soc. London Ser. A**302**, 113 (1967); G. J. Morgan, Proc. Phys. Soc. **89** (1966) 365.

[66] N. Papanikolaou, R. Zeller, and P. H. Dederichs, J. Phys. Cond. Mat **14** (2002) 2799.

[67] R. Zeller and P. H. Dederichs, Phys. Rev. Lett. **42** (1979) 1713.

[68] A. Gonis, Theoretical Materials Science, Materials Research Society (2000).

[69] J. C. Slater, Advances in Quantum Chemistry **1** (1964) 35.

[70] Johannes Grotendorst, Stefan Blugel, Dominik Marx. Computational Nanoscience: Do It Yourself!, Winter School. Forschungszentrum Julich, Germany (2006).

[71] Hedin L, Phys. Rev.A. **139** (1965) 796.

[72] Hybertsen M S, Louie S G. Phys. Rev. Lett. **55** (1985) 1418.

[73]Godby R W, Shluter M, Sham L J. Phys. Rev. B **37** (1988) 10159.

[74] Becke A D, Johnson E R. J. Chem. Phys. **124** (2006) 221101.

[75] Tran F, Blaha P. J. Phys. Rev. Lett. **102** (2009) 226401.

[76] Tran F, Blaha P, Schwars K. J. Phy. Cond. Mat **19** (2007) 196208.

[77] Heyd J, Peralta J E, Scuseria G E and Martin R L. J. Chem. Phys. **123** (2005) 174101.

[78] Paier J, Marsman M, Hummer K, Kresse G, Gerber I C, Angyan J G. J. Chem. Phys. **124** (2006) 154709.

[79] Paier J, Marsman M, Hummer K, Kresse G, Gerber I C, Angyan J G. J. Chem. Phys. **125** (2006) 249901.

[80] Aulbur W G, Stadele M, Gorling A. J. Phys. Rev. B **62** (2000) 7121.

[81] Faleev S V, Schilfgaarde M V, Kotani T, Phys. J. Rev. Lett. **93** (2004) 126406.

[82] Shishkin M, Marsman M, Kresse G, Phys. J. Rev. Lett. **99** (2007) 246403.

[83] V.K. Sharma, R. Xalxo, G.D. Varma. J. Cryst. Res. Technol. **42** (2007) 34.

[84] J.K. Furdyna. J. Appl. Phys. **64** (1988) 29.

[85] J. Kossut, A.C. Beer, K. Furdyna, Academic, New York, **25 (**1988).

[86] M. Jain, J.L. Robbins, Material preparation, crystal structure and energy gap of diluted magnetic semiconductors, in: M. Jain (Ed.), Diluted Magnetic Semiconductors, World Science Publishing Co. Pvt. Ltd., Singapore (1991) 13.

[87] K. Sato. J. Advances in Crystal Growth Research. (2001) 303.

[88] Y. Ohno, D.K. Young, B. Beschoten, F. Matsukura, H. Ohno, D.D. Awschalom. J. Nature . **402** (1999) 790.

[89] J.K. Furdyna. J. Appl. Phys. **64** (1988) R29.

[90] D. Ferrand, A. Wasiela, S. Tatarenko, J. Cibert, G. Richter, P. Grabs, G. Schmidt, L.W. Molenkamp, T. Dietl. J. Solid State Commun. **119** (2001) 237.

[91] A. Haury, A. Wasiela, A. Arnoult, J. Cibert, S. Tatarenko, T. Dietl, Y. Merle d'Aubigné, J. Phys. Rev. Lett. **79** (1997) 511.

[92] D. Ferrand, J. Cibert, C. Bourgognon, S. Tatarenko, A. Wasiela,G. Fishman, A. Bonanni, H. Sitter, S. Kolesnik, J. Jaroszynski,A. Barcz, T. Dietl. J. Cryst. Growth **214** (2000) 387.

[93]F. Takano et al. Physica E **40** (2008) 1166.

[94] J.-Y. Ahn, M. Imamura. Journal of Magnetism and Magnetic Materials **272–276** (2004) 2002.

[95] A.E. Merad et al. Journal of Magnetism and Magnetic Materials **302** (2006) 536.

[96] S.A. Touat et al. Physica B **405** (2010) 625.

[97] Y. Hwang et al. Journal of Magnetism and Magnetic Materials **304** (2006) 309.

[98] A.D. Becke. J. Phys. Rev. A. **38** (1988) 3098.

[99] J.P. Perdew , J.A Chevary ,S.H. Vosko, K.A. Jackson, M.R. Pederson, D.J. Singh, C Fiolhais. J. Phys. Rev. B **46** (1992) 6671.

[100]www.sham.phys.sci.osaka-u.ac.jp/~kkr/.

[101] V. L. Mouruzzi, J. F. Janak and A. R. Williams Properties of Metals. Pergramon,

New York (1998).

[102] O. Madelung (Ed.), Numerical Data and Functional relationships inScience and Technology, Landolt Bornstein, New Series, Group III, vol.22, Springer, Berlin, 1987 .

[103] K. Durose et al. Journal of Crystal Growth **197** (1999) 733.

[104] J.A. Gaj, R. Planel, G. Fishman. J. Solid State Commun. **29** (1984) 861.

[105]Andriy I. Savchuk, Mykola P. Gavaleshko, Anatoliy M. Lyakhovich. IEEE TRANSACTIONS ON MAGNETICS. **29** (1993) 6.

[106]J.-Y. Ahn, M. Imamura. Journal of Magnetism and Magnetic Materials. **272–276** (2004) 2002.

[107] J.A. Gaj, R. Planel, G. Fishman. J. Solid State Commun. **29** (1984) 861.

[108] Andriy I. Savchuk, Mykola P. Gavaleshko, Anatoliy M. Lyakhovich, Transactions on Magnetics **29** (1993) 6.

[109] H. Katayama-Yoshida, et al. J. Physica Status Solidi a-Applications and Materials Science **204** (2007) 15.

[110] M. Toyoda, et al. J. Physica B-Cond. Mat **376** (2006) 647.

[111] M. Toyoda et al. J. phys. Stat. sol. C **3** (2006) 4155.

[112] J.A. Gaj, R. Planel, G. Fishman. J. Sol. Stat. Commun. **29** (1984) 861.

[113] Andriy I. Savchuk, Mykola P. Gavaleshko, Anatoliy M. Lyakhovich. IEEE TRANSACTIONS ON MAGNETICS. **29** (1993) 6.

[114] V.K. Sharma, R.Xalxo, G.D. Varma. J. Cryst. Res. Technol. **42** (2007) 34.

[115] Y. Sbai, A. AitRaiss, E. Salmani, L. Bahmad, A. Benyoussef. J. Magn. Magn. Mat. **396** (2015) 153.

[116] A. Ait Raiss, Y.Sbai, L.Bahmad, A. Benyoussef. J. Magn. Magn. Mat. **385** (2015) 295.

[117] A. Ait Raiss, Y. Sbai, Z. Zarhri, L. Bahmad and A. Benyoussef. J. Supercond. Nov. Magn. **28** (2015) 3545.

[118] J.K. Furdyna. J. Appl. Phys. **64** (1988) 29.

[119] J. Kossut, A.C. Beer, K. Furdyna, Diluted Magnetic Semiconductors, Semiconductors and Semimetals, Academic, New York, **25** (1988).

[120] K. Sato et al., First-principles theory of dilute magnetic semiconductors, Reviews of Modern Physics. **82** (2010) 1633.

[121] M. Jain, J.L. Robbins, Material preparation, crystal structure and energy gap of diluted magnetic semiconductors, in: M. Jain (Ed.), Diluted Magnetic Semiconductors, World Science Publishing Co. Pvt. Ltd., Singapore (1991) 13.

[122] K. Sato. Advances in Crystal Growth Research. (2001) 303.

[123] Y. Ohno, D.K. Young, B. Beschoten, F. Matsukura, H. Ohno, D.D. Awschalom. J. Nature **402** (1999) 790.

[124] D. Ferrand, A. Wasiela, S. Tatarenko, J. Cibert, G. Richter, P. Grabs, G. Schmidt, L.W. Molenkamp, T. Dietl. J. Sol. Stat. Commun. 1**19** (2001) 237.

[125] J. Gutowski, N, Presser and G. Kudlek. J. Phys. Stat. Sol. **120** (1990) 11.

[126] T.L. Chu, S.S. Chu, G. Chen, J. Britt, C. Ferekides and C.Q Wu. J.Appl. Phys. **71** (1992) 3865.

[127] A. Guillen-Cervantes, Z. Rivera-Avarez, M. Lopez-Lopez, E. Lopez-Luna, and I. Henandez-Calderon , Thin Solid Films **373** (2000) 159.

[128] A. A. Shakhmin, I. V. Sedova, S. V. Sorokin, M. V. Zamoryanskaya, Superlattices Microstruct, **56** (2013) 27.

[129] R. Kumaresan, M. Ichimura and E. Arai, Thin Solid Films. **414** (2002) 25.
[130] A. D. Becke, Phys. Rev. A **38** (1988) 3098.
[131]www.sham.phys.sci.osaka-u.ac.jp/~kkr/.

[132] V. L. Mouruzzi, J. F. Janak and A. R. Williams, Properties of Metals. Pergramon,

New York (1998).